NTNU

Norwegian University of
Science and Technology

Leak Detection in Two-Phase Oil and Gas Pipelines by Parameter- and State Estimation

Kjetil Hodne

Master of Science in Engineering Cybernetics
Submission date: June 2008
Supervisor: Ole Morten Aamo, ITK

Norwegian University of Science and Technology
Department of Engineering Cybernetics

Problem Description

Oppgaven har bakgrunn i et behov for overvåking av oljerør og gassrør. StatoilHydro opererer flere slike, bl.a. mellom Kollsnes og Mongstad. En modell for slik overvåking er myndighetspålagt. Her er det viktig med en god modell, bl.a. slik at Mongstad vet i forkant hva som kommer, og for å avdekke lekkasjer. Oppgaven bygger på tidligere prosjektoppgave hvor deteksjon av lekkasje i tofase lagdelt strømning ble studert. Følgende punkter skal belyses:

1. Gjør rede for tidligere arbeid, og motiver for oppgaven. Her kan du i stor grad støtte deg på tidligere arbeid.
2. I tidligere arbeid er matematisk modell brukt for å finne gunstige grensebetingelser for tilstandsestimatordelen av lekkasjedeteksjonssystemet eksplisitt i form av en koordinattransformasjon. Mens dette er mulig for enfase strømning, er det ikke hensiktsmessig for de kompliserte sammenhengene som oppstår mellom faser i flerfase strømning. Det skal derfor undersøkes hvorvidt målinger kan benyttes til å finne grensebetingelser for tilstandsestimatoren numerisk.
3. Utfør simuleringer hvor OLGA benyttes både som prosess og tilstandsestimator, og undersøk konvergensegenskaper.
4. Utfør simuleringer hvor OLGA benyttes både som prosess og tilstandsestimator, og undersøk evnen til å utføre lekkasjedeteksjon.
5. Foreslå videre arbeid basert på dine erfaringer.

Assignment given: 15. January 2008
Supervisor: Ole Morten Aamo, ITK

Abstract

A two-fluid model is used to derive a set of boundary conditions. The conditions are produced numerically, and try to imitate the behavior of output injection by using a linearized version of the model. In order to ensure that the model is hyperbolic, virtual mass terms are included in the momentum equations. An observer is presented, using OLGA, a fluid simulator, as its model. The boundary conditions derived are employed in the observer, and its convergence properties are shown to improve. A set of adaption laws for estimating parameters in a two-phase leak model is derived. Estimation of the leakage mass fraction is sacrificed in order to increase performance and stability. A model, also based on OLGA, is used to simulate a leak, and the observer prove to give good estimates of leak parameters as long as estimates of leakage mass fraction is available. Mass flow fraction seem to be a sufficient estimate. A wide range of scenarios are simulated, inspecting the weaknesses of the observer.

Preface

This report is the result of a Master of Science thesis performed at the department of engineering cybernetics at the Norwegian University of Science and Technology (NTNU) during the period from January '08 until June '08. The thesis is a collaboration between NTNU and StatoilHydro R&D, department of process control, at Rotvoll, Trondheim.

I would like to thank my adviser at StatoilHydro, John-Morten Godhavn, and especially my adviser at NTNU, Ole Morten Aamo.

Contents

Nomenclature

$\bar{f}_G$	Mean gas leakage estmiate deviation [kg/s]
$\bar{f}_L$	Mean oil leakage estmiate deviation [kg/s]
$\bar{w}$	State vector based on conserved variables
$\bar{x}_l$	Mean leak position estmiate deviation [m]
$\breve{w}$	Outgoing dynamics mapped into states
δ	Virtual mass parameter
ϵ	Volumetric gas fraction
ϵ_G	Gas volumetric fraction
ϵ_L	Oil volumetric fraction
ϵ_l	Gas mass fraction of leakage
γ	Pipeline inclination [°]
Γ_w	Wall friction force
Γ_{Gi}	Interphase friction working on gas phase
Γ_{Gw}	Wall friction working on gas phase
Γ_{Li}	Interphase friction working on oil phase
Γ_{Lw}	Wall friction working on oil phase
$\hat{\epsilon}$	Estimated leakage gas fraction
$\hat{q}$	State vector of observer on characteristic form
$\hat{w}$	State vector of observer
$\hat{w}_c$	Observer variables set by boundary conditions
$\hat{w}_m$	Observer variables not set by boundary conditions
κ_{u_G}	Leakage magnitude adaption coefficient
κ_{u_L}	Leakage magnitude adaption coefficient
κ_{x_G}	Position adaption coefficient
κ_{x_L}	Position adaption coefficient
Λ	System matrix on characteristic form
Λ^*	Observer system matrix on characteristic form
λ_k	System eigenvalue
μ_g	Partial derivative of pressure with respect to m_G
μ_l	Partial derivative of pressure with respect to m_L
ρ	Average density in a cross section $[kg/m^3]$
ρ_G	Gas density $[kg/m^3]$
ρ_L	Oil density $[kg/m^3]$
ρ_{refl}	Reference density in oil density model $[kg/m^3]$
$\tilde{q}$	Deviation state vector of observer on characteristic form
$\tilde{w}$	Observer deviation state vector

$\tilde{w}_c$	Deviation $w_c - \hat{w}_c$
$\tilde{w}_m$	Deviation in measured values$w_m - \hat{w}_m$
A	Area of a pipeline cross-section $[m^2]$
$A(w)$	System matrix
c_G	Sonic velocity in gas $[m/s]$
c_L	Sonic velocity in oil $[m/s]$
c_{vm}	Virtual mass coefficient
D_0	Tuning coefficient matrix for output injection at inlet
D_1	Tuning coefficient matrix for output injection at outlet
$f_G(x)$	Gas leakage at point x $[kg/s]$
f_l	Leakage magnitude $[kg/s]$
$f_L(x)$	Oil leakage at point x $[kg/s]$
k_L	Constant coefficient in the oil density model [Pa]
M	Length of window of convergence $[m]$
m_G	Gass mass in a cross section, $\epsilon_G \rho_G$
m_L	Gass mass in a cross section, $\epsilon_L \rho_L$
M_{vm}	Virtual mass term
p	Pressure [Pa]
P_G	Pressure in gas phase [Pa]
P_L	Pressure in oil phase [Pa]
p_{ref}	Reference pressure in oil density model [Pa]
q	Model characteristic state vector
q^+	Part of state vector in characteristic form corresponding to positive eigenvalues
q^-	Part of state vector in characteristic form corresponding to negative eigenvalues
R	System eigenvector matrix
t_c	Measure of convergence time $[s]$
t_{end}	End of simulation $[s]$
u_G	Gas phase velocity $[m/s]$
u_L	Oil phase velocity $[m/s]$
w	Model state vector
w_c	Model state vector with variables chosen as boundary condition in the observer
w_G	Gas mass flux $[kg/m^2 s]$
w_L	Oil mass flux $[kg/m^2 s]$
w_m	Model state vector with variables which are not set by boundary condition in the observer

Chapter 1

Introduction

Two-phase flow pipelines are used extensively in the petroleum industry. With growing public concern for the environment, the demand for pipeline monitoring is increasing. Being able to detect, quantify and position a leak clearly has its environmental motivation factors, but also has economical aspects. Most leak detection systems able to estimate leak position only work for single-phase flow.

Several leak detection systems are available, using dynamic modeling to quantify and locate leakage in single-phase flow. This report is based on the Luenberger-type observer presented in (Aamo, Salvesen & Foss 2005), which is throughly tested in (Hauge 2007). The objective of this thesis is to derive a similar observer for two-phase flow, using measurements from the pipeline inlet and outlet to estimate leak position.

An observer works by simulating a process using a model, while the real process is monitored. What distinguishes a Luenberger observer is the way it monitor the process and reacts to it. Measurements from the process are compared to values from the observer. The deviation is used to modify observer states in order to make the observer states converge to those of the real process. The observer used in this thesis has a similar set-up, where the real process is a pipeline with two-phase oil and gas flow, and the states are fluid conditions throughout the pipeline. However, directly modifying the states inside the pipeline will in most cases violate conservation laws. This may unfortunately lead to unphysical responses and strange behavior. Measurements are taken at inlet and outlet, but instead of using them to modify states inside the pipeline, they are used to control the states at the ends only, the boundary conditions. This ensures conservation of mass and momentum inside the pipeline, which makes it far easier to obtain convergence. In addition, it allows the use of OLGA as its model, which is a state of the art computational fluid dynamics simulator.

For this set-up to work, a set of boundary conditions must be derived. These condi-

tions must make all states converge even if only the boundary states are controlled. In this case, the observer variables are defined throughout the entire pipeline, and consequently there are endlessly many states in the model. In the observer, however, the pipeline is partitioned into sections with averaged values. These averaged values have to converge to the average in the corresponding section of the real pipeline.

The most obvious choice of boundary conditions is simply setting the observer boundaries equal to that of the process. Assuming that a transport pipeline is strictly dissipative, these simple conditions would eventually make the observer converge. On the other hand, in single-phase flow, faster convergence has been obtained using the characteristics of the system employing output injection instead. This means separating ingoing and outgoing dynamics, and then let the ingoing dynamic at each end be controlled by the outgoing (Aamo et al. 2005). As convergence is important to be able to estimate leak parameters, output injection is desired also in the two-phase observer. This is straight forward partial differential equation theory, but employing the method on a two-phase model has proved difficult (Hodne 2007). The interaction between the two phases make the model complex, and simple analytic expressions for eigenvectors were not found. Analytic expressions for the characteristics might not exist. Since it has failed to derive output injection analytically, an objective in this thesis is to develop something equivalent, only numerically.

In addition to controlling boundary conditions, the error $\hat{e}$ will also be used to estimate leak parameters. In order for this to work, the model in the observer has to converge faster than the adaption. If not, deviation in behavior between the model and the real process might corrupt the adaption and lead to false estimates. The adaption laws also have to be derived, which is another objective.

The resulting set-up is presented in Figure 1.1. As seen, Matlab will be used as interface between the process and the observer. Process measurements will be generated by another OLGA model. First boundary conditions and adaption laws have to be found, before the observer is implemented and tested.

1.1 Previous work

Many types of leak detection systems exist, both hardware- and software-based. Lately, software-based methods have been the most popular, including mass balance methods, flow or pressure change methods or dynamic modeling methods (Zhang 1996). The majority of solutions fall into the pressure change type, where measurements of pressure are examined, looking for specific wave or gradient signatures. Two such systems are presented in (Feng, Zhang & Liu 2004) and in (Hu, Ye, Wang & Lu 2004), which both look for negative pressure waves.

In (Nilssen 2005), a work founded on previous work by (Aamo et al. 2005), a leak detection system for single-phase flow is designed. The system, which uses a type

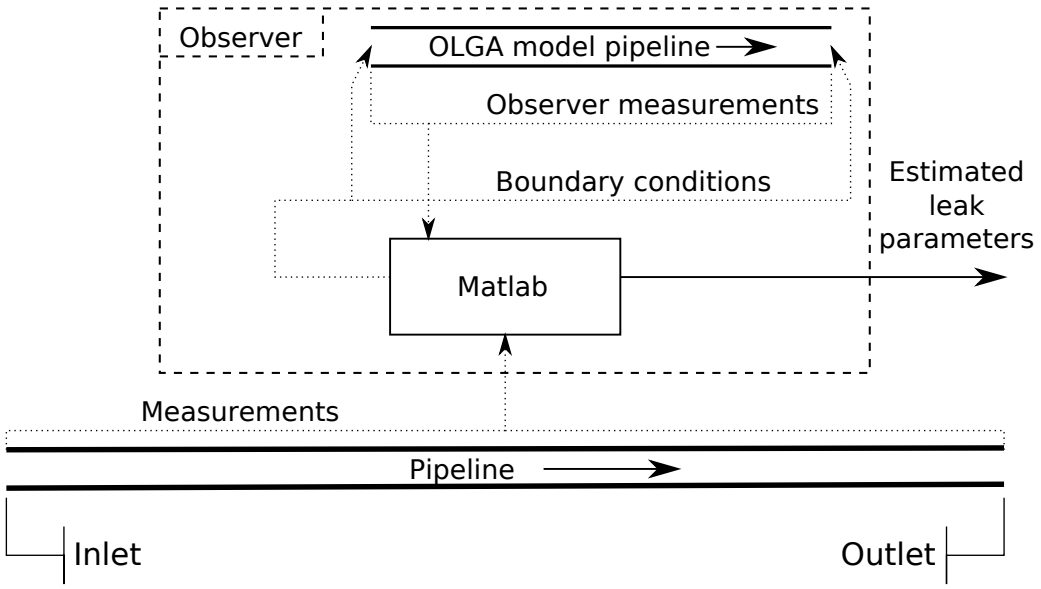

Figure 1.1: Observer setup using OLGA as model and estimating leak parameters.

of dynamic modeling, is based on two coupled one dimensional first order nonlinear hyperbolic partial differential equations. An observer, as the one described above, is derived with time-varying boundaries guaranteeing fast convergence. These boundary conditions employ output injection, which is obtained by finding the model and observer characteristics. The ingoing dynamics of the observer are set equal to that of the process. A set of adaption laws are also presented, both adapting friction and leak parameters, including leak position. The observer only uses measurements of pressure and flow rates at inlet and outlet, measurements which often are available, and hence the observer can be used without installing new equipment.

In (Hauge 2007), two instances of this observer-type is implemented. One of them was a Matlab observer already presented in (Nilssen 2005), which solves the two equations using a finite differential method. The other uses OLGA as its model, which is already a widely used fluid dynamic simulator. The observers are throughly tested in many scenarios, including cases with shutdown and varying production. Simulations showed that the OLGA observer was superior to the Matlab observer. The OLGA observer also has the option of modeling pipelines with varying inclination, and temperature could easily be included.

Chapter 2

Theory

This chapter will cover different topics within the science of leak detection and pipeline flow. First a set of general boundary conditions, which are valid for any hyperbolic flow model, will be developed. These boundary conditions mimic output injection, and are compared to the conditions which already have proved useful for single-phase flow. A two-fluid model is derived, made hyperbolic by adding a virtual force term, and used in the general boundary conditions. Subsequently, boundary responses in a two-phase pipeline are examined. A leak in the pipeline has its parameters altered. Leak adaption laws for two-phase flow are developed based on the examples.

2.1 Numerical boundary conditions

In this section, a general expression for boundary conditions in hyperbolic systems will be derived. The goal is to utilize this set of conditions on the boundaries of a pipeline observer model and have the observer converge to the real system fast. In (Aamo et al. 2005), a set of boundary conditions was derived, by analysis of the characteristics of a single phase flow system and utilizing output injection. Multi-phase flow models are often very complex due to their interphase interaction terms. Such models are often hard to work with analytically. For this reason, a set of boundary conditions will be derived, which behave like output injection. They are derived using a linearized model, and should be applicable to a number of different flow models, and hence named general boundary conditions. Later these conditions will be analyzed and compared to the single-phase boundary conditions which are throughly investigated in (Hauge 2007). They will also be used in a two-fluid observer with the same type of setup as that of the single-phase observer.

Consider a strictly hyperbolic system on the quasilinear form

$$w_t + A(w)w_x = B(w)w. \tag{2.1}$$

$w \in \mathbb{R}^n$ is a vector of dependent variables. For abbreviation, we write $w(x,t)$ as w and $\partial w/\partial x$ as w_x. $(x,t) \in (0,1) \times \mathbb{R}^+$, and $A \in \mathbb{R}^{n\times n}$ is the system matrix. Consider the transform into

$$q_t + \Lambda q_x = \varphi q, \tag{2.2}$$

by using $w = Rq$, $A = R\Lambda R^{-1}$ and $B = R\varphi R^{-1}$. As with w, we write $q(x,t)$ as q. The columns of R are the eigenvectors of A, which gives Λ non-zero values only on the diagonal. This follows from the fact that A is hyperbolic, and these values are the eigenvalues of the system.

Let $\Lambda \in \mathbb{R}^{n\times n}$ and $q \in \mathbb{R}^n$ be arranged such that

$$\Lambda = \begin{bmatrix} \Lambda^- & 0 \\ 0 & \Lambda^+ \end{bmatrix} \qquad\qquad q(x,t) = \begin{bmatrix} q(x,t)^- \\ q(x,t)^+ \end{bmatrix} \tag{2.3}$$

where

$$\begin{aligned} \Lambda^- &= \mathtt{diag}(\lambda_1, \lambda_2, \ldots, \lambda_p), & \lambda_1, \lambda_2, \ldots, \lambda_p < 0, \\ \Lambda^+ &= \mathtt{diag}(\lambda_p, \lambda_{p+1}, \ldots, \lambda_n), & \lambda_p, \lambda_{p+1}, \ldots, \lambda_n > 0, \end{aligned}$$

while $q^- \in \mathbb{R}^p$ and $q^+ \in \mathbb{R}^r$. Now consider $a(x)$ and $b(x)$ as the time-invariant versions of A and B respectively within a time-step. $a(x)$ and $b(x)$ will converge toward A and B when the time of one step approaches zero. Within each time step, (Besson, Tchousso & Xu 2006) proves that the following boundary conditions will give profitable convergence:

$$q^+(0,t) = D_0 q^-(0,t), \tag{2.4}$$
$$q^-(1,t) = D_1 q^+(1,t). \tag{2.5}$$

where $D_0 \in \mathbb{R}^{p\times r}$ and $D_1 \in \mathbb{R}^{r\times p}$. According to (Besson et al. 2006) these boundary conditions guaranties exponential convergence towards zero as long as for all $\omega_- \in \mathbb{R}^p, \omega_+ \in \mathbb{R}^r$,

$$\omega_-^T \left[\Lambda^-(1) + D_1^T \Lambda^+(1) D_1\right] \omega_- \leq +r_1 \left\|\omega_+\right\|_{\mathbb{R}^p}^2 \tag{2.6}$$
$$\omega_+^T \left[\Lambda^+(0) + D_0^T \Lambda^-(0) D_0\right] \omega_+ \geq -r_2 \left\|\omega_-\right\|_{\mathbb{R}^r}^2 \tag{2.7}$$
$$\begin{bmatrix} \omega_- \\ \omega_+ \end{bmatrix}^T \left[\delta + \varphi^T - \frac{\partial}{\partial x}\Lambda\right] \begin{bmatrix} \omega_- \\ \omega_+ \end{bmatrix} \leq 0 \tag{2.8}$$

In addition, the system has to be hyperbolic, which is true for the above mentioned system. These conditions generally say that the system has to be strictly dissipative.

Not investigating these restrictions further at this point, focus is put on a general system with an observer. Consider an observer on the same form as the model,

$$\hat{q}_t + \Lambda^* \hat{q}_x = \varphi^* \hat{q} \tag{2.9}$$

The hat above variables indicate it is an observer value, corresponding to the variable from the model without the hat. Consider now the two systems put together,

$$\tilde{q}_t + \Lambda \tilde{q}_x + (\Lambda - \Lambda^*)\hat{q}_x = \varphi \tilde{q} + (\varphi - \varphi^*)\hat{q}, \tag{2.10}$$

where $\tilde{q}$ denote the difference between the model and the observer, $\tilde{q} = q - \hat{q}$. $\tilde{q}$ is the vector that is desired to converge to zero. In order to use the theorem mentioned, the observer is assumed to be a linearized version of the model, and the difference is ignored. This difference between Λ and Λ^* is assumed small as long as the observer states are close to those of the model. This will clearly be a cause for error, but results later prove that the assumption give profitable conditions. The resulting system is

$$\tilde{q}_t + \Lambda \tilde{q}_x = \varphi \tilde{q}. \tag{2.11}$$

In an observer based on n system equations, there are n boundary conditions which must be set, and n measurements. Often, there is an even number of measurements and controlled variables at each end. Assume w is arranged such that the top variables are measured and used when deciding values on the controlled variables at the bottom. The following derivation is almost identical if you let the top variables be controlled variables. Measured and controlled variables will be denoted with subscript m and c respectively. Note that it is only in the observer some variables are named controlled variables. In the real process, all n variables are measured.

$$\tilde{w} = \begin{bmatrix} \tilde{w}_m \\ \tilde{w}_c \end{bmatrix} \qquad , \tilde{w}_m \in \mathbb{R}^m, \tilde{w}_c \in \mathbb{R}^c. \tag{2.12}$$

$\tilde{w}$ again denote the difference between the model and the observer, $\tilde{w} = w - \hat{w}$. Similarly, the eigenvector matrix is split into four,

$$R^{-1} = \begin{bmatrix} S_- \\ S_+ \end{bmatrix} = \begin{bmatrix} S_{m-} & S_{c-} \\ S_{m+} & S_{c+} \end{bmatrix}. \tag{2.13}$$

$S_{m-} \in \mathbb{R}^{p \times m}$ is the part of the eigenvector-matrix mapping measured variables into the characteristic values corresponding to negative eigenvalues. Equal interpretations can easily be found for the other sub matrices. It now follows that

$$\tilde{q}^- = S_- \tilde{w} = S_{m-}\tilde{w}_m + S_{c-}\tilde{w}_c, \tag{2.14}$$

$$\tilde{q}^+ = S_+ \tilde{w} = S_{m+}\tilde{w}_m + S_{c+}\tilde{w}_c. \tag{2.15}$$

Inserting (2.14)-(2.15) into (2.4)-(2.5),

$$S_{m+}\tilde{w}_m + S_{c+}\tilde{w}_c = D_0(S_{m-}\tilde{w}_m + S_{c-}\tilde{w}_c) \tag{2.16}$$
$$S_{m-}\tilde{w}_m + S_{c-}\tilde{w}_c = D_1(S_{m+}\tilde{w}_m + S_{c+}\tilde{w}_c) \tag{2.17}$$

Remember that (2.16) is a condition at inlet, while (2.17) is valid at the outlet. After some manipulation,

$$(S_{m+} - D_0 S_{m-})\tilde{w}_m = (D_0 S_{c-} - S_{c+})\tilde{w}_c, \tag{2.18}$$
$$(S_{c-} - D_1 S_{c+})\tilde{w}_c = (D_1 S_{m+} - S_{m-})\tilde{w}_m, \tag{2.19}$$

it is easy to obtain the following boundary conditions:

Inlet:

$$\hat{w}_c = w_c - (D_0 S_{c-} - S_{c+})^{-1}(S_{m+} - D_0 S_{m-})(w_m - \hat{w}_m), \tag{2.20}$$

Outlet:

$$\hat{w}_c = w_c - (S_{c-} - D_1 S_{c+})^{-1}(D_1 S_{m+} - S_{m-})(w_m - \hat{w}_m). \tag{2.21}$$

The convergence-performance for these conditions will be discussed in later sections, where they will be labeled output injection. This is to some extent a misuse of this term, as they are based on a linearized model, where the working point is that of the model. Note from (2.4)-(2.5), what goes into the pipe depends on what comes out. When implementing these conditions, the system matrix A must be evaluated at both ends where you want to apply the conditions. Hence S_{m-} in (2.20) will probably not have the same values in (2.21).

By rearranging (2.12) and (2.13), (2.20)-(2.21) is valid with the controlled variables on top also.

2.2 General boundary conditions and single phase flow

In this section, the general boundaries, (2.20) and (2.21), will be compared to the boundary conditions found by (Aamo et al. 2005). In order to do so, the eigenvector matrix for the single-phase system is found and used in (2.20)-(2.21). First, the one-phase model is given,

$$\frac{\partial p}{\partial t} + u\frac{\partial p}{\partial x} + \rho c^2 \frac{\partial u}{\partial x} = 0, \tag{2.22}$$
$$\frac{\partial u}{\partial t} + u\frac{\partial u}{\partial x} + \frac{1}{\rho}\frac{\partial p}{\partial x} = 0, \tag{2.23}$$

where the first equation is derived from mass conservation, while the second from momentum conservation(Nilssen 2005). Putting the system on the general form by (2.1),

$$\frac{\partial}{\partial t}\begin{bmatrix} p \\ u \end{bmatrix} + A(p,u)\frac{\partial}{\partial x}\begin{bmatrix} p \\ u \end{bmatrix} = 0 \tag{2.24}$$

where, using the general density model

$$\rho = \rho_{ref} + \frac{p - p_{ref}}{c^2} \tag{2.25}$$

and $k = \rho_{ref}c^2 - p_{ref}$, the system matrix becomes

$$A(p,u) = \begin{bmatrix} u & k+p \\ \frac{c^2}{k+p} & u \end{bmatrix}. \tag{2.26}$$

Knowing that the eigenvalues are $\lambda_1 = u - c$ and $\lambda_2 = u + c$, the eigenvector matrix can easily be shown to be

$$R(p,u) = \begin{bmatrix} \frac{k+p}{c} & \frac{k+p}{c} \\ -1 & 1 \end{bmatrix}, \qquad R^{-1}(p,u) = \begin{bmatrix} 1 & -\frac{k+p}{c} \\ 1 & \frac{k+p}{c} \end{bmatrix}. \tag{2.27}$$

Using the general boundary conditions found, utilizing full output injection, i.e. $D_0 = 0$,$D_1 = 0$, we get the following expressions. At inlet, the velocity to be set is

$$\hat{u} = u + \frac{c}{k+p}(p - \hat{p}) \tag{2.28}$$

Equally, for pressure at outlet,

$$\hat{p} = p - \frac{k+p}{c}(u - \hat{u}) \tag{2.29}$$

In comparison, (Aamo et al. 2005) found, with $k_0 = 0$ and $k_L = 0$

$$\hat{u}_a = u + c\ln(\frac{k+p}{k+\hat{p}}), \tag{2.30}$$

$$\hat{p}_a = (k+p)e^{\frac{\hat{u}-u}{c}} - k \tag{2.31}$$

Looking closely into the two expressions for velocity, the difference between $\hat{u}$ and $\hat{u}_a$ is what is multiplied with c on the right hand side. That is, how does $\frac{p-\hat{p}}{k+p}$ compare to $\ln(\frac{k+p}{k+\hat{p}})$. Using

$$\ln x = (x-1) + \sum_{n=2}^{\infty}(-1)^{n+1}\frac{(x-1)^n}{n} \qquad [0 < x < 2] \tag{2.32}$$

and considering $\frac{k+p}{k+\hat{p}} < 2$ which is valid for most practical cases, (2.30) can be written as

$$\hat{u}_a = u + \frac{c}{k+p}(p-\hat{p}) + \sum_{n=2}^{\infty} \frac{(-1)^{n+1}}{n}(\frac{p-\hat{p}}{k+p})^n \tag{2.33}$$

Similar, by using

$$e^x = \sum_{n=0}^{\infty} \frac{x^n}{n!} \tag{2.34}$$

(2.31) can be written

$$\hat{p}_a = p - \frac{k+p}{c}(u-\hat{u}) + \sum_{n=2}^{\infty} \frac{(\hat{u}-u)^n}{c^n n!}(k+p) \tag{2.35}$$

Both $\hat{u} - \hat{u}_a$ and $\hat{p} - \hat{p}_a$ are the higher order terms of a series expansion, and in both cases the difference is linearly dependent on the difference between model measurements and observer values. It is not possible to gain any higher order terms of $\tilde{p}$ or $\tilde{u}$ into the general boundary conditions, as they are built up of a linear mapping between physical and characteristic variables. Also note that for large c (remember that a large c means a large k), the sums become infinitesimal, and the two sets of boundary conditions are practically identical. This is the case for oil flow, where high sound velocity c and density makes k very large. These boundaries are throughly tested in (Hauge 2007). For gas the difference is notable, however.

2.3 Flow patterns in oil and gas pipelines

There are many flow patterns in two-phase flow. For oil and gas flow, the most common patterns are stratified smooth flow, stratified wavy flow, slug flow, bubble flow and annular flow (Liu, Yang & Wang 2008). The regimes depend on pipe diameter, and large diameter gas and oil transportation pipelines are mostly limited to stratified flow and slug flow (Lu, Wang & Jia 2006).

Prediction of flow patterns are important when flow resistance is concerned, and it is not an easy task with frequent pattern transitions. At low flow rates the regime will be stratified, whereby the liquid phase flows along the bottom and the gas above it. Phase velocities might vary, but when the liquid velocity increases, slugging occurs. Slugging is characterized by large bubbles of gas alternated with liquid or bubbly flow. At even higher rates, pure bubbly or annular flow might occur.

Adaption will be depending on estimates of both interphase and wall friction forces. Being able to predict the correct flow regime is crucial, but will be flawed. Wall friction adaption would be able to compensate for some of that error, but perhaps not satisfactory at transient behavior with frequent transitions.

Another problem concerning flow regimes occurs when a small change in flow rate or valve opening causes a pattern transition. This may drastically change the flow resistance and hence also the pressure drop. When this happens to an observer attempting to converge toward a model, it will probably end up as an unexpected response, and might be hard to distinguish from the response of a small leak.

All considered, there is no doubt, different flow regimes and transitions will cause problems when attempting leak detection in a two-phase gas and oil pipeline. If the observer was limited to to a single pattern, this would certainly also limit the means of convergence to a limited interval of boundary conditions which maintain that pattern. The most general approach would be to create an observer able to handle any flow regime, accepting the error this might cause.

2.4 Two-Fluid Model

In this section the Two-Fluid model for gas and oil flow in pipelines will be derived. This is a model based on conservation laws and interphase terms. The interphase interaction terms depend on flow pattern, while the conservation laws are universal. Energy equations will be ignored, and all variables averaged over a cross section, leaving an isothermal one dimensional model. Negative sources are added in order to account for leakage. In the next section, further terms are added in order to make the model strictly hyperbolic.

Figure 2.4 shows a pipeline segment of length dx. The cross section area A is constant. As all variables are averaged over a cross section, the length x is the only dimension in the system. The pipe is inclined with an angle γ compared to the horizon.

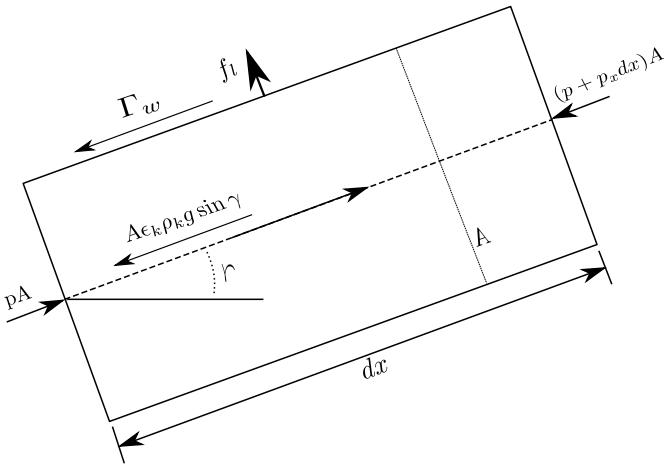

Figure 2.1: A segment of a pipeline illustrating forces.

2.4.1 Mass balance

Adding up the mass flow in and out of a segment, for both phases individually, leads to the following mass balance equations:

$$A\frac{\partial(\epsilon_k\rho_k)}{\partial t}dx + \left[\epsilon_k\rho_k A u_k - A\frac{\partial(\epsilon_k\rho_k u_k)}{\partial x}dx\right] - \epsilon_k\rho_k A u_k + f_k(x)dx = 0 \tag{2.36}$$

for $(x,t) \in (0,L) \times \mathbb{R}^+$. ϵ_k, ρ_k and u_k are volume fraction, density and velocity respectively. Two versions of this equation exists, one for each phase, and variables for the two phases are indexed $k \in \{G, L\}$ for gas and oil respectively. Note that the volumetric fractions sum up to one, $\epsilon_G + \epsilon_L = 1$. f_k is a function describing gas leakage at position x, and is modeled as

$$f_G(x) = f_l\epsilon_l\delta(x - x_l), \tag{2.37}$$
$$f_L(x) = f_l(1 - \epsilon_l)\delta(x - x_l). \tag{2.38}$$

f_l is mass leakage, ϵ_l is the fraction of gas leaking, and x_l is the position of the leak. δ is the Dirac distribution.

Dividing (2.36) by Adx, rearranging and inserting phase variables leads to the two mass conservation equations

$$\frac{\partial}{\partial t}(\epsilon_G\rho_G) + \frac{\partial}{\partial x}(\epsilon_G\rho_G u_G) = -\frac{f_G(x)}{A}, \tag{2.39}$$

and

$$\frac{\partial}{\partial t}(\epsilon_L\rho_L) + \frac{\partial}{\partial x}(\epsilon_L\rho_L u_L) = -\frac{f_L(x)}{A}. \tag{2.40}$$

2.4.2 Momentum balance

When deriving momentum balance, consider a material volume, i.e. a fixed set of particles contained in a volume $V(t)$. This allow the use of Newton's second law,

$$\frac{d(\bar{m}_G u_G)}{dt} = \sum F \tag{2.41}$$

for $(x,t) \in (0,L) \times (0,\infty)$. The derivation will consider the gas phase, but momentum balance for liquid phase can be derived in the exact same way. Let the mass inside the material volume, as the one illustrated in Figure 2.4, be $\bar{m}_G = \rho_G\epsilon_G A dx$.

$$\frac{d(\rho_G\epsilon_G u_G A dx)}{dt} = \sum F \tag{2.42}$$

As the control volume is the time-varying volume of which a specific set of particles is contained, the mass is constant, and it follows that

$$\frac{d}{dt}(\bar{m}_G u_G) = \frac{du_G}{dt}\bar{m}_G + \frac{d\bar{m}_G}{dt}u_G = \frac{du_G}{dt}\rho_G \epsilon_G A dx \tag{2.43}$$

By combining the mass balance with Reynolds' transport theorem (Egeland & Gravdahl 2002), it follows that

$$\frac{du_G}{dt}\bar{m}_G = \frac{\partial}{\partial t}(\rho_G \epsilon_G u_G) + \frac{\partial}{\partial x}(\rho_G \epsilon_G u_G u_G) \tag{2.44}$$

Newton's law, (2.41), may now be written as

$$A\frac{\partial}{\partial t}(\rho_G \epsilon_G u_G) + A\frac{\partial}{\partial x}(\rho_G \epsilon_G u_G u_G) = \sum F \tag{2.45}$$

The forces working on the material volume are

$$\sum F = -A\epsilon_G \frac{\partial P_G}{\partial x} + \Gamma_{Gw} + \Gamma_{Gi} - A\epsilon_G \rho_G g \sin\gamma + M_{vm} \tag{2.46}$$

The first term in the sum is the pressure gradient. P_G is the gas phase pressure. Since the model is one-dimensional, P_G is considered equal to the liquid phase pressure P_L. The second and third term, Γ_{Gw} and Γ_{Gi}, are wall and interphase friction forces respectively, and depend on flow regime. g is the gravity and γ the pipe angle relative to the horizon, but by assuming horizontal pipes, the fourth term will be neglected. The fifth term is the virtual mass force term, which will be accounted for in section 2.4.5. Following the same procedure for the liquid phase, momentum balances are summed up as

$$A\frac{\partial}{\partial t}(\epsilon_G \rho_G u_G) + \frac{\partial}{\partial x}(A\epsilon_G \rho_G u_G u_G) + A\epsilon_G \frac{\partial P_G}{\partial x} + M_{vm} = \Gamma_{Gw} + \Gamma_{Gi}, \tag{2.47}$$

$$A\frac{\partial}{\partial t}(\epsilon_L \rho_L u_L) + \frac{\partial}{\partial x}(A\epsilon_L \rho_L u_L u_L) + A\epsilon_L \frac{\partial P_L}{\partial x} - M_{vm} = \Gamma_{Lw} + \Gamma_{Li}. \tag{2.48}$$

2.4.3 Density models

The number of dependent variables has to be reduced in order to solve this equation set, hence models for density is introduced. Densities are modeled as a functions of pressure, and pressure is assumed equal in both phases over a cross section, i.e. $p = P_G = P_L$. The ideal gas law, (2.49), replace gas density. Oil density is modeled as in the single phase model,(2.25), and repeated in (2.50).

$$\rho_G = \frac{p}{c_G^2} \tag{2.49}$$

$$\rho_L = \rho_{refl} + \frac{p - p_{ref}}{c_L^2} = \frac{k_L + p}{c_L^2} \tag{2.50}$$

where $k_L = c_L^2 \rho_{refl} - p_{ref}$.

2.4.4 Conserved variables

The desired quasi-linear form of the system is

$$\frac{\partial \bar{w}}{\partial t} + A(\bar{w}) \frac{\partial \bar{w}}{\partial x} = S(\bar{w}), \tag{2.51}$$

where $\bar{w}$ is the state vector. Basing states on the conserved variables simplifies the system matrix, hence $\bar{w}$ is chosen as

$$\bar{w} = \begin{bmatrix} m_G \\ w_G \\ m_L \\ w_L \end{bmatrix} = \begin{bmatrix} \rho_G \epsilon_G \\ \rho_G \epsilon_G u_G \\ \rho_L \epsilon_L \\ \rho_L \epsilon_L u_L \end{bmatrix}, \tag{2.52}$$

Substituting the conserved variables into system equations, they may be written as

$$\frac{\partial}{\partial t}(m_G) + \frac{\partial}{\partial x}(w_G) = -\frac{f_{lG}}{A}, \tag{2.53}$$

$$\frac{\partial}{\partial t}(m_L) + \frac{\partial}{\partial x}(w_L) = -\frac{f_{lL}}{A}, \tag{2.54}$$

$$\frac{\partial}{\partial t}(w_G) + \frac{\partial}{\partial x}(\frac{w_G^2}{m_G}) + \epsilon_G \frac{\partial P_G}{\partial x} + M_{vm} = \Gamma_{Gw} + \Gamma_{Gi}, \tag{2.55}$$

$$\frac{\partial}{\partial t}(w_L) + \frac{\partial}{\partial x}(\frac{w_L^2}{m_L}) + \epsilon_L \frac{\partial P_L}{\partial x} - M_{vm} = \Gamma_{Lw} + \Gamma_{Li}. \tag{2.56}$$

In order to replace pressure as a variable, the following function is introduced:

$$P_k = P(m_G, m_L) \qquad k \in \{G, L\}. \tag{2.57}$$

It follows that

$$\frac{\partial p}{\partial x} = \mu_g \frac{\partial m_G}{\partial x} + \mu_l \frac{\partial m_L}{\partial x}, \tag{2.58}$$

where

$$\mu_g = \frac{\partial P_p(m_{G_i}, m_{L_i})}{\partial m_G}, \tag{2.59}$$

$$\mu_l = \frac{\partial P_p(m_{G_i}, m_{L_i})}{\partial m_L}. \tag{2.60}$$

In search of the function $P(m_G, m_L)$, consider now the conserved variables, and insert the density models:

$$m_G = \rho_G \epsilon_G = \frac{p\epsilon}{c_G^2}, \tag{2.61}$$

$$m_L = \rho_L \epsilon_L = \frac{(p + k_L)(1 - \epsilon)}{c_L^2}, \tag{2.62}$$

where $\epsilon = \epsilon_G = 1 - \epsilon_L$ is introduced. By eliminating ϵ from the two equations above, the following equation is obtained:

$$\frac{m_G {c_G}^2}{p} = \frac{-m_L {c_L}^2 + p + k_L}{p + k_L}. \tag{2.63}$$

This is a second order equations in terms of p, and can easily be shown to have the following solutions:

$$P(m_G, m_L) = \varsigma \pm \sqrt{\varsigma^2 + m_G {c_G}^2 k_L}, \tag{2.64}$$

where

$$\varsigma = \frac{m_G {c_G}^2 + m_L {c_L}^2 - k_L}{2}. \tag{2.65}$$

Looking carefully into the solutions, one of them can be eliminated, as the physical solution must be positive. This leaves the solution

$$P(m_G, m_L) = \varsigma + \sqrt{\varsigma^2 + m_G {c_G}^2 k_L}, \tag{2.66}$$

its partial derivatives are

$$\mu_G = \frac{\partial P}{\partial m_G} = \frac{c_G^2}{2}(1 + \frac{\varsigma + k_L}{\sqrt{\varsigma^2 + m_G c_G^2 k_L}}), \tag{2.67}$$

and

$$\mu_L = \frac{\partial P}{\partial m_L} = \frac{c_L^2}{2}(1 + \frac{\varsigma}{\sqrt{\varsigma^2 + m_G c_G^2 k_L}}). \tag{2.68}$$

Similarly fraction is converted as

$$\epsilon_k = E_k(m_G, m_L). \tag{2.69}$$

Following the same procedure as for pressure, pressure is eliminated from (2.61) and (2.62), which leads to

$$\frac{m_G {c_G}^2}{\epsilon} = -\frac{m_L {c_L}^2 - k_L + k_L \epsilon}{-1 + \epsilon}. \tag{2.70}$$

This is also a second order equations, with the following physical solutions:

$$E_G(m_G, m_L) = \epsilon_G = \frac{-\varsigma + \sqrt{\varsigma^2 + m_G {c_G}^2 k_L}}{k_L}, \tag{2.71}$$

$$E_L(m_G, m_L) = \epsilon_L = 1 - \frac{-\varsigma + \sqrt{\varsigma^2 + m_G {c_G}^2 k_L}}{k_L}. \tag{2.72}$$

2.4.5 Virtual Mass

The basic two-fluid model is ill-posed with complex eigenvalues of the Jacobian matrix. However, adding a few additional differential terms to the momentum equation can make the equations well-posed. These terms are named virtual mass terms, and represents the interphase force which is created by difference in the phase accelerations. As interpretation, consider the virtual mass as the liquid a gas-bubble has to relocate in order to accelerate relative to the liquid phase. The virtual mass terms are an attempt to model the extra forces needed to accelerate because of the virtual mass.

The motivation for adding the virtual mass terms to the system is not to model the relatively insignificant force they represents, but to make the model hyperbolic. This method is commonly used, but the form of the virtual mass terms in realistic two-phase flow is not known exact, and consequently the differential terms used vary. Common for all formulations are that they do not appreciably change the momentum results, but cause the system to be hyperbolic.

In this work, we choose the general virtual mass term (2.73) presented in (Toumi & Kumbaro 1996). (Chung, Lee & Chang 2001) present an even more general term, but eventually use (2.73) in the code.

$$M_{vm} = -\epsilon_G \epsilon_L \rho c_{vm} \left(\frac{\partial}{\partial t}(u_G - u_L) + u_L \frac{\partial u_G}{\partial x} + u_G \frac{\partial u_L}{\partial x}\right) \tag{2.73}$$

where

$$\rho = m_G + m_L. \tag{2.74}$$

c_{vm} is the virtual mass coefficient. One of the disadvantages of virtual mass terms is that this coefficient is determined empirically without any theoretical reasoning. For a single, non-deformable, spherical particle in an alien fluid, according to (Drew 1979), $c_{vm} = 0.5$. For two-phase flow of practical concern c_{vm} is likely to give values less than 0.5, independent of flow regime.

In a mixed bubbly flow, with bubbles close to spheres, c_{vm} should have a value between zero and 0.5. However, in a regime of smooth separated flow, the amount of alien fluid a particle must relocate in order to accelerate is close to zero. Clearly, c_{vm} depend on flow regime.

(Chung et al. 2001) add interphacial pressure jump terms to his equations, in addition to the virtual mass terms. This guarantee hyperbolicity, but might add unphysical responses. Instead a condition suggested by (Tiselj & Petelin 1997) is used,

$$c_{vm} = \begin{cases} (1+2\epsilon)/(2-2\epsilon), & \epsilon < 0.5 \\ \sqrt{(\frac{3-2\epsilon}{2\epsilon})^2 - \frac{(\epsilon-1)(2\epsilon-1)}{(1+\epsilon\rho_G/\rho_L-\epsilon)^2}}, & \epsilon > 0.5 \end{cases}, \tag{2.75}$$

which guarantees hyperbolicity as long as the relative velocity $u_G - u_L$ is less than 30% of sonic velocity in the medium, i.e. $u_G - u_L < 0.3c$ where c is the sonic velocity in the medium.

2.4.6 Hyperbolic Two-Fluid model on quasi-linear form

Consider again the quasi-linear form

$$\frac{\partial w}{\partial t} + A(w)\frac{\partial w}{\partial x} = S(w)w, \tag{2.76}$$

The inclusion of virtual mass has complicated the model significantly, and for to ease the derivation, another change of variables is introduced. In order to eliminate the virtual mass term from one of the momentum equations, the variable w_G is replaced with $w_G + w_L$. In addition, the virtual mass terms are separated from the main equations as follows, where subscript δ denote matrices with virtual mass terms.

$$(I + M_\delta(\bar{w}))\bar{w}_t + (A_s(\bar{w}) + A_\delta(\bar{w}))\bar{w}_x = S(\bar{w})\bar{w} \tag{2.77}$$

A_s contains the system matrix without virtual mass terms. $\bar{w}$ and $A_s(\bar{w})$ are given by

$$\bar{w} = \begin{bmatrix} m_G \\ m_L \\ w_G + w_L \\ w_L \end{bmatrix} \tag{2.78}$$

$$A_s(\bar{w}) = \begin{bmatrix} 0 & 0 & 1 & -1 \\ 0 & 0 & 0 & 1 \\ \mu_G - \frac{w_G^2}{m_G^2} & \mu_L - \frac{w_L^2}{m_L^2} & \frac{2w_G}{m_G} & 2(\frac{w_L}{m_L} - \frac{w_G}{m_G}) \\ \epsilon_L\mu_G & \epsilon_L\mu_L & 0 & \frac{2w_L}{m_L} \end{bmatrix} \tag{2.79}$$

The matrices corresponding to the virtual mass terms are given by

$$A_\delta(\bar{w}) = \delta \begin{bmatrix} 0 & 0 & 0 & 0 \\ 0 & 0 & 0 & 0 \\ 0 & 0 & 0 & 0 \\ (1-c)u_G u_L & -cu_G u_L & -(1-c)u_L & u \end{bmatrix} \tag{2.80}$$

and

$$M_\delta(\bar{w}) = \delta \begin{bmatrix} 0 & 0 & 0 & 0 \\ 0 & 0 & 0 & 0 \\ 0 & 0 & 0 & 0 \\ (1-c)u_G & -cu_L & -(1-c) & 1 \end{bmatrix} \tag{2.81}$$

where

$$\delta = \frac{\rho^2}{\rho_G \rho_L} c_{vm} \tag{2.82}$$

$$u = \frac{w_G + w_L}{m_G + m_L}, \tag{2.83}$$

$$c = \frac{m_G}{m_G + m_L}, \tag{2.84}$$

$$S_s(\bar{w}) = (I + M_\delta(\bar{w}))^{-1} S(\bar{w}) \tag{2.85}$$

This leaves the system matrix $A = (I + M_\delta(\bar{w}))^{-1}(A_s(\bar{w}) + A_\delta(\bar{w}))$ which has real eigenvalues for sufficiently large $c_{vm} > 0$.

Ignoring the leak at this point, $S(\bar{w})$ is found to be

$$S(\bar{w}) = \begin{bmatrix} 0 & 0 & 0 & 0 \\ 0 & 0 & 0 & 0 \\ 0 & 0 & \frac{\Gamma_{Gw}}{w_G} & \frac{\Gamma_{Lw}}{w_L} \\ 0 & 0 & 0 & \frac{\Gamma_{Lw}}{w_L} + \frac{\Gamma_{Li}}{w_L} \end{bmatrix} \tag{2.86}$$

Simulation show that the system has two eigenvalues in the range between sound velocities in the two phases, one negative and one positive. The third eigenvalue is in the range between velocity of gas and velocity of oil. The fourth eigenvalue is very small, negative, and vary much with c_{vm}. A smaller c_{vm} tends to give smaller fourth eigenvalue.

While the two eigenvalues with the largest magnitude have opposite signs, the smaller eigenvalues might change sign. If there are not two negative eigenvalues, a pseudo-inverse is used instead of the inverse in equation (2.20) and (2.21). When

these are implemented in the OLGA observer, there will only be set three boundary conditions, which means some information is lost anyway. The pseudo-inverse should not prevent the output injection appreciably, but the optimal solution would be to set a number of conditions at one end of the pipeline equal to the amount of ingoing waves at that position. This number depends on the signs of the eigenvalues.

2.4.7 Modeling leakage

Leakage is modeled as

$$\hat{f}_l = \hat{c}_v \sqrt{\rho_l(\hat{p}_l - \hat{p}_l^{amb})}, \tag{2.87}$$

$$\hat{f}_G = \hat{f}_l \epsilon_l \delta(x - \hat{x}_l) \tag{2.88}$$

$$\hat{f}_L = \hat{f}_l (1 - \epsilon_l) \delta(x - \hat{x}_l) \tag{2.89}$$

where

$$\rho_l = \epsilon \rho_G + (1 - \epsilon)\rho_L. \tag{2.90}$$

Subscript l denote values at leak position. $\hat{f}_G$ and $\hat{f}_L$ are leakage of gas and oil respectively. $\hat{c}_v$ is a general leak magnitude parameter. $\hat{p}_l^{amb}$ is the ambient pressure outside the leak.

The reason for this structure is justified in Section 2.5 where adaption laws for the parameters are derived.

2.4.8 General boundary conditions and restrictions

The general boundary conditions were derived with the assumptions (2.6)-(2.8). First, note, when concerned with these restrictions, the optimal value for D_0 and D_1 must be zero. This can be seen by rearrange the left hand side of (2.6) to

$$w_-^T \Lambda^-(1) w_- + (D_1 w_-)^T \Lambda^+(1)(D_1 w_-). \tag{2.91}$$

Since the Λ^+ is positive definite, the second term can never be negative, and its lowest value is when $D_1 = 0$. Equivalent, $D_0 = 0$ is the best choice when it comes to comply with restriction (2.7).

Now consider the condition (2.8). For the two-fluid model, $\varphi = S_s(\bar{w})$, which depend on friction-forces. A high φ will cause the condition to become invalid, and hence the general boundary conditions are limited to low friction flow. Exactly where the limit is, will not be investigated, but this should be kept in mind when conducting simulations.

Using the general boundary conditions (2.20)-(2.21) with $D_0 = D_1 = 0$ and the model derived, results in the boundary conditions,

$$\begin{bmatrix} \hat{w}_G + \hat{w}_L \\ \hat{w}_L \end{bmatrix} = \begin{bmatrix} w_G + w_L \\ w_L \end{bmatrix} + S_{c+}^{-1} S_{m+} \begin{bmatrix} m_G - \hat{m}_G \\ m_L - \hat{m}_L \end{bmatrix} \tag{2.92}$$

at inlet, and

$$\begin{bmatrix} \hat{m}_G \\ \hat{m}_L \end{bmatrix} = \begin{bmatrix} m_G \\ m_L \end{bmatrix} + S_{c-}^{-1} S_{m-} \begin{bmatrix} w_G + w_L - \hat{w}_G - \hat{w}_L \\ w_L - \hat{w}_L \end{bmatrix} \tag{2.93}$$

at outlet. The controlled variables are chosen to correspond with OLGA boundary conditions as will be clear through the next chapter. S_{c-} and S_{m-} are part of the eigenvector matrix at outlet while S_{c+} and S_{m+} are part of the eigenvector matrix at inlet. The system matrix from where the eigenvector matrix is derived is $A = (I + M_\delta(\bar{w}))^{-1}(A_s(\bar{w}) + A_\delta(\bar{w}))$.

2.4.9 Flow Regimes

The model derived this far is based on mass and momentum conservation only, and is thus not limited to any flow regime. What makes up the difference between flow regimes in the two-fluid model is the phase interaction terms, including Γ_{kw} and Γ_{ki}. The interaction is easiest modeled for a stratified flow pattern. The virtual mass term, however, has the parameter c_{vm} which is dependent on the flow regime, and is easiest adopted to mixed flow.

Still, what is derived this far can be used on any two-fluid flow regime without specifying the phase interaction terms. However, it must be expected to have varying success on the different flow patterns. The linearization on boundaries assume states to be somewhat equal throughout the pipe, which is the case for stratified and mixed flow. As was pointed out in Section 2.3, slugging is often present, which would give alternating conditions on boundaries. However, as will be discussed in Section 3.3, by filtering the alternation on boundaries during slugging, the conditions derived may also be employed on this flow pattern. Simulations presented in Chapter 4 will test adaption on both major flow regimes; stratified flow and mixed flow with slugging.

2.5 Adaption laws

The goal of the thesis is to create an observer adapting to the behavior of a model both in order to detect a leak and to estimate the leak parameters. This is done with adaption based on measurements on the boundaries of the pipeline.

A set of adaption laws has to be produced, using boundary deviation between observer and model. These adaption laws must be based on dynamics coming from inside the pipeline, limiting the variables used for adaption to $q^-(0)$ and $q^+(L)$. $q^+(0)$ and $q^-(L)$ is set by the boundary conditions derived in section 2.1, and obviously give no new information on what is happening inside the pipeline. In order to draw information out of these variables, they are transfered into physical variables,

$$\begin{aligned} \check{w}(0) &= R^-(0)\tilde{q}^-(0) \\ \check{w}(L) &= R^+(L)\tilde{q}^+(L) \end{aligned} \tag{2.94}$$

where R^- and R^+ are matrices consisting of the eigenvectors corresponding to $q^-(0)$ and $q^+(L)$ respectively. $\check{w}(0)$ and $\check{w}(L)$ give information on how the observer differs from the model.

In order to use this information to decide which leak parameters needs to be adjusted and in which direction, a few examples are considered. The source is simulations in OLGA of a straight pipeline and constant boundary conditions. For pipe-properties, see Table B.1 in the appendix.

2.5.1 Leak position parameter adaption

Figure 2.2 illustrate two examples, where the blue graphs show boundary response with a leak at $x_l = 1150m$ and the green graphs show boundary response with a leak at $x_l = 3250m$. Flow rates at inlet and pressure at outlet are constant, and the flow-regime is stratified flow. The leaks does not occur until 3 minutes after the simulation starts. For simulation-parameters, see Table B.2.

Figure 2.3 show another set of boundary-values in a mixed flow regime. The leak position is $x_l = 1150m$ for the blue graphs and $x_l = 3250m$ for the green graphs, exactly like in the previous examples. Simulation-parameters are presented in Table B.3.

When considering these examples, the convergence-properties of the observer is not yet known, and the adaption-laws should as little as possible depend on transient behavior on the boundaries. For these laws to be stable, they should work with endlessly slow adaption. Consequently, when looking for a pattern on the boundaries, only steady state values are considered.

From what it seems, the only steady state indication on whether the leak position parameter is to be increased or decreased, which is apparent in both figures, is m_G and m_L at inlet. Consider the heuristic law

$$\dot{\hat{x}}_l = \kappa_{x_G}\check{m}_G(0) + \kappa_{x_L}\check{m}_L(0). \tag{2.95}$$

In Figure 2.2 the values at outlet seem to change toward the end of the simulation. In this flow pattern, fluid velocity is slower than in the mixed flow examples. When

a leak occurs, the fraction will change at the point of the leak, and the change propagate at a velocity in the range of the phase velocities. This change propagating toward the outlet will be labeled a fraction-wave. An example of this is illustrated in Figure 2.7. In the stratified flow example with a leak at 3250m, this fraction wave reaches outlet before the simulation is stopped. In the example with a leak at 1150m, however, it does not. This phenomena is also observed in mixed flow. In both examples with a mixed flow pattern, plotted in Figure 2.3, the fraction wave reaches outlet within 10 minutes after the leak occurs. This is due to the higher phase velocities in mixed flow.

Notice the small peaks at inlet flow rates, even though it was stated that these rates are constant. These peaks are due to the way flow rates are measured, which is described in section 3.1.

Also note the y-axis in Figure 2.2. The difference at inlet is very small. Actually, the inlet pressure only differs by 0.25 bar between the two cases. This is because interphase friction is lower in stratified flow in addition to the lower friction against pipe wall due to lower velocity. Also, fraction changes are only marginally different, which is why m_G and m_L does not change much. The difference is more noticeable in the cases of mixed flow. This suggests such flow regimes might be more robust, in that the response is more distinguishable. Adaption in mixed flow should be less vulnerable to noise, measurement error and perhaps also modeling error.

2.5.2 Leak magnitude parameter adaption

Figure 2.4 illustrate three new examples in a stratified flow regime, where the leak position x_l is kept constant, but magnitude of leakage, c_v, is changed. Also this pipe is described by the parameters in Table B.1. The black graphs show a default case where total leakage is 40 kg/s and gas fraction in leakage is $\epsilon_l = 0.1$. The green graphs show an identical leak, only the amount of gas leaking is reduced from 4 kg/s to 1 kg/s. The blue graphs show a similar case, only where oil leakage is reduced from 36 kg/s to 9 kg/s. Simulation-parameters are listed in Table B.4.

Similar examples in a mixed flow regime are given in Figure 2.5, with corresponding simulation-parameters in Table B.5. As in the previous examples, green graphs show a drop in gas leakage and blue graphs a drop in oil leakage.

In both flow regimes, when a leak occurs, there is an initial change and a delayed response visible only when the fraction-wave reaches outlet. This is easier to see in the stratified flow regime, where the fraction-wave propagate slower. This will be illustrated by two examples. Figure 2.6 show pressure profiles shortly after the leak occur in a stratified flow regime. Within a few seconds, the change in pressure has propagated throughout almost half the pipeline. Fraction profile from the same example is plotted in Figure 2.7. Note that these profiles range over 15 minutes. One can clearly see the change in fraction propagating toward the outlet, but at a

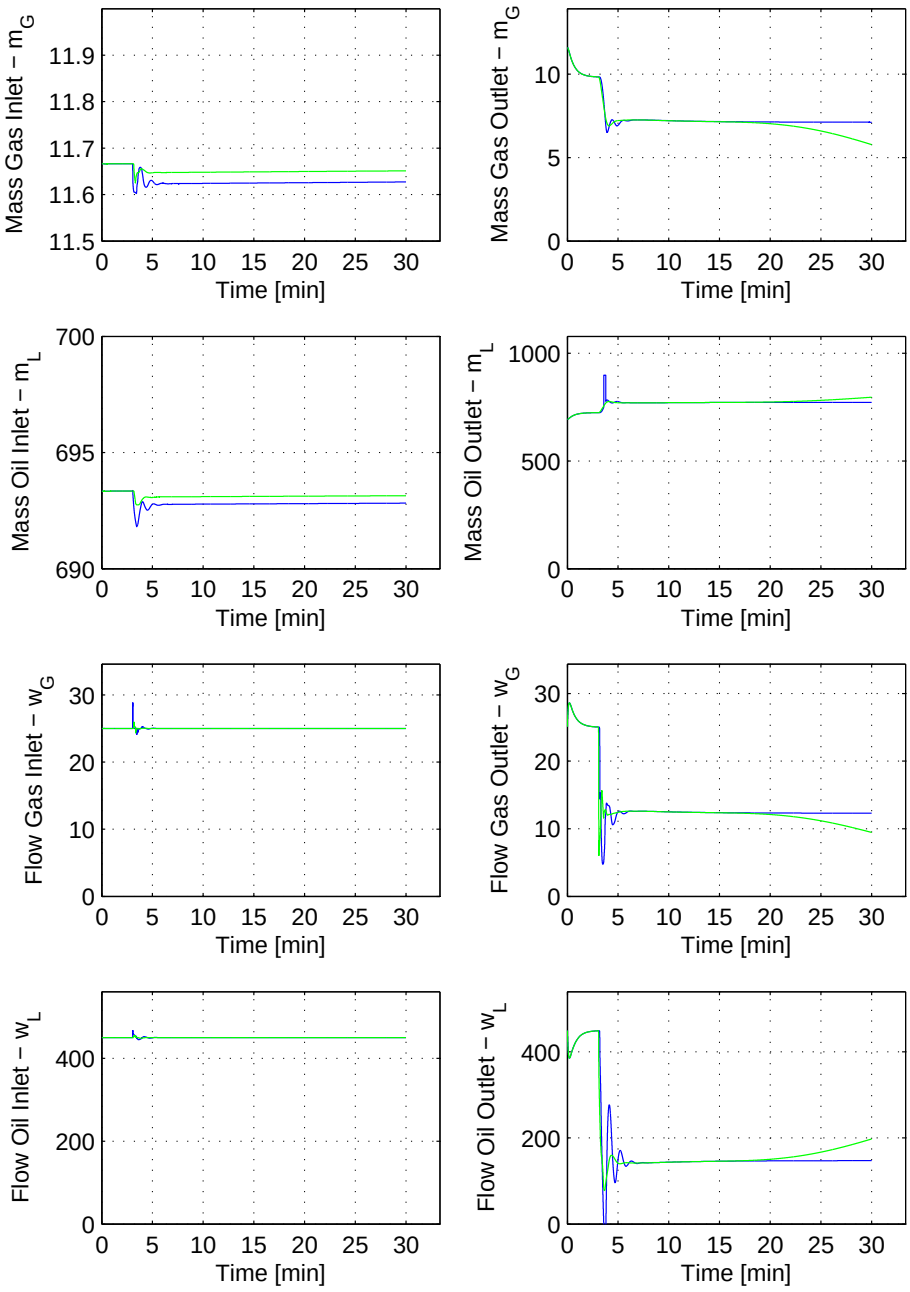

Figure 2.2: Boundary values of simulations with leaks at 1150m(blue) and 3250m(green) - Stratified flow

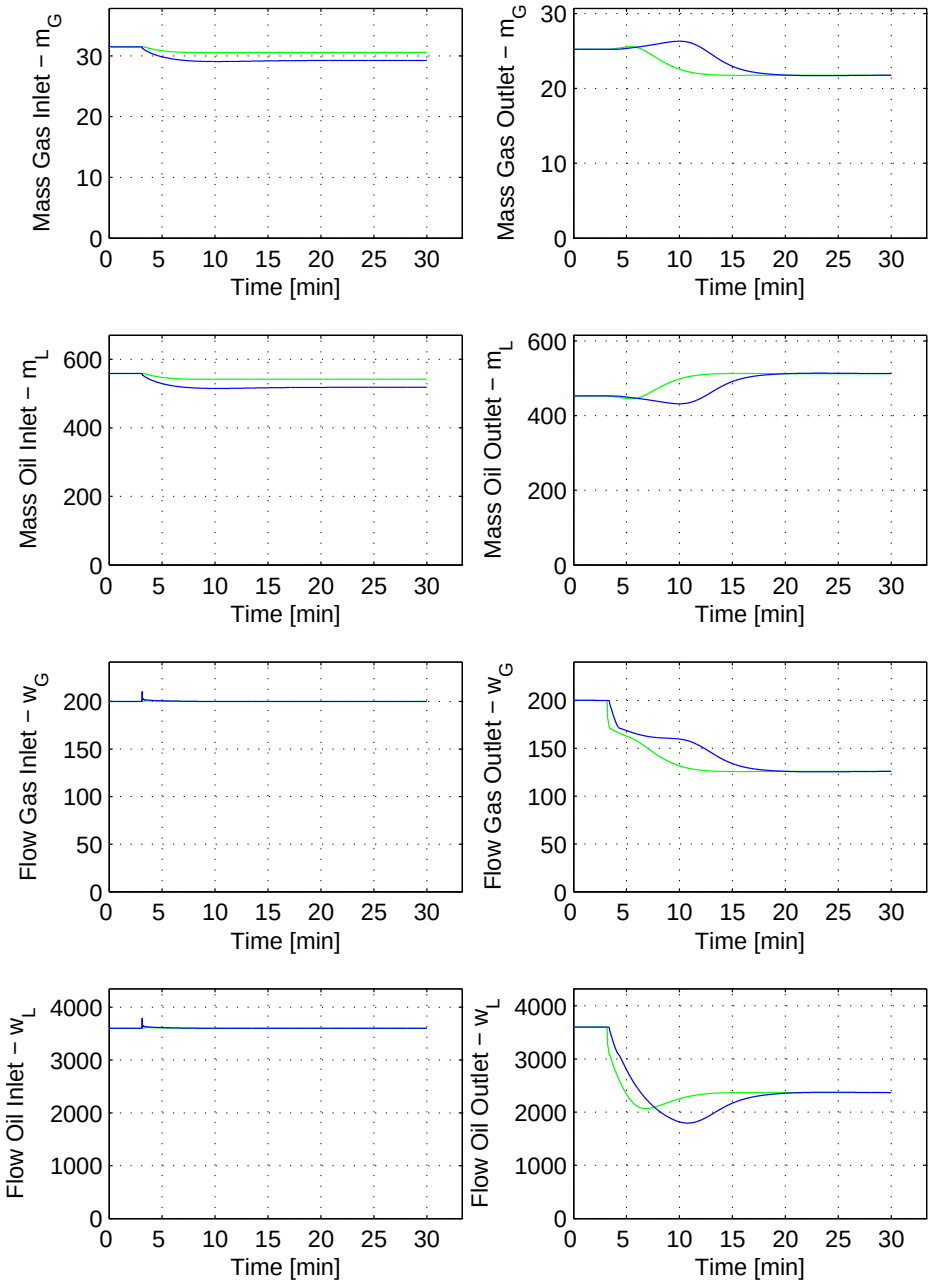

Figure 2.3: Boundary values of simulations with leaks at 1150m(blue) and 3250m(green) - Mixed flow

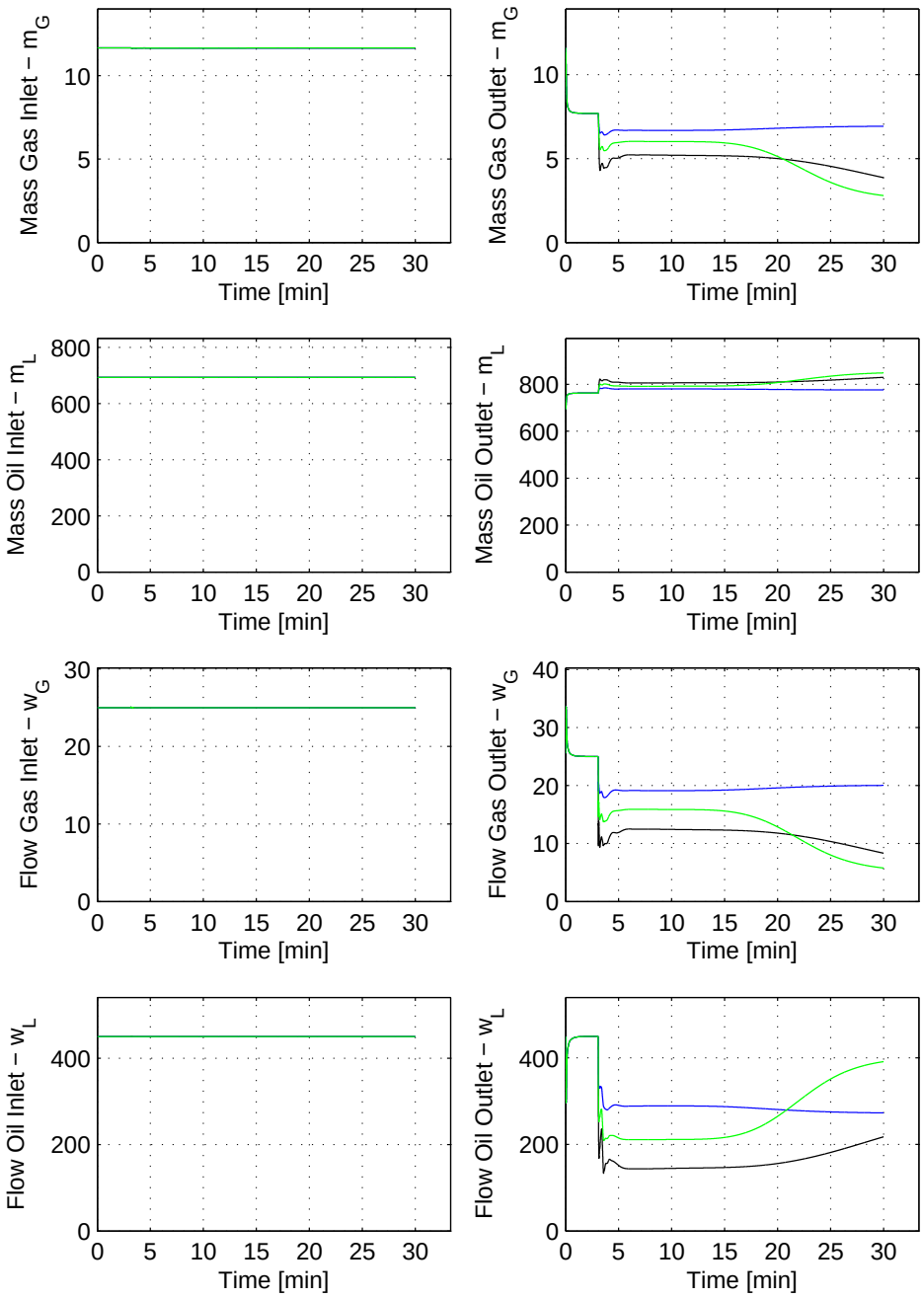

Figure 2.4: Boundary values in pipeline with stratified flow and a leak at 3450m. Black graphs show default leak. Green graphs show decrease in gas leakage, while blue graphs show decrease in oil leakage.

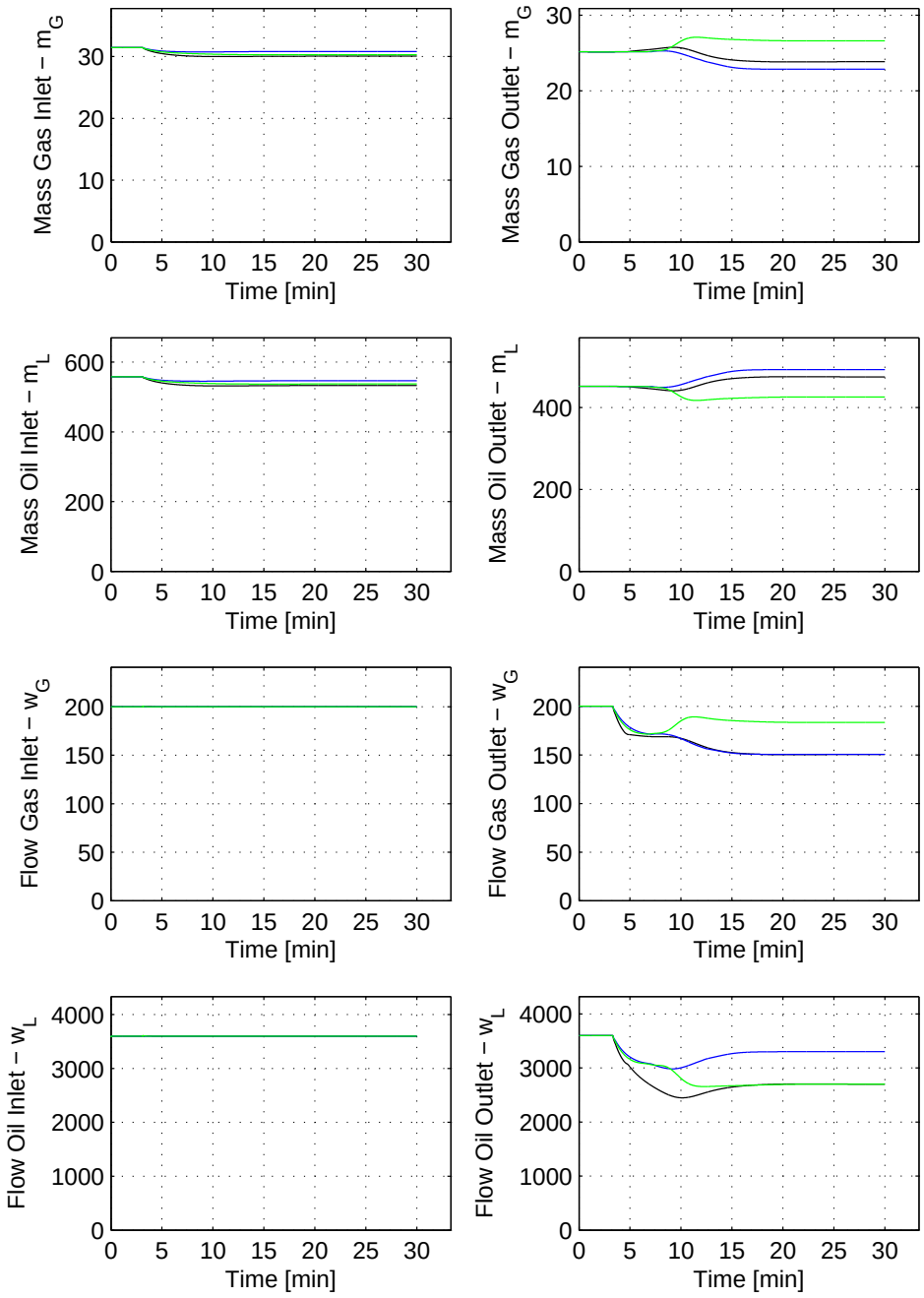

Figure 2.5: Boundary values in pipeline with stratified flow and a leak at 3450m. Black graphs show default leak. Green graphs show decrease in gas leakage, while blue graphs show decrease in oil leakage.

much slower rate than the pressure did. Notice also how fraction seem to drop at outlet. This is caused when the pressure wave reaches outlet. All states will change once when the pressure wave reaches outlet and once later, when the fraction wave does the same. Let us denote these two changes as the first drop and the second drop, although not all variables drop in value.

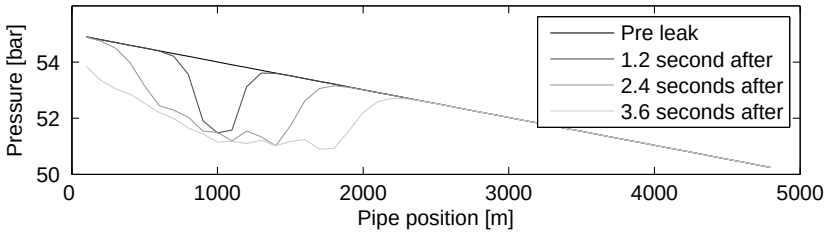

Figure 2.6: Pressure profiles before and after a leak occurs in a stratified flow pattern.

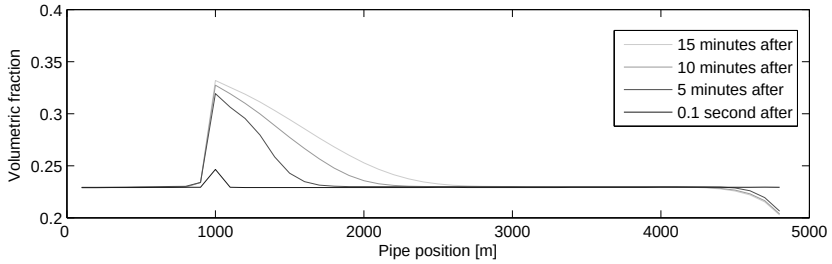

Figure 2.7: Fraction profiles after a leak occurs in a stratified flow pattern.

For all six simulations, the first drop causes flow rates at outlet to decrease. Even when very little gas is leaking, there will be a distinct drop in gas rate at outlet. Actually, two leaks at the same position, but with different leakage fraction ϵ_l, might give nearly identical responses at outlet. This, however, changes when the fraction wave reaches outlet. Eventually flow rates at outlet is the difference between what flows into the pipeline, and what is leaking. In the event of pure gas leakage, oil flow should go back to pre-leak values after the fraction wave reaches outlet.

Consider a case when an observer settle at a leak with $\epsilon_l = 0$ while the real value is 1. When the fraction wave reaches outlet, and the observer detect it is mistaken, the last part of the pipeline is already filled up with too much gas. In an extreme case, the last part of the pipeline might be filled entirely with oil, while the same part of the observer is filled with gas only. The adaption laws would be corrupted with this error until the observer could replace the excessive oil with gas. Regardless of pipe length, this would clearly be time-consuming. Although this example is rather extreme, and perhaps not possible, it suggests that when the fraction wave generated by a leak reaches outlet, it might be too late to change ϵ_l. Actually, at this point a very good estimate of ϵ_l could be concluded from model inlet minus outlet flow.

So, its not possible to estimate ϵ_l before the fraction wave reaches outlet, and when it does, it is probably too late. And there is more reasons for why adaption should not depend on information from the fraction wave. The flow into the pipeline would probably be shut down as soon as a leak is detected, and the fraction wave would never reach outlet. The leak might be placed at arbitrary length from outlet, causing the fraction wave to take an arbitrary amount of time before it reaches outlet. Also, adaption laws would most probably have to change when the fraction wave reached outlet, in order to cope with responses different from the initial ones. All of this considered, ϵ_l will not be adapted, but set to the best estimate available.

Leaving out fraction from our considerations, the only parameter left to adapt is $\hat{c}_v$. Looking at the examples, the general tendency is a drop in flow rates relative to the amount of leakage. As w_G and w_L are not directly affected by the pressure set at outlet, they are used for adapting $\hat{c}_v$ with adaption-law

$$\dot{\hat{c}}_v = \kappa_{u_G} \breve{w}_G(L) + \kappa_{u_L} \breve{w}_L(L). \tag{2.96}$$

where κ_{u_G} and κ_{u_G} are positive constants.

This adaption law is based on boundary responses before the fraction wave reaches outlet. Adaption beyond this point would be corrupted in many ways. First, if the estimate of ϵ_l is wrong, it will take quite a while before the observer has converged toward the model. Also, after the fraction wave has settled, the model is at steady state, and the real value of ϵ_l is directly available through mass conservation. Adaption would be unnecessary, also on c_v, which at steady state can be read directly. Third, but not least, with a wrong estimate of ϵ_l, there would be no way the observer could settle to the steady state boundary values of the model. Whatever it did, the leakage could never be the same as the model, and outlet flow rates would never settle at the values of the model.

Based on these facts, adaption will be limited to a window in time. On the other hand, adaption may be repeated for this window many times, keeping the parameter values from previous runs. This also gives a chance to change ϵ_l, and if data is available past this window, perhaps ϵ_l and c_v can be estimated through mass balance. If during each run through the time-window, leak parameters have converged toward its true value, this method should produce correct parameters eventually. Leaks very close to the outlet would have a very short time window, which might complicate the adaption, but should also provide good leak estimates through mass balance.

2.6 Observer summary

In the chapters to come, the general boundary conditions will be implemented on the boundaries of an OLGA model. OLGA is based on the two-fluid model, but

have more equations than the basic two-fluid model presented in this chapter. The main results of this chapter for use in later chapters are summarized here.

At the boundaries of the observer, the following conditions will be used:

Inlet:

$$\begin{bmatrix} \hat{w}_G + \hat{w}_L \\ \hat{w}_L \end{bmatrix} = \begin{bmatrix} w_G + w_L \\ w_L \end{bmatrix} + S_{c+}^{-1} S_{m+} \begin{bmatrix} m_G - \hat{m}_G \\ m_L - \hat{m}_L \end{bmatrix} \tag{2.97}$$

Outlet:

$$\begin{bmatrix} \hat{m}_G \\ \hat{m}_L \end{bmatrix} = \begin{bmatrix} m_G \\ m_L \end{bmatrix} + S_{c-}^{-1} S_{m-} \begin{bmatrix} w_G + w_L - \hat{w}_G - \hat{w}_L \\ w_L - \hat{w}_L \end{bmatrix} \tag{2.98}$$

where S_{c-} and S_{m-} are part of the eigenvector matrix at outlet while S_{c+} and S_{m+} are part of the eigenvector matrix at inlet. The system matrix from where the eigenvector matrix is derived is $A = (I + M_\delta(\bar{w}))^{-1}(A_s(\bar{w}) + A_\delta(\bar{w}))$.

The leak is parameterized as

$$\hat{f}_l = \hat{c}_v \sqrt{\rho_l(\hat{p}_l - \hat{p}_l^{amb})}, \tag{2.99}$$

$$\hat{f}_G = \hat{f}_l \epsilon_l \delta(x - \hat{x}_l) \tag{2.100}$$

$$\hat{f}_L = \hat{f}_l (1 - \epsilon_l) \delta(x - \hat{x}_l) \tag{2.101}$$

where $\hat{x}_l$ and $\hat{c}_v$ is adapted using adaption-laws

$$\dot{\hat{x}}_l = \kappa_{x_G} \check{m}_G(0) + \kappa_{x_L} \check{m}_L(0), \tag{2.102}$$

and

$$\dot{\hat{c}}_v = \kappa_{u_G} \check{w}_G(L) + \kappa_{u_L} \check{w}_L(L). \tag{2.103}$$

ϵ_l is kept constant, based on an initial guess, but a search algorithm may be used to fit it to the data running through the dataset several times.

Chapter 3

Method

This chapter will give a brief explanation on how to construct both model and observer. OLGA is a state of the art computational fluid dynamics simulator, and is employed as both observer and model. OLGA has limited options for leaks, and how this is handled is also explained in this chapter. In addition there is a section on adaption and one on result comparison.

The software used is Mathworks Matlab version 7.4.0.287 (R2007a), and OLGA 5.2.1 with OLGAMatlabToolbox version 1.1.

3.1 Measurements in OLGA

Two instances of a pipeline is modeled in OLGA, whereof one is used to generate model measurements, and the other is used as the model in an observer. Both OLGA pipelines are simulated through Matlab and Matlab OLGA Toolbox. Matlab is used to store model data-sets and in the case of the observer, load measurements, generate the correct boundary conditions, and control the OLGA simulations in general.

When Matlab is reading data from OLGA, there are two types of variables readable. One type is defined as volume-variable and values can be obtained in the middle of an OLGA pipe section. The second type of variables is boundary-variable, which can be read only at the boundaries between two sections. This type of scheme is normal for numerical partial differential solvers, such as Roe-solvers, which is also the reason why variables are defined this way in OLGA. General boundary conditions derived in the previous chapter require model measurements of state variables at two specific points labeled inlet and outlet. The separation of measurement-points makes this impossible as half the variables are measured at one set of points and the rest at another. Figure 3.1 illustrate the points at which measurements are taken relative to a section.

The pipeline is partitioned into n segments of length Δx. The OLGA pipeline model, on the other hand, is partitioned into sections, which should not be mixed with segments. Inlet is defined as the start of segment 1 and outlet at the end of segment n. The boundary variables, as velocity and flow rate, are read directly at these points. Pressure and fraction, however, must be estimated from the neighboring measurement-points. For better estimates, the distance between the inlet/outlet and the closest measurement-points should be small. On the other hand, small segments drastically increase the runtime of simulations. In order to get good measurements while keeping the simulation-time down, the first and last segment is partitioned into several sections as illustrated in Figure 3.1 and 3.2. A section in OLGA must be no more than twice the length of neighboring sections, which leads to a setup with sections at different lengths.

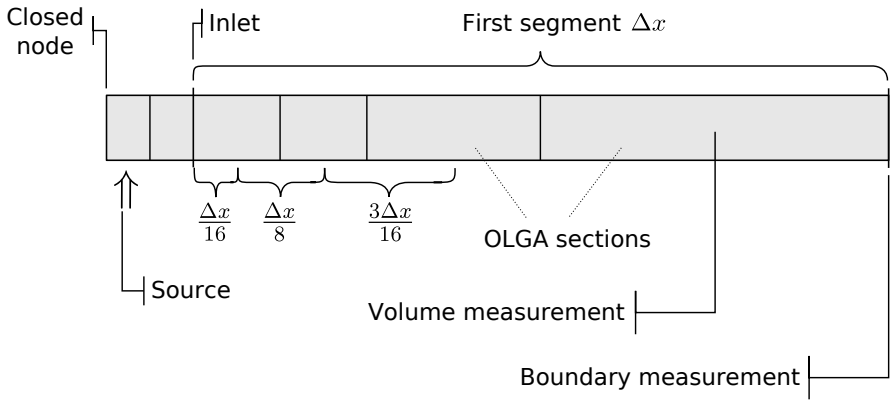

Figure 3.1: OLGA sections and segment overview at inlet. Illustrates the first six sections in OLGA whereof the last four form the first segment in the model.

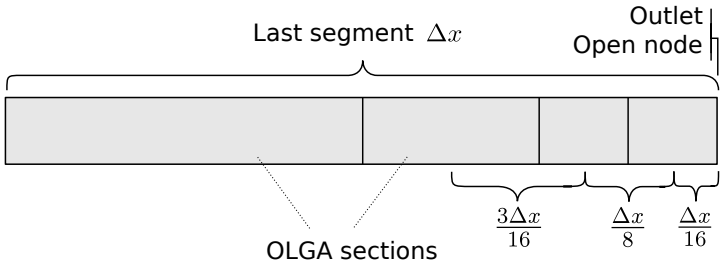

Figure 3.2: OLGA sections and segment overview at outlet. Illustrates the last four sections in OLGA which form the last segment in the model.

For to estimate the values of volume variables at inlet and outlet, an interpolation scheme is introduced, using the three closest measurements. Following (Nilssen 2005), only with varying section length, the following relations are derived in Appendix A,

$$\alpha_0 = \frac{9}{5}\alpha_1 - \alpha_2 + \frac{1}{5}\alpha_3 \tag{3.1}$$

$$\alpha_m = \frac{9}{5}\alpha_{m-1} - \alpha_{m-2} + \frac{1}{5}\alpha_{m-3} \tag{3.2}$$

α is any volume variable, and $\alpha_0 = \alpha(0)$, $\alpha_1 = \alpha(\Delta x/16)$, $\alpha_2 = \alpha(3\Delta x/16)$, $\alpha_3 = \alpha(6\Delta x/16)$, $\alpha_m = \alpha(L)$,$\alpha_{m-1} = \alpha(L - \Delta x/16)$, $\alpha_{m-2} = \alpha(L - 3\Delta x/16)$ and $\alpha_{m-3} = \alpha(L - 6\Delta x/16)$.

3.2 Setting boundary conditions in OLGA

At inlet, an OLGA source-element is added to control inlet flow rates of both gas and oil in the OLGA pipelines. The inflow is separated into two different sources in order to let one be negative while the other is positive, which would not be possible otherwise.

At outlet, which is an open node, OLGA let the user set pressure, but not fraction or any other variable appearing in the system equations presented in Section 2.4. The two-fluid model presented in the previous chapter has four system equations, and thus has four boundary conditions to be set. The reason OLGA only has three boundary conditions, is probably because of the inclusion of a slip relation. Unfortunately, the details of the OLGA model is not known.

3.2.1 Observer boundary conditions

The general boundary conditions derived in the previous chapter give four conditions in total, two at inlet and two at outlet. The inlet boundary-conditions are flow rates of gas and oil, taken directly from equation (2.97). The outlet boundary-condition is pressure. The pressure would be found using (2.66) mapping the values of $\hat{m}_G$ and $\hat{m}_L$ found by using (2.98) into pressure. However, another problem arise as the density-models are not exact. Even if $\hat{m}_G$ and $\hat{m}_L$ are equal to m_G and m_L, equation (2.66) will never give the same pressure as the model, and a steady state error is unavoidable. For this reason, when implementing output injection at outlet, the pressure set is a modification of the model pressure rather than the value produced by (2.66). Model measurements for m_G and m_L are used to find a pressure value with the density models, which is then compared to the same result using $\hat{m}_G$ and $\hat{m}_L$. The difference between the two is added to the model pressure, which is what is used at the outlet for the observer. This value can be expressed as

$$\hat{p} = p + (P(\hat{m}_G, \hat{m}_L) - P_p(m_G, m_L)). \tag{3.3}$$

where $\hat{m}_G$ and $\hat{m}_L$ are values generated from (2.98).

As fraction is not set, it is not possible to control both m_G and m_L as desired, and this drastically reduces the benefit of output injection.

In Figure 3.1, notice that there is two sections prior to inlet. The first of them include the source elements controlling inlet flow rates. Sources are always placed in the middle of their sections. This structure is necessary for steady flow rate measurements at inlet. Without the empty second section, fraction would not correspond to the flow rates. This, however, create a delay before the set flow rate affects measurements at inlet, and if the distance is large, this is clearly a source for error. On the other hand, it is yet another reason to make the first few sections shorter than average.

A filter is put on the inlet flow rates, as changes faster than the mentioned delay will only cause oscillation and in some cases strange behavior. Consider the filter

$$w^*_{k,n} = w^*_{k,n-1} - \frac{dt}{T}(w^*_{k,n-1} - w_{k,n}) \qquad k \in \{G, L\} \tag{3.4}$$

where the time constant T is set relative to the delay. Subscript n denote time step, while superscript * denote filtered variable. In this thesis, T is found heuristic and $T = L_{delay}/min(u_G, u_L)$ was found to yield good results. L_{delay} is the distance from source to inlet, and dt is the length of one time step.

Output injection is set off the first 15 seconds in order to let OLGA settle, as there is often an initial peak. If this peak give a pressure too high or too low, OLGA will produce an error and terminate the simulation. This is due to the lack of values in fluid properties tables used in OLGA. The peak occur because OLGA steady state pre-processor does not give exact steady state conditions. The 15 seconds is enough for the observer to settle.

3.3 Flow patterns in OLGA

OLGA has two basic flow regime classes, distributed and separated flow. Distributed flow include both mixed flow and slugging. Separated flow contains stratified and annular flow. The most common flow patterns in oil and gas flow is stratified flow and mixed flow with slugging (Lu et al. 2006). This is confirmed by OLGA, as annular flow was never observed throughout this thesis. Pure mixed flow may be observed, but when a leak is present, slugging will most probably occur. Also, an observer trying to mimic a model with a pure mixed flow pattern is likely to adopt slugging.

OLGA calculate the dominant flow regime for every section alone, and mostly independent of the flow regime in neighboring sections. When slugging is appointed to one section, OLGA applies an averaged slug flow. The slug flow is assumed to be infinitely many identical slug cells, and mass flow is averaged. This means flow

out of the section will be the average flow, and for the neighboring section, is hardly distinguishable from mixed flow.

While mixed flow and slugging is closely related, transitions between mixed/slug flow and stratified flow, however, is less common. In addition to being hard to separate from slugging, pure mixed flow only appear at high flow rates, which again leads to high friction. Considering the restriction in friction by (2.8), simulations will be limited to stratified flow and a mix between mixed and slug flow. This latter mix will be denoted as mixed flow only, but in some cases slugging might be dominant both in the model and the observer.

While the flow through the pipeline is averaged in slug flow, the leakage seems to be dependent on slug bubbles. When slugging occur, small ripples occur on gas leakage. These are relatively small compared to leakage magnitude in total, and does not seem to affect boundaries.

3.4 Modeling the leak

Recall the leak-equations (2.87)-(2.89). The leak is modeled as two leaks, one for each phase, but at the exact same position. The magnitude of leakage will be distributed over two segments depending on the estimated position of the leak. The segments at which the leak is distributed are the two closest to estimated leak position. Their positions are x_1 and x_2, where $x_1 < x_2$.

OLGA has an element named "leak", but this feature does not allow the user to specify what phase is leaking, only the leak magnitude. For this reason, a negative source element is used instead. The leak distribution from (Hauge 2007) is adopted, slightly modified to account for two phases. Distribution among the two neighboring sections is

$$\begin{bmatrix} f_{G,1} \\ f_{G,2} \\ f_{L,1} \\ f_{L,2} \end{bmatrix} = \begin{bmatrix} G_l^{-1} & 0 \\ 0 & G_l^{-1} \end{bmatrix} \begin{bmatrix} \hat{f}_G \\ \hat{f}_G \\ \hat{f}_L \\ \hat{f}_L \end{bmatrix} \tag{3.5}$$

where

$$G_l = \begin{bmatrix} \Delta x & \Delta x \\ \Delta x + 2l - \frac{l^2}{\Delta x} & \frac{l^2}{\Delta x} \end{bmatrix} \tag{3.6}$$

Δx is the segment length and l is the distance between x_1 and the actual leak position. $f_{G,1}$ and $f_{L,1}$ denote the leakage at x_1 of gas and oil respectively, while $f_{G,2}$ and $f_{L,2}$ correspond to x_2.

For this method to work properly, the pipe must be divided into sufficiently small segments. It is argued in (Hauge 2007) that segment-length under a certain constant Δx_s will only marginally change convergence properties, and this segment-length suffice.

Pressure at the leak position has to be estimated, and this is done in a similar way as distributing the leakage. This pressure is used in the density-model to generate ρ_l as well, together with volumetric fraction. By assuming constant spatial derivative of pressure in segments, one can set up the following equations,

$$\frac{\Delta \hat{p}}{\Delta x} = \frac{p_2 - p_1}{\Delta x}, \tag{3.7}$$

$$\hat{p_l} = p_1 + l\frac{\Delta \hat{p}}{\Delta x}. \tag{3.8}$$

p_1 and p_2 are pressures at x_1 and x_2 respectively, while p_l is pressure at the leak position. Fraction can be found using the same method, but do not mistake this fraction for ϵ_l which is the leakage fraction.

3.5 Restarting simulations

In section 2.5, it was pointed out that adaption beyond the point in time when the fraction-wave reaches outlet, would diverge. The fraction-waves in question is the one generated from the occurrence of a leak, illustrated in Figure 2.7. This fraction wave travel at a speed relative to phase velocities, and can be expected to have velocity equal to one of the eigenvalues of the system. It was previously mentioned that the largest of these eigenvalues has a value in the range of gas and oil velocity. Based on an estimate of its velocity, the observer and model will be reset before the fraction wave is expected to reach outlet. Consider the following inequality,

$$max(\bar{u}_G, \bar{u}_L)(t_r - t) < L - \hat{x}_l \tag{3.9}$$

where t_r is the time of the previous reset. $\bar{u}_G$ and $\bar{u}_L$ are phase velocities averaged over a time window. The window will be set as the last minute before time t. Any time the inequality is not valid, all variables will be reset to pre-leak values, but leak parameters will be kept. t_r is set to t again. Figures where the values are reset illustrate this with vertical lines, but it will be mentioned when this happens.

Note this is by no means a perfect condition for when to restart the simulations, but in most cases it gives a satisfactory window of convergence. The observer will be vulnerable when $\hat{x}_l$ is too small, as the observer will not expect a fraction-wave at outlet until it is too late. If this error is large, the estimates may fluctuate enough for the total adaption within the time-window to diverge. In that case, adaption will not converge independent of how many times the dataset is used to adapt onto.

3.6 Observer tuning

Note that adaption coefficients are both lower and upper bounded. If adaption is faster than the pressure wave response leak parameters generate, it will oscillate or diverge. If adaption is slower than the fraction wave it will also diverge.

Tuning of the observers was done by a heuristic method, but with theory in mind. Remember how leak position did not affect the steady state flow rates at outlet. Leak magnitude, or c_v in this case, should then be identifiable independent of leak position adaption. This is, of course, only true the interval before the previously described fraction-wave reaches outlet. The transient response within this time interval, however, will be different. Too aggressive tuning will make the magnitude drift too far away until response is settled, and cause oscillation. During tuning, ignoring adaption of position, coefficients κ_{u_G} and κ_{u_L} are set such that quantification is stable within a few minutes. This is done, basically, by setting a low value on the two coefficients, and increasing until oscillations occur, and then lower them slightly.

When correct quantification is found, the position can obtain its correct value. Tuning of κ_{x_G} and κ_{x_L} is done similar, by setting low values initially, and increasing them until adaption on $\hat{x}_l$ start oscillating. At this point, they are lowered slightly. In this thesis, κ_{u_G} is kept equal to κ_{u_L}, and κ_{x_G} equal to κ_{x_L}.

3.7 Computing measures of performance

In order to express adaption performance with values, consider the following definitions. These measures are almost identical to those found in (Hauge 2007), and when using the same parameters, can be compared directly.

3.7.1 Observer error

Observer error is described using the $\mathbb{L}_2$-norm through the pipeline. The error of an arbitrary variable v will be denoted $e(v,t)$ and expressed through

$$e(v,t) = \left[\sum_{i=2}^{N-1} \|v_i(t) - \hat{v}_i(t)\|^2\right]^{\frac{1}{2}}, \qquad t \in (0,t) \tag{3.10}$$

where i denote one of N segments of the pipeline. As the first and last segment of the OLGA pipeline is partitioned into four sections, and no measurement is available at the center, the first and last segment is left out of this measure.

3.7.2 Leak adaption time

As a measure of how close the adapted leak position is to the actual value, consider

$$\Phi(t) = \frac{1}{T}\int_{T}^{t-T} |\hat{x}_l(\tau) - x_l|\, d\tau \tag{3.11}$$

which is the average position deviation in a window in time of duration T. Now let $t \in [t_m, t_{end}]$ be the longest interval where the inequality

$$\Phi(t) < M \tag{3.12}$$

is valid, where t_{end} is the end of simulation. The time between a leak occurs and t_m will be denoted t_c, and used as a measure of performance in terms of convergence. Note that t_c might not exist if the adaption do not converge to the correct values. This is indicated with the value -1. M will be set to 300 in this thesis.

3.7.3 Average deviation

Leak position and leakage magnitude will be averaged as

$$\bar{v} = \int_{t_l}^{t_{end}} v(\tau) - \hat{v}(\tau) d\tau \tag{3.13}$$

where v is either x_l, f_G or f_L and t_l is the time when the leak occur.

Chapter 4

Results

This chapter presents the main results of simulations conducted throughout the course of this thesis. All results come from simulations of two-phase oil and gas flow in the fluid simulator OLGA. Performance in terms of convergence is inspected at first. Afterward, the observer presented is run with data produced by an OLGA model of a straight pipeline. Many different scenarios are tested, and the results will be discussed in the following chapter.

4.1 Convergence

In this section, performance of the observer will be investigated in terms of convergence. Through several simulations it will be tested with and without output injection both for mixed flow and for stratified flow.

An OLGA model is run at steady state, first with a mixed flow pattern. Boundary conditions are given in Table 4.1. Remember that mixed flow, in this case, may include averaged slug flow in some or all sections. Even if the model only had the pure mixed flow pattern, the observer would likely include slugging at some point. Read more on this in Section 3.3. Pipe properties are listed in Table B.1.

Table 4.1: OLGA model boundary conditions - Mixed flow

Property	*Value*
Inlet flow rate gas	20 kg/s
Inlet flow rate oil	375 kg/s
Outlet pressure	50 bar

The observer is run three times with an initial steady state where inflow of gas and oil rate 50% higher than the model. Also, outlet pressure is 5% higher than that of the model. During the first simulation, boundary conditions are set equal to those of

the model, i.e. no output injection is employed. The second time, output injection is employed at the inlet through boundary condition (2.97). Finally, the observer is run with output injection at both ends, employing (2.98) at outlet. Figure 4.1 show the $\mathbb{L}_2$-norm of observer error for the three cases.

For a real pipeline, boundaries will vary with production, and fast convergence is vital for adaption to work. If convergence is slow, the observer error will corrupt adaption. In addition, sudden changes may be mistaken for a leak. In section 2.5 it was pointed out how leak adaption is restricted in time, and it follows that convergence during the first few minutes is of most importance. Therefore, Figure 4.2 show the same $\mathbb{L}_2$-norm for the first 10 minutes only.

Another steady state mixed flow example was tested, with twice the flow rate of the first. The aim was to obtain pure mixed flow, which should be present at high flow rates (Liu et al. 2008). The result was that the boundary conditions diverged, and OLGA aborted the simulations. This is probably connected with the high friction force at these velocities, and the restriction (2.8), as mentioned in Section 2.4.8.

Next, the same pipeline model is simulated at steady state with stratified flow pattern. This is achieved lowering flow rates, and simulation-parameters are given by Table 4.2. As for the previous case, $\mathbb{L}_2$-norms are plotted in Figure 4.3, with the first 10 minutes repeated in Figure 4.4.

Table 4.2: OLGA model boundary conditions - Stratified flow

Property	*Value*
Inlet flow rate gas	5 kg/s
Inlet flow rate oil	91 kg/s
Outlet pressure	50 bar

When adapting to a real pipeline, it will probably not be in steady state as above, but a change might be followed by another change soon after. The mixed flow case above is run with a pulse-like oil flow rate at inlet as plotted in Figure 4.5. The observer is run again, three times, with the resulting $\mathbb{L}_2$-norms plotted in Figure 4.6.

Comment Remember how it was pointed out in the previous section that pressure-waves are used for adaption, and thus convergence in terms of pressure is of greater importance than other variables.

4.2 Leak adaption

In this section, the observer presented will be tested in many different scenarios, with focus on adaption of leak parameters. Performance will be presented as graphs and

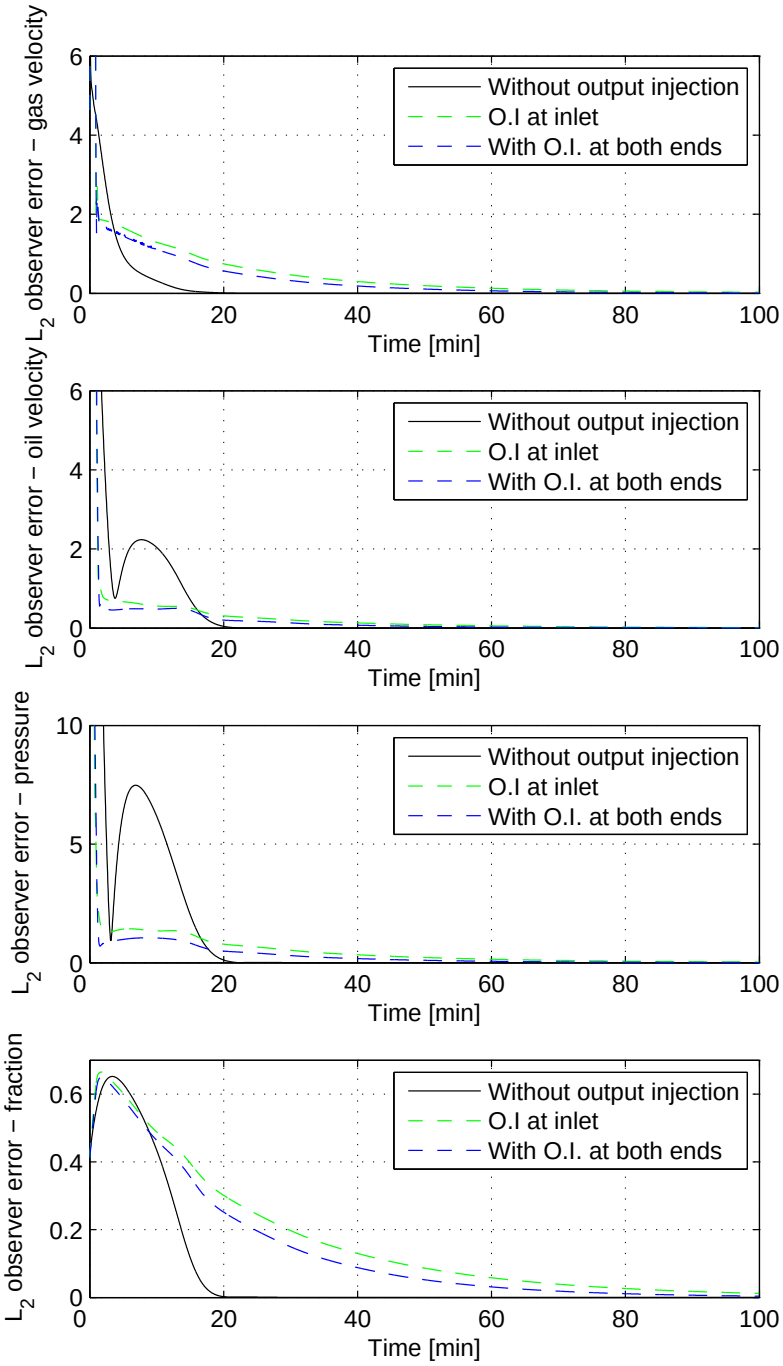

Figure 4.1: $\mathbb{L}_2$-norm of observer error in mixed flow. Black graphs show $\mathbb{L}_2$-norm of observer error without output injection. Green graphs show error when output injection is employed at inlet only, while the blue graphs show error when output injection is employed at both inlet and outlet.

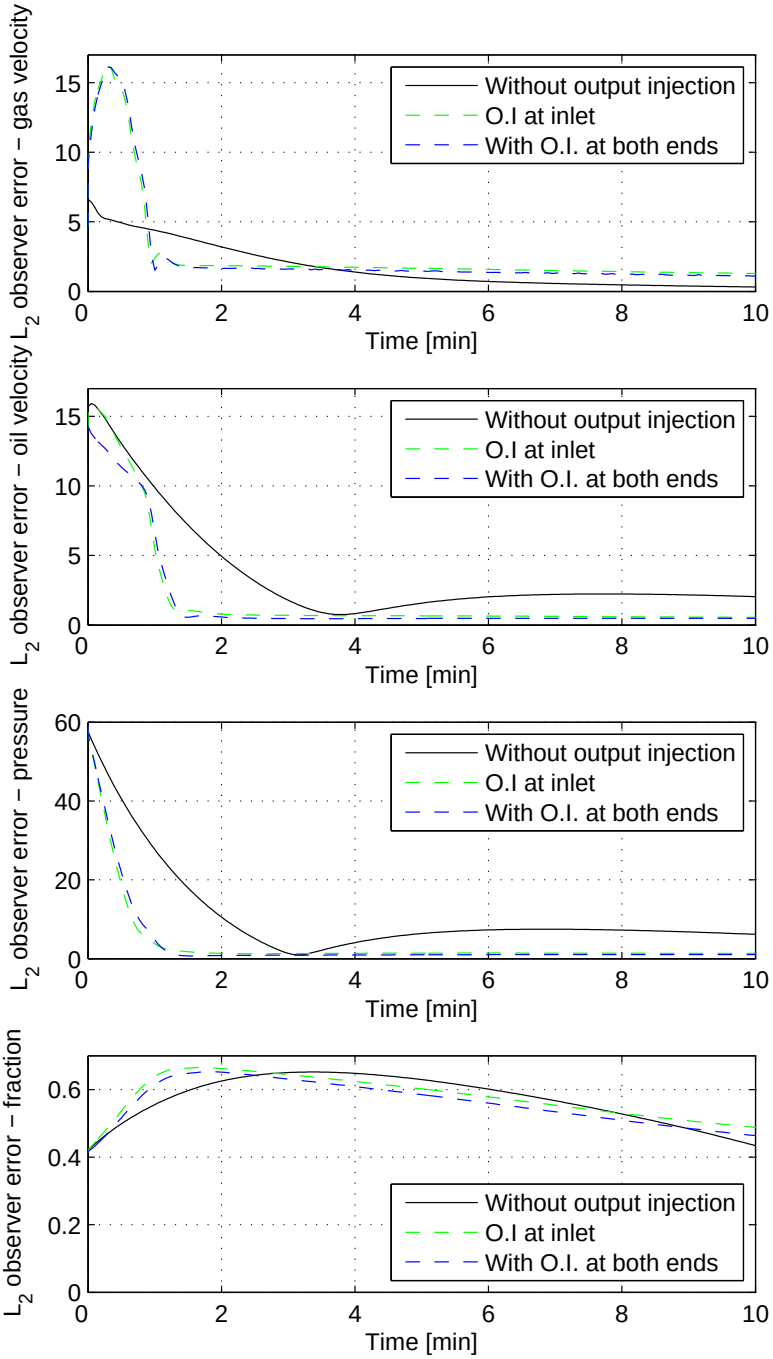

Figure 4.2: $\mathbb{L}_2$-norm of observer error in mixed flow during first 10 minutes only. Black graphs show $\mathbb{L}_2$-norm of observer error without output injection. Green graphs show error when output injection is employed at inlet, while the blue graphs show error when output injection is employed at both inlet and outlet.

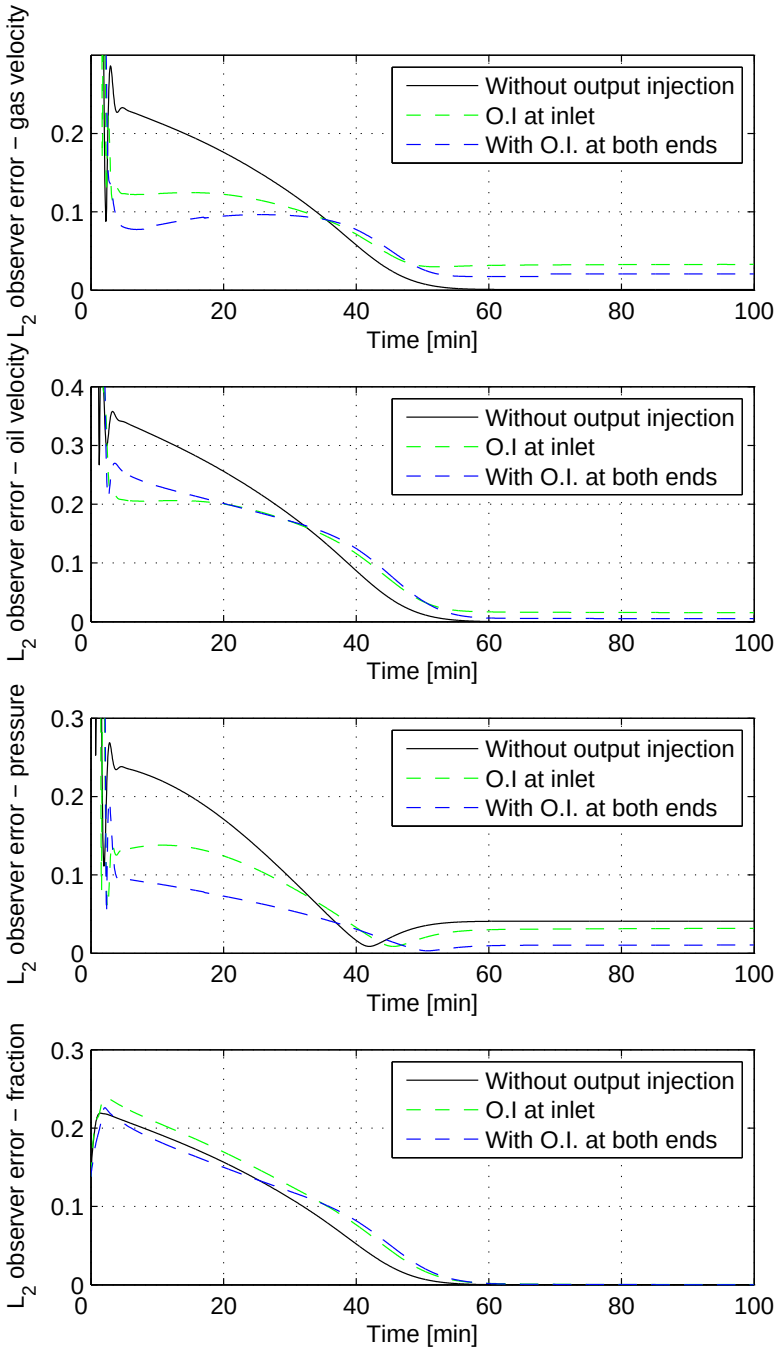

Figure 4.3: $\mathbb{L}_2$-norm of observer error in stratified flow. Black graphs show $\mathbb{L}_2$-norm of observer with no output injection. Green graphs show error when output injection is employed at inlet only, while the blue graphs show error when output injection is employed at both inlet and outlet.

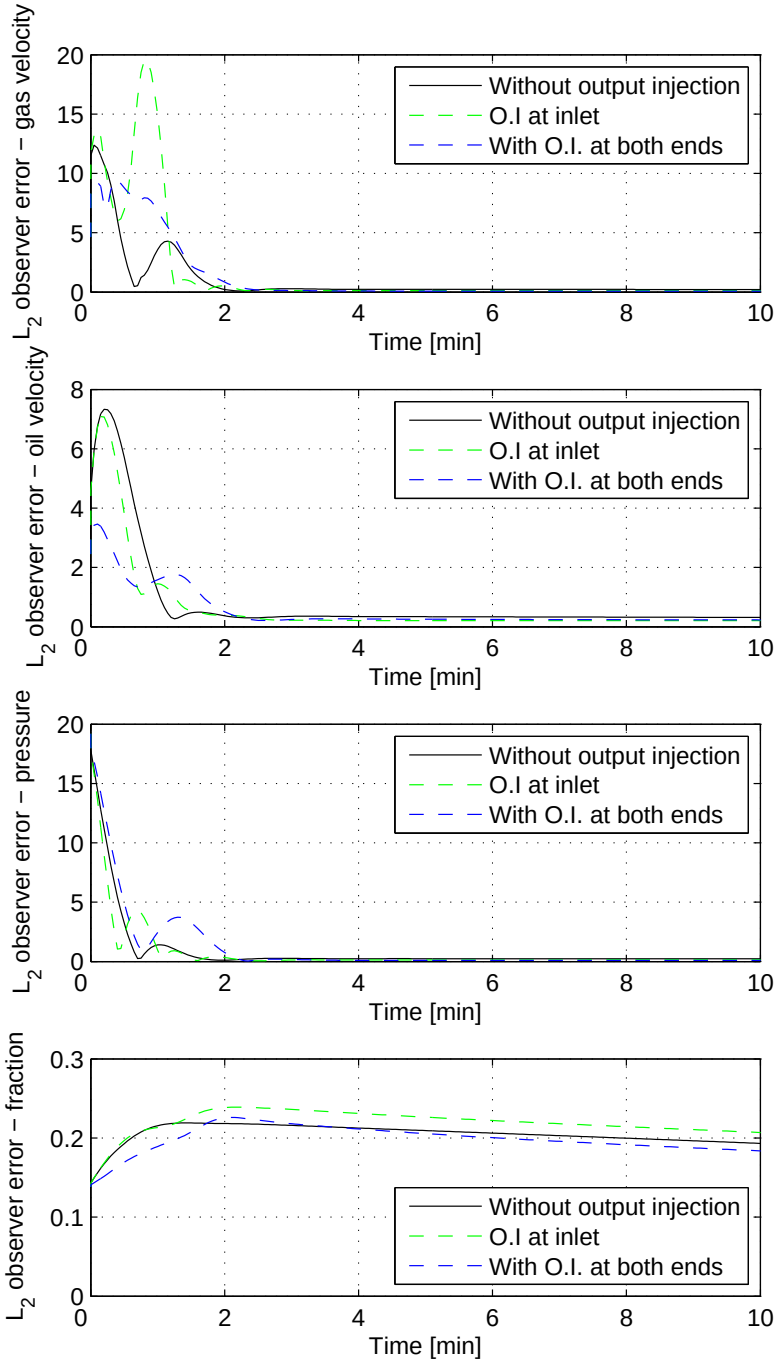

Figure 4.4: $\mathbb{L}_2$-norm of observer error in stratified flow during first 10 minutes only. Black graphs show $\mathbb{L}_2$-norm of observer with no output injection. Green graphs show error when output injection is employed at inlet only, while the blue graphs show error when output injection is employed at both inlet and outlet.

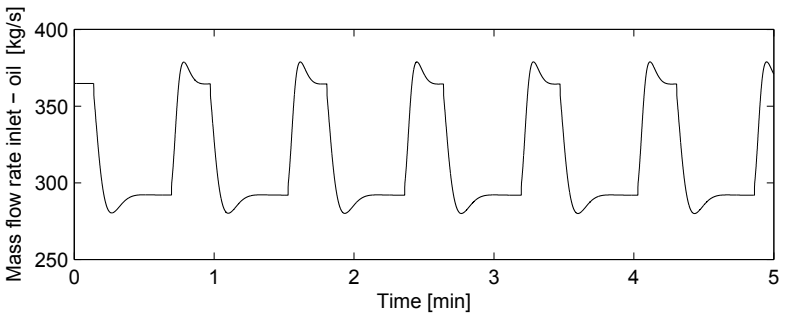

Figure 4.5: Oil mass flow at inlet.

in terms of the measures given in the previous chapter. The section is divided into subsections, where each subsection concerns one subject. A discussion of the results will follow in the next chapter. Based on results in the previous section, where output injection at both ends proved to give better convergence, it is employed at both inlet and outlet in all simulations unless stated otherwise.

4.2.1 Steady flow and perfect leakage fraction estimate

First, a simple case is considered, with the intention to compare adaption performance with and without output injection. The case include a nominal model with stratified flow, perfect measurements, and ϵ_l known prior to the leak. Model parameters and observer parameters are listed in Table 4.2 and Table B.6 respectively. Leak parameters are listed in Table 4.3. Note that the leakage is constant, and not relative to pressure at the point of the leak. The observer is run twice, once with output injection and once without. Both cases are plotted in Figure 4.7. A summary of the performance is listed in Table 4.4.

Table 4.3: Leak parameters - Leakage relative to pre-leak flow rate

Property	*Value*
Leak position	1650m
Leakage gas	20%
Leakage oil	20%

Next, a similar case in a mixed flow regime is considered. The leak is placed at 2250m in the same pipeline as above, and model boundary conditions are given by Table 4.1. Observer coefficients equal those in the previous case, and the result is plotted in Figure 4.8. Values of performance are listed in Table 4.4.

Notice that in this case, the Matlab script reset simulation before it expect the previously described fraction wave to reach outlet. Several times both the model and observer is reset to the states when the leak was detected. In these simulations,

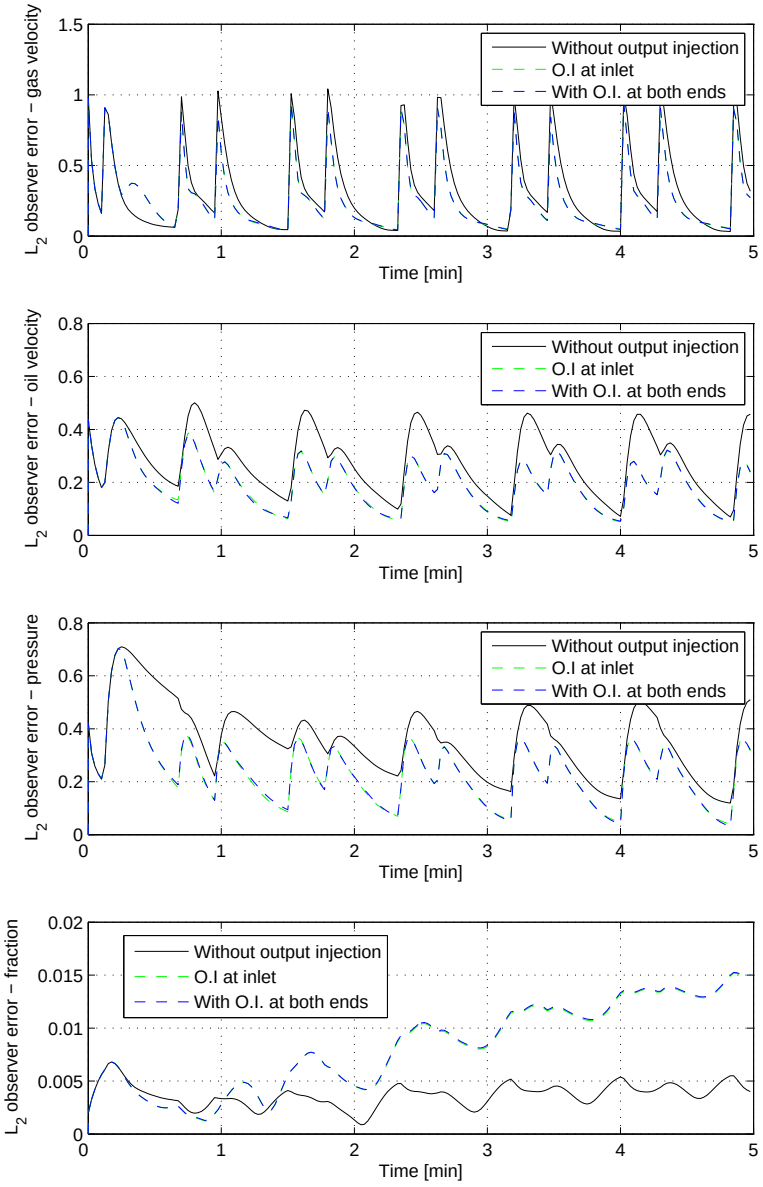

Figure 4.6: $\mathbb{L}_2$-norm of observer error with pulse flow at inlet. Black graphs show $\mathbb{L}_2$-norm of observer with no output injection. Green graphs show error when output injection is employed at inlet only, while the blue graphs show error when output injection is employed at both inlet and outlet.

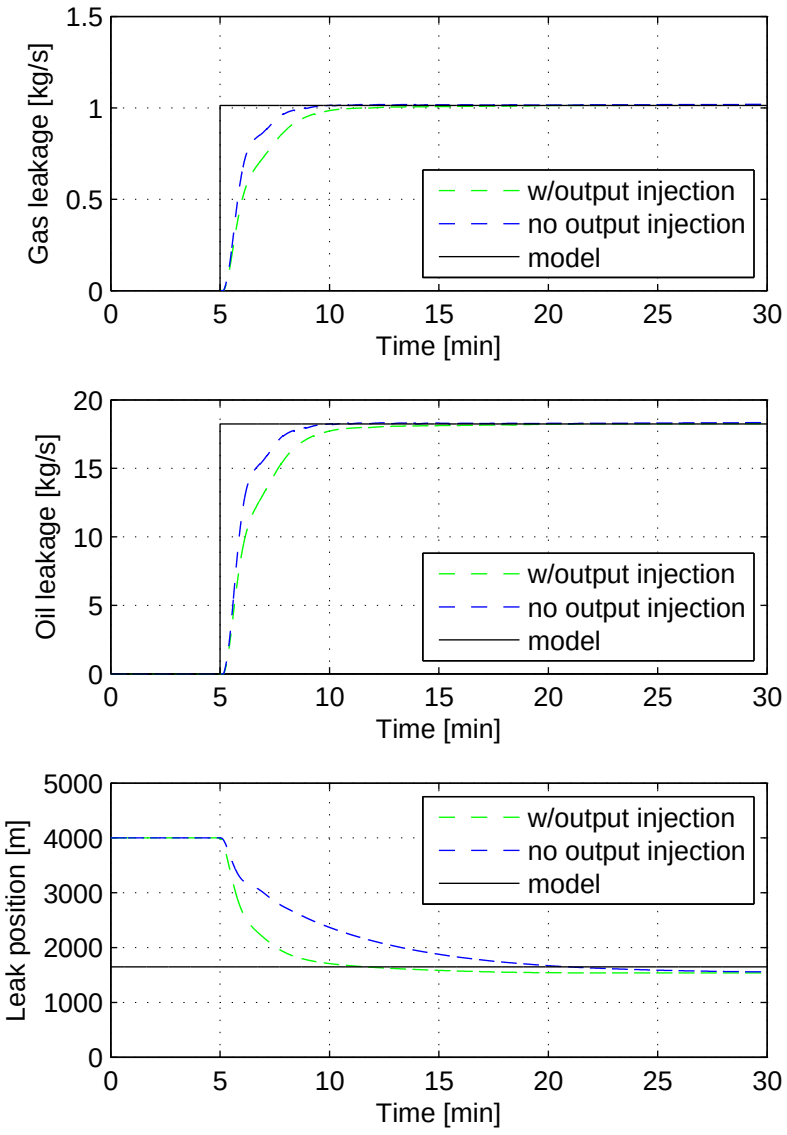

Figure 4.7: Leak adaption in stratified flow with a leak at 1650m.

a reset was programmed every seven minutes instead of using the formula 3.9. In the figure, a reset is indicated by stippled horizontal lines. Boundary values for the state vector $\bar{w}$ is plotted in Figure 4.9. The left column show inlet values, while the right column show values at outlet. Also in this figure, restarts are indicated with horizontal lines.

Table 4.4: Summary of leak adaption

		Measure			
		t_c[min]	$\bar{x}_l$[m]	$\bar{f}_G$[kg/s]	$\bar{f}_L$[kg/s]
Stratified flow	With Output Injection	2.4	-56.5	0.065	1.17
	Without Output Injection	7	-345	0.042	0.75
Mixed flow	With Output Injection	5.5	175	0.32	5.78
	Without Output Injection	6.4	319	0.56	10.1

Output injection has proved to give increased performance, and from now on, is employed in every simulation. A set of simulations will follow, where the observers stability will be tested. A single observer with a fixed set of coefficients will be tested on a range of different leaks, including all flow regimes. The observer parameters are listed in Table B.7.

First, the observer is tested in stratified flow, with model boundary conditions equal to the previous stratified cases. The leak object in OLGA is used, modeling the leakage. This model depend on both internal variables and flow regime, while the observer leak model is still unchanged. In the model, leakage magnitude, leakage fraction and leak position are varied. The results from adapting leak parameters are listed in Table 4.5.

The same observer is now run on the same model, only with a mixed flow pattern. For model inlet and outlet conditions, again, see Table 4.1. Model leak parameters are varied as for stratified flow, and the resulting adaption performance is listed in Table 4.6.

4.2.2 Leakage fraction unknown

The two models from above are now considered again, but now with wrong estimates of ϵ_l. Four different values are used, $\hat{\epsilon}_l = \langle 0.02, 0.1, 0.5, 0.95 \rangle$. The real value is $\epsilon_l = 0.0526$, and was set constant by using two negative source elements instead of a leak element in the OLGA pipeline. First consider the model from Table 4.2, the stratified flow case. Observer coefficients are unchanged, and is listed in Table

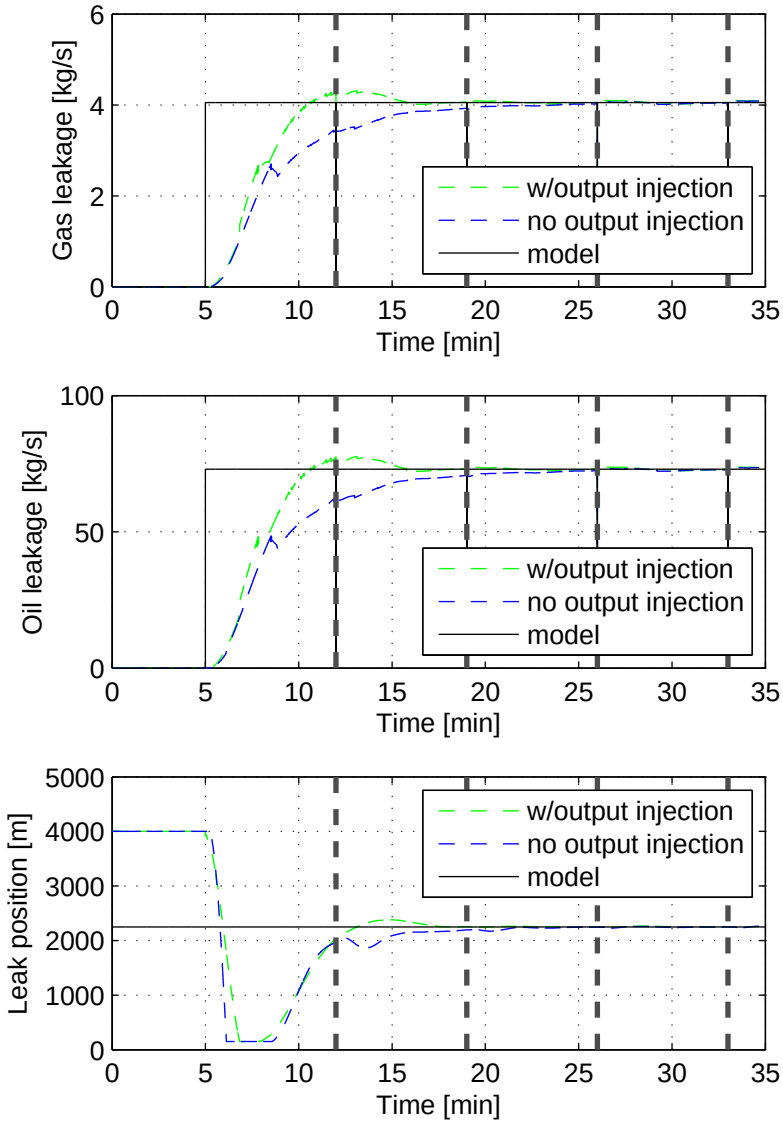

Figure 4.8: Leak adaption in mixed flow with a leak at 2250m. The horizontal stippled lines indicate a restart of observer and model states, while leak parameters are kept.

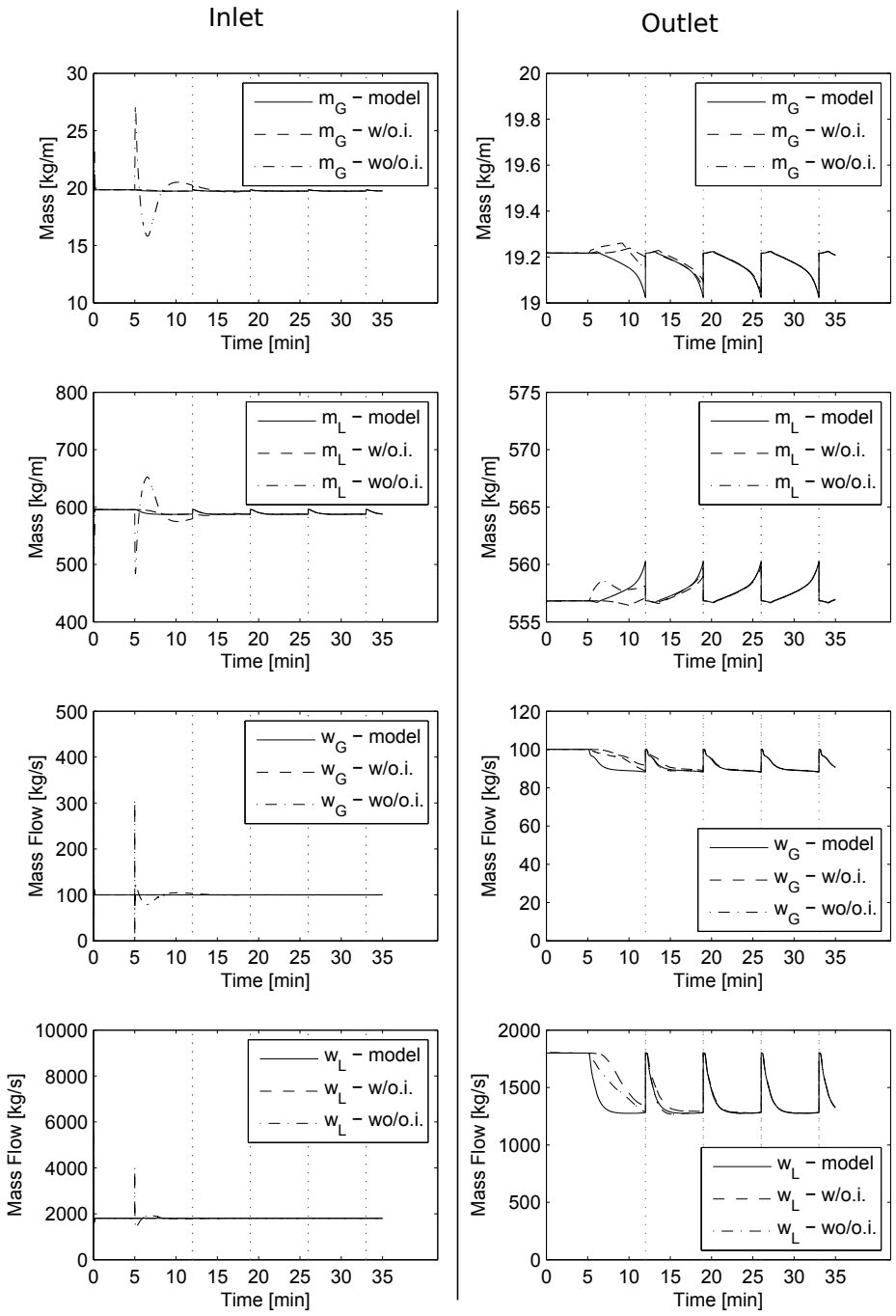

Figure 4.9: Boundary values when adapting a leak in a mixed flow regime. Horizontal stippled lines indicate that model and observer is reset. Left column correspond to inlet values, while the right column show outlet values.

Table 4.5: Summary of leak adaption with different leak parameters in a stratified flow regime.

		Stratified Flow			
Leak size	Measure	Leak position 950m	1950m	2950m	3950m
$f_G \approx 2\%$ $f_L \approx 7\%$	t_c[min]	14.2	-1	-1	-1
	$\bar{x}_l$[m]	-489	-44.6	436	943
	$\bar{f}_G$[kg/s]	0.0222	0.0144	0.00723	0.000247
	$\bar{f}_L$[kg/s]	1.29	0.839	0.423	0.0158
$f_G \approx 11\%$ $f_L \approx 33\%$	t_c[min]	2.8	6.1	9	10.6
	$\bar{x}_l$[m]	59.1	165	292	438
	$\bar{f}_G$[kg/s]	0.0281	0.0188	0.00983	0.000138
	$\bar{f}_L$[kg/s]	1.53	1.04	0.563	0.0443
$f_G \approx 25\%$ $f_L \approx 63\%$	t_c[min]	2.3	3.7	4.7	21.8
	$\bar{x}_l$[m]	-63.4	2.96	74.1	69.6
	$\bar{f}_G$[kg/s]	0.0224	0.0128	0.0016	-0.0137
	$\bar{f}_L$[kg/s]	1.18	0.76	0.245	-0.463
$f_G \approx 40\%$ $f_L \approx 85\%$	t_c[min]	13.4	19.8	15.9	NA
	$\bar{x}_l$[m]	-357	359	-199	NA
	$\bar{f}_G$[kg/s]	-0.0104	0.5	-0.0313	NA
	$\bar{f}_L$[kg/s]	-0.108	19.2	-0.773	NA

Table 4.6: Summary of leak adaption with different leak parameters.

		Mixed Flow			
Leak size	Measure	Leak position 950m	1950m	2950m	3950m
$f_G \approx 4.2\%$ $f_L \approx 7.2\%$	t_c[min]	21	9.5	8.3	8.1
	$\bar{x}_l$[m]	448	230	210	272
	$\bar{f}_G$[kg/s]	0.15	0.0675	0.0505	0.0307
	$\bar{f}_L$[kg/s]	4.56	2.04	1.51	0.911
$f_G \approx 17\%$ $f_L \approx 27\%$	t_c[min]	17.3	6.4	5.6	4.9
	$\bar{x}_l$[m]	327	241	204	180
	$\bar{f}_G$[kg/s]	0.394	0.241	0.18	0.153
	$\bar{f}_L$[kg/s]	11.7	7.32	5.5	4.58
$f_G \approx 29\%$ $f_L \approx 45\%$	t_c[min]	11.8	5.4	4.9	4.3
	$\bar{x}_l$[m]	235	201	169	131
	$\bar{f}_G$[kg/s]	0.512	0.339	0.262	0.24
	$\bar{f}_L$[kg/s]	14.5	10.1	7.86	6.93
$f_G \approx 38\%$ $f_L \approx 55\%$	t_c[min]	11.3	4.9	4.7	4.2
	$\bar{x}_l$[m]	194	170	142	106
	$\bar{f}_G$[kg/s]	0.555	0.374	0.304	0.276
	$\bar{f}_L$[kg/s]	15.2	11	9.02	7.77

B.6. Output injection is employed in all simulations, both at inlet and outlet. The resulting leak adaption corresponding to all four values of $\hat{\epsilon}_l$ are plotted in Figure 4.10. Values of performance are listed in Table 4.7.

Next, the same four values are tested for the mixed flow model. Also in this case, the real value is $\epsilon_l = 0.0526$. For model boundary values, see Table 4.1. The results are plotted in Figure 4.11. Values of performance are listed in Table 4.7 together with values from cases with stratified flow.

Table 4.7: Summary of leak adaption with varying fraction. The real fraction is $\epsilon_l = 0.0526$.

		Measure			
		t_c[min]	$\bar{x}_l$[m]	$\bar{f}_G$[kg/s]	$\bar{f}_L$[kg/s]
Mixed flow	$\hat{\epsilon}_l = 0.02$	9.2	218	2.16	-19.9
	$\hat{\epsilon}_l = 0.1$	6.7	250	-1.08	26.7
	$\hat{\epsilon}_l = 0.5$	-	313	-3.62	65.3
	$\hat{\epsilon}_l = 0.95$	-	342	-4.10	72.5
Stratified flow	$\epsilon_l = 0.02$	-	-130	0.51	-6.59
	$\hat{\epsilon}_l = 0.1$	-	20.3	-0.26	6.82
	$\hat{\epsilon}_l = 0.5$	-	158	-0.80	16.42
	$\hat{\epsilon}_l = 0.95$	-	384	-0.82	18.1

Consider now varying ϵ_l, as an OLGA leak element is used to model the leak. A good estimate of fraction in leakage may be the mass flow fraction immediately upstream of the leak position. Especially in mixed flow, this should be a good estimate. In stratified flow, however, fraction is dependent on where the leak is present in a cross section, i.e whether it is on top or on bottom of the pipeline. Still, $\hat{\epsilon}_l$ is set equal to mass fraction of flow inside the pipeline, and the observer is tested on several different leaks in both the mixed and stratified flow case above. The results are listed in Table 4.9 for adaption in stratified flow and Table 4.8 for adaption in mixed flow.

Table 4.8: Summary of leak adaption in mixed flow with different leak parameters. $\epsilon_l \approx 0.033$ while $\hat{\epsilon}_l$ is based on mass flow fraction and equal $\hat{\epsilon}_l \approx 0.05$.

		Mixed Flow			
Leak size		Leak position			
	Measure	950m	1950m	2950m	3950m
$f_G \approx 29\%$ $f_L \approx 45\%$	t_c[min]	18.6	9.4	8.2	4.2
	$\bar{x}_l$[m]	252	264	204	143
	$\bar{f}_G$[kg/s]	-0.3	-0.855	-1.05	-1.11
	$\bar{f}_L$[kg/s]	27.5	29.3	28.8	27.5

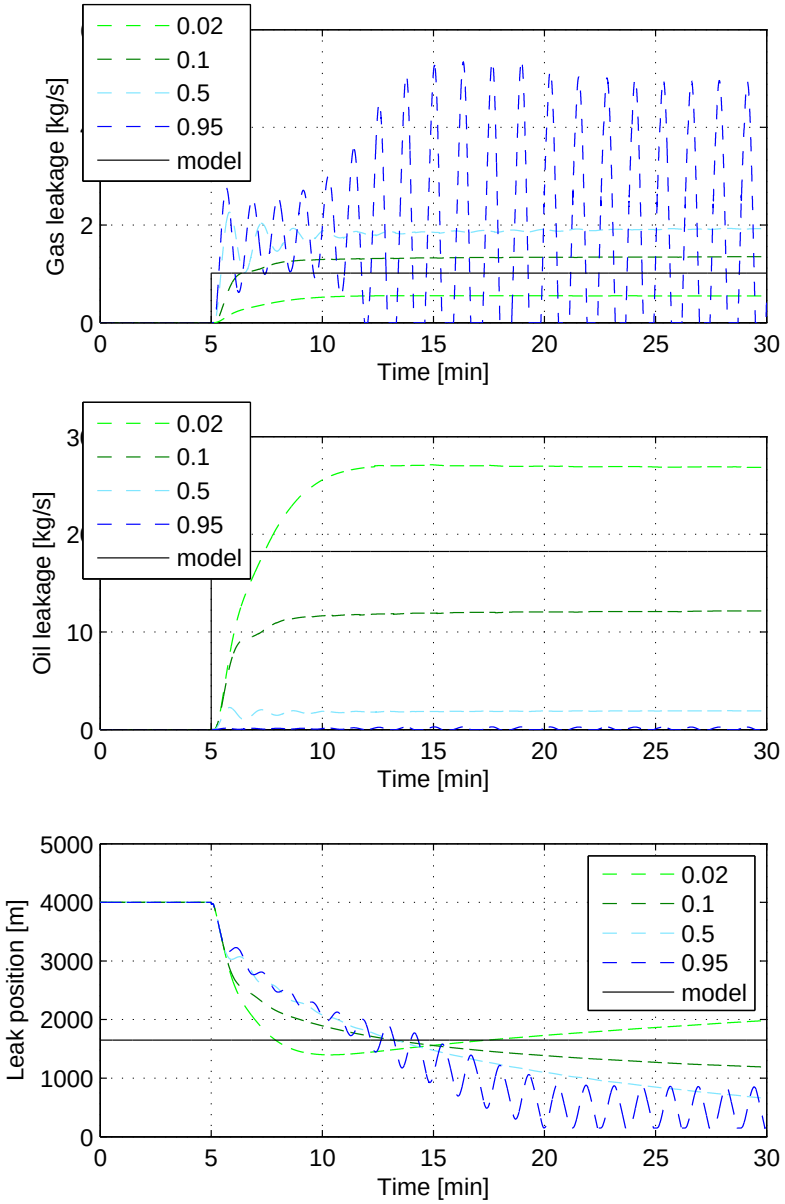

Figure 4.10: Leak adaption with varying guesses of $\hat{\epsilon}_l$ in a stratified flow regime. The real fraction is $\epsilon_l = 0.0526$.

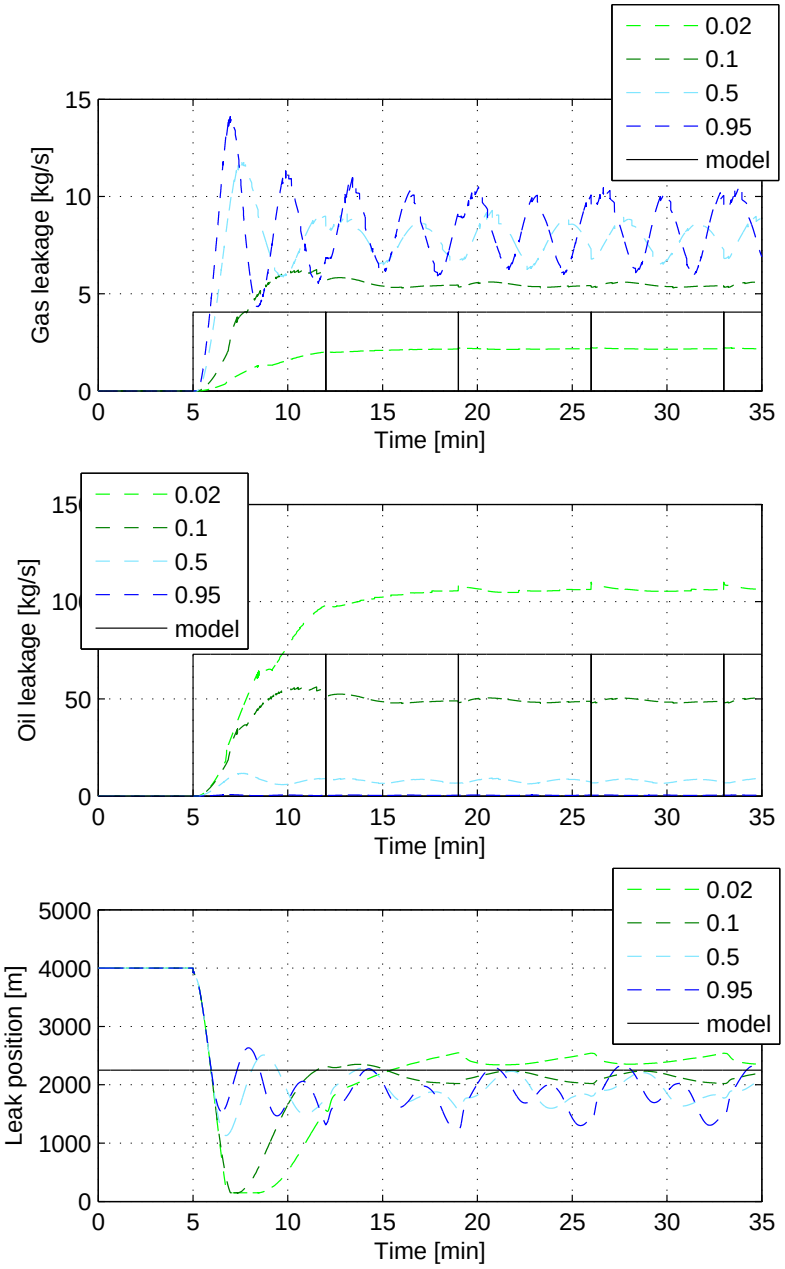

Figure 4.11: Leak adaption with varying guesses of $\hat{\epsilon}_l$ in a mixed flow regime. The real fraction is $\epsilon_l = 0.0526$.

Table 4.9: Summary of leak adaption in stratified flow with different leak parameters. $\epsilon_l \approx 0.028$ while $\hat{\epsilon}_l$ is based on mass flow fraction and equal $\hat{\epsilon}_l \approx 0.05$.

		Stratified Flow		
Leak size	Measure	Leak position 950m	1950m	2950m
$f_G \approx 43\%$ $f_L \approx 83\%$	t_c[min]	10.6	12.5	11.9
	$\bar{x}_l$[m]	-320	26.9	-164
	$\bar{f}_G$[kg/s]	-1.41	-1.3	-1.3
	$\bar{f}_L$[kg/s]	24.3	27	21.2

4.2.3 Varying boundaries

It is not likely that the inflow will stay constant very long. Production changes will cause varying boundaries, hence in this section a few scenarios with sinusoidal inlet flow will be presented. The same OLGA model is used, only with the change in flow rates. The observer parameters are listed in Table B.7.

First, for stratified flow, the inflow rates are given in Figure 4.12. The amplitude of the sinusoids is 20% of the average value except in the case with the higest frequency which has 30% amplitude. Note that there is a 180° phaselag between the sinusoids for gas and oil flow rate. Estimated leak position is plotted in Figure 4.13, and measures of performance in Table 4.10. For plots of leak magnitude, see Figure C.1-C.3 in the appendix.

Next follows the same procedure for mixed flow, with sinusoidal inflow rates at three different frequencies. The case with the highest frequency also has a higher amplitude. The inflow is illustrated in Figure 4.14, and the resulting leak adaption is presented in Figure 4.15. Resulting measures of performance are listed in Table 4.10. Again, adaption of magnitude is found in the appendix, in Figure C.4-C.6.

Table 4.10: Summary of leak adaption performance during scenarios with sinusoidal varying flowrates.

		Measure			
		t_c[min]	$\bar{x}_l$[m]	$\bar{f}_G$[kg/s]	$\bar{f}_L$[kg/s]
Stratified flow	Case 1	-	1060	0.053	0.87
	Case 2	-	692	0.047	0.83
	Case 3	-	1461	0.16	2.86
Mixed flow	Case 4	8.6	106	0.063	1.08
	Case 5	19.9	190	0.073	1.01
	Case 6	-	248	0.021	0.37

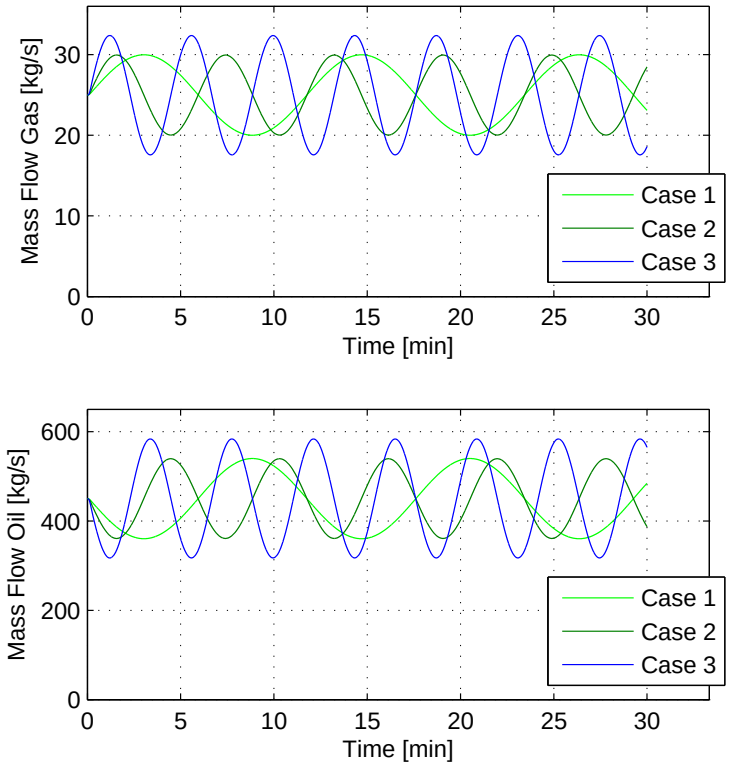

Figure 4.12: Sinusoidal varying inflow for Case 1-3 - Stratified flow

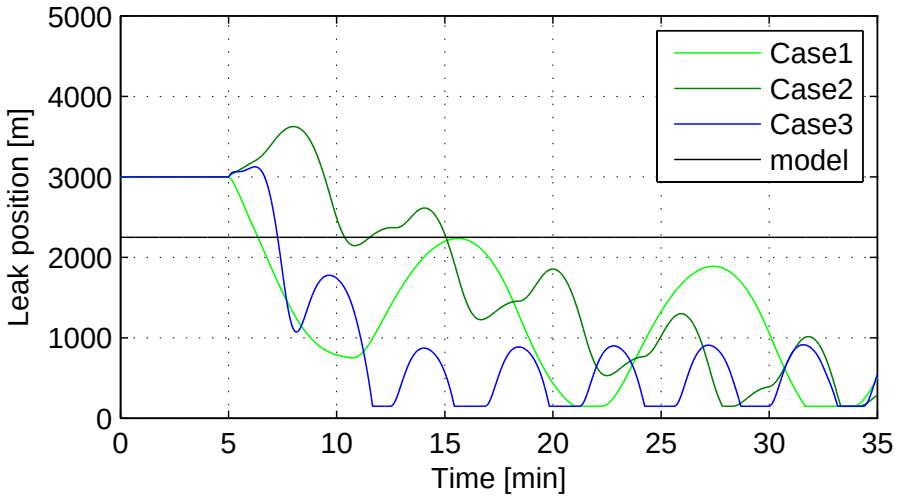

Figure 4.13: Leak adaption in stratified flow with varying boundaries.

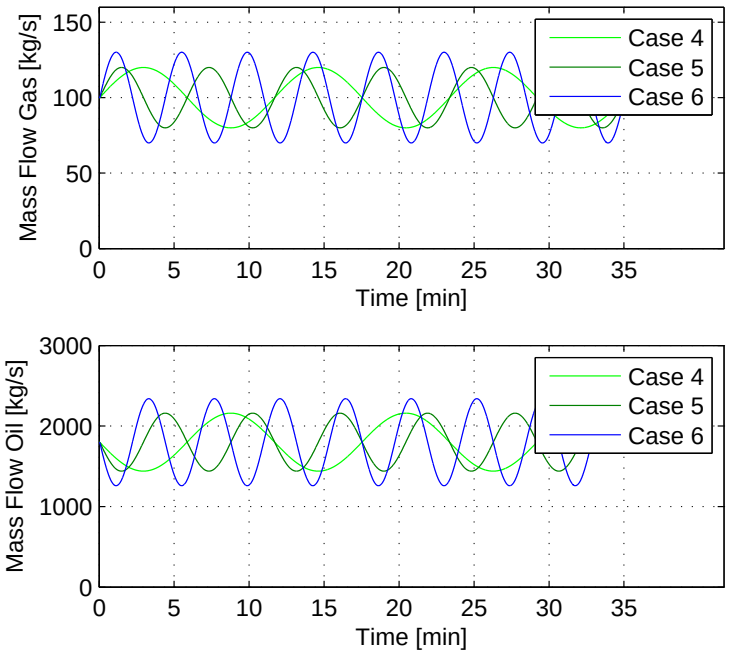

Figure 4.14: Sinusoidal varying inflow for Case 4-6 - Mixed flow

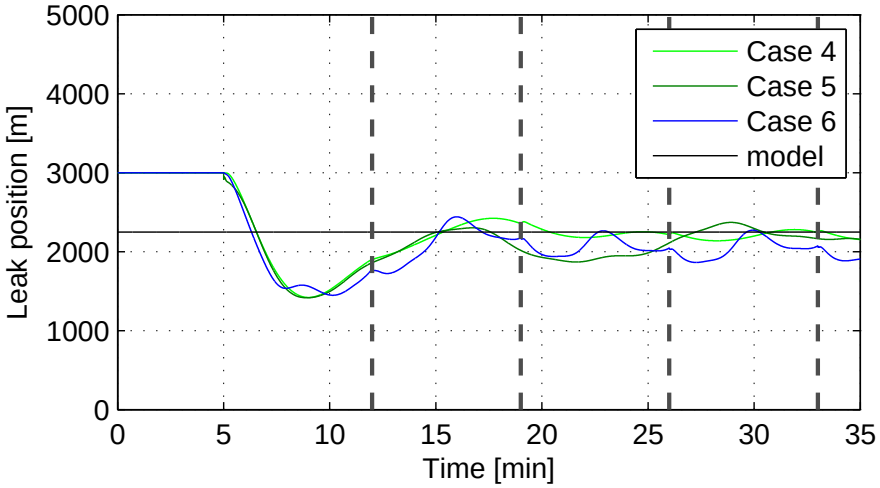

Figure 4.15: Leak adaption in mixed flow with varying boundaries. Horizontal lines indicate a reset of model and observer.

4.2.4 Biased Measurements

Until now, measurements have been perfect. In this section, a wide range of simulations will be conducted, inspecting the effect of biased measurements. There are four measurements, both phase flow rates, pressure and volumetric fraction. These will be inspected in pairs, cross-checking the effect of bias on both flow rates before the same is done with pressure and fraction.

The models will be the same as in previous scenarios, with flow rates given in Table 4.2 and Table 4.1 for stratified and mixed flow respectively. The observer listed in Table B.7 is still used. The bias is present at both inlet and outlet. Perfect estimates of ϵ_l are used.

Four sets of simulations follow. First, flow rates are changed with ±1% or kept constant. The results from all nine simulations for each flow regime are presented in Table 4.11. The left column list bias on gas flow, while the top row show the bias on oil flow. Afterwards, the bias is increased to ±5%, and an identical set of results for the new biases are presented in Table 4.12.

Table 4.11: Summary of leak adaption with minor bias on measurements of flow rates.

		Mixed Flow			Stratified Flow		
Error		Error w_L			Error w_L		
w_g	Measure	-0.01%	0%	+0.01%	-0.01%	0%	+0.01%
-0.01%	t_c[min]	8.5	5.6	5.9	2.8	2.6	2.5
	$\bar{x}_l$[m]	-56	95.2	242	-132	-24	82
	$\bar{f}_G$[kg/s]	0.20	0.18	0.16	0.043	0.040	0.037
	$\bar{f}_L$[kg/s]	3.56	3.18	2.88	0.78	0.73	0.67
0%	t_c[min]	8.4	5.7	5.9	2.6	2.5	2.4
	$\bar{x}_l$[m]	-6	145	282	-63	44	149
	$\bar{f}_G$[kg/s]	0.18	0.164	0.149	0.040	0.037	0.034
	$\bar{f}_L$[kg/s]	3.29	2.96	2.69	0.72	0.67	0.62
+0.01%	t_c[min]	8.4	5.7	6	2.5	2.4	-1
	$\bar{x}_l$[m]	43	188	329	7	110	214
	$\bar{f}_G$[kg/s]	0.17	0.15	0.14	0.037	0.034	0.031
	$\bar{f}_L$[kg/s]	3.06	2.75	2.51	0.66	0.61	0.56

Following the same procedure, similar simulations are conducted only with a bias on measurements of pressure and fraction instead. For the first set of results, pressure bias is ±0.1 bar and fraction bias is ±0.01. The results are presented in Table 4.13. Next, the bias is increased to ±0.2 bar for pressure and ±0.05 for fraction. Results are presented in Table 4.14.

Table 4.12: Summary of leak adaption with large bias on measurements of flow rates.

		Mixed Flow			Stratified Flow		
		Error w_L			Error w_L		
Error w_G	Measure	-0.05%	0%	+0.05%	-0.05%	0%	+0.05%
-0.05%	t_c[min]	-1	-1	-1	-1	-1	2.6
	$\bar{x}_l$[m]	-1031	-117	607	-858	-330	129
	$\bar{f}_G$[kg/s]	0.329	0.223	0.131	0.067	0.049	0.025
	$\bar{f}_L$[kg/s]	5.92	4.01	2.36	1.20	0.88	0.45
0%	t_c[min]	-1	5.7	-1	-1	2.5	-1
	$\bar{x}_l$[m]	-679	145	807	-510	44	540
	$\bar{f}_G$[kg/s]	0.266	0.164	0.118	0.049	0.037	0.020
	$\bar{f}_L$[kg/s]	4.79	2.96	2.12	0.88	0.67	0.36
+0.05%	t_c[min]	-1	-1	-1	8.7	-1	-1
	$\bar{x}_l$[m]	-388	351	966	-239	350	873
	$\bar{f}_G$[kg/s]	0.17	0.10	0.082	0.024	0.018	0.007
	$\bar{f}_L$[kg/s]	3.12	1.77	1.48	0.43	0.32	0.12

Table 4.13: Summary of leak adaption with minor bias on measurements of pressure and volumetric fraction.

		Mixed Flow			Stratified Flow		
		Error p			Error p		
Error ϵ	Measure	-0.1 bar	0	+0.1 bar	-0.1 bar	0	+0.1 bar
-0.01	t_c[min]	8.5	8.4	8.4	2.4	2.4	2.4
	$\bar{x}_l$[m]	-56	-6	42	-18	-21	-55
	$\bar{f}_G$[kg/s]	0.198	0.18	0.17	0.011	0.033	0.052
	$\bar{f}_L$[kg/s]	3.56	3.29	3.06	0.20	0.60	0.94
0	t_c[min]	5.6	5.7	5.7	2.5	2.5	2.5
	$\bar{x}_l$[m]	95	145	188	48	44	42
	$\bar{f}_G$[kg/s]	0.18	0.164	0.15	0.015	0.037	0.060
	$\bar{f}_L$[kg/s]	3.18	2.96	2.75	0.27	0.67	1.07
+0.01	t_c[min]	5.9	5.9	6.0	2.6	2.6	2.6
	$\bar{x}_l$[m]	242	282	329	88	85	79
	$\bar{f}_G$[kg/s]	0.16	0.15	0.14	0.016	0.038	0.060
	$\bar{f}_L$[kg/s]	2.88	2.69	2.51	0.28	0.68	1.08

Table 4.14: Summary of leak adaption with large bias on measurements of pressure and volumetric fraction.

		Mixed Flow			Stratified Flow		
		Error p			Error p		
Error ϵ	Measure	-0.2 bar	0	+0.2 bar	-0.2 bar	0	+0.2 bar
-0.05	t_c[min]	-1	-1	-1	-1	-1	-1
	$\bar{x}_l$[m]	-694	-727	-766	-518	-518	-529
	$\bar{f}_G$[kg/s]	0.12	0.18	0.24	-0.041	0.002	0.047
	$\bar{f}_L$[kg/s]	2.20	3.24	4.29	-0.74	0.04	0.85
0	t_c[min]	5.7	5.7	8.1	2.5	2.5	2.5
	$\bar{x}_l$[m]	165	145	121	53	44	38
	$\bar{f}_G$[kg/s]	0.10	0.164	0.23	-0.007	0.037	0.082
	$\bar{f}_L$[kg/s]	1.80	2.96	4.15	-0.13	0.67	1.48
+0.05	t_c[min]	-1	-1	-1	-1	-1	-1
	$\bar{x}_l$[m]	992	972	951	237	225	212
	$\bar{f}_G$[kg/s]	0.27	0.33	0.39	-0.004	0.041	0.085
	$\bar{f}_L$[kg/s]	4.85	5.89	6.97	-0.06	0.73	1.53

4.2.5 Shutdown

In many cases, when a leak is detected, especially in gas and oil pipelines, flow into the pipeline is halted. A leak identification system should certainly be able to handle such conditions. In this section, such a scenario is simulated, but because of OLGA fluid property file limitations, it is not a complete shutdown. Neither was it possible to reduce flow in stratified flow sufficiently for to simulate such a scenario. Therefore, only mixed flow with slugging is tested in this section.

The inflow rates are illustrated in Figure 4.16 while the outlet pressure is kept constant at 50 bar. Two minutes after the leak occurs, shutdown is initiated, which lasts for one and a half minute. The final flow is then 40% of initial flow. The observer is still unchanged, and listed in Table B.7. Leak parameter estimates are plotted in Figure 4.17. During this simulation, a perfect value of ϵ_l is used. A second simulation where there is a 10% error in $\hat{\epsilon}_l$ is presented in Figure 4.18. Results are summed up in Table 4.15. $\tilde{\epsilon}_l$ denote the error in $\hat{\epsilon}_l$ in percentage of ϵ_l.

In these cases the adaption would converge eventually, but in a real shutdown, adaption would cease when flow was halted. In such a scenario, the only data available would be the first few minutes after leak occurense. Next, a simulation is conducted, reusing the first two minutes before a shutdown is initiated. This will cause adaption to restart every two minutes, but leak parameters are kept. Consider the case from above, including the error in $\hat{\epsilon}_l$. Figure 4.19 show the leak adaption, while values of the state vector $\bar{w}$ is illustrated in Figure C.7 in the appendix. Results are also listed in Table 4.15.

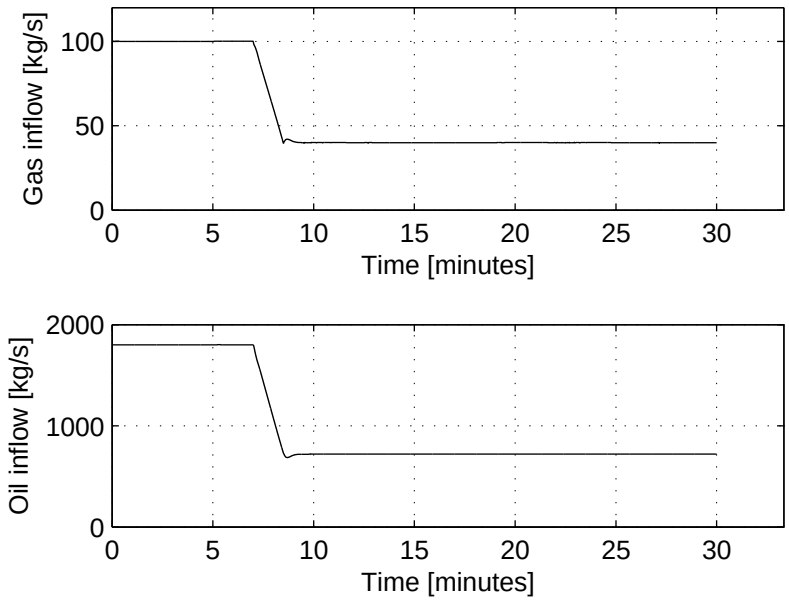

Figure 4.16: Inflow rates of gas and oil during the shutdown scenario.

Table 4.15: Summary of leak performance during shutdown scenario, both for perfect $\hat{\epsilon}_l$ and $\hat{\epsilon}_l$ with a 10% error. Stippled lines indicate estimates while the solid line is real values.

	Scenario		
Measure	$\tilde{\epsilon}_l = 0$	$\tilde{\epsilon}_l = 10\%$	$\tilde{\epsilon}_l = 10\%$ w/restarts
t_c[min]	11.6	-	8
$\bar{x}_l$[m]	120	378	290
$\bar{f}_G$[kg/s]	0.149	0.036	0.12
$\bar{f}_L$[kg/s]	4.99	8.09	10.46

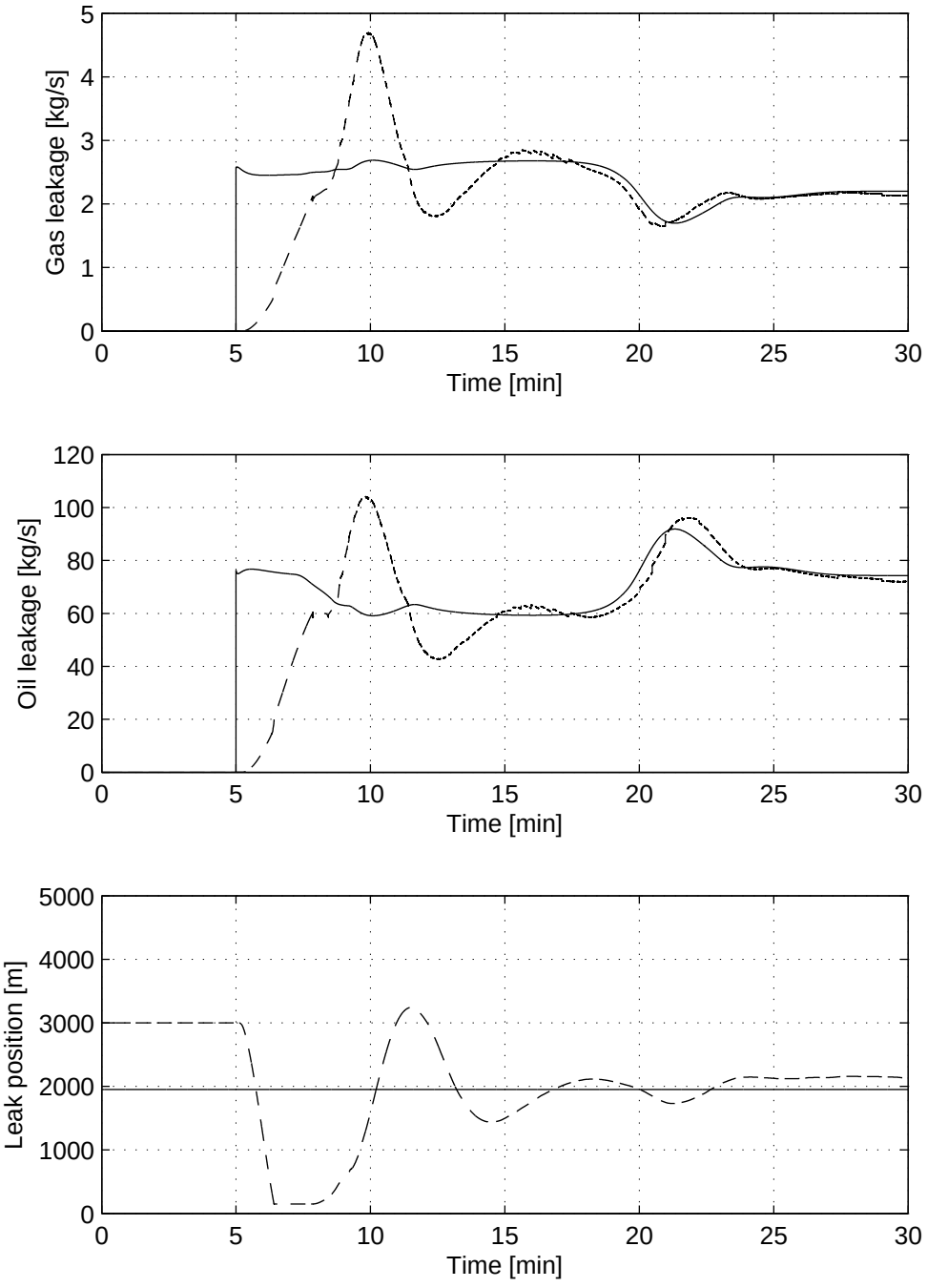

Figure 4.17: Estimates of leak parameters during the shutdown scenario. ϵ_l is known. Stippled lines indicate estimates while the solid line is real values.

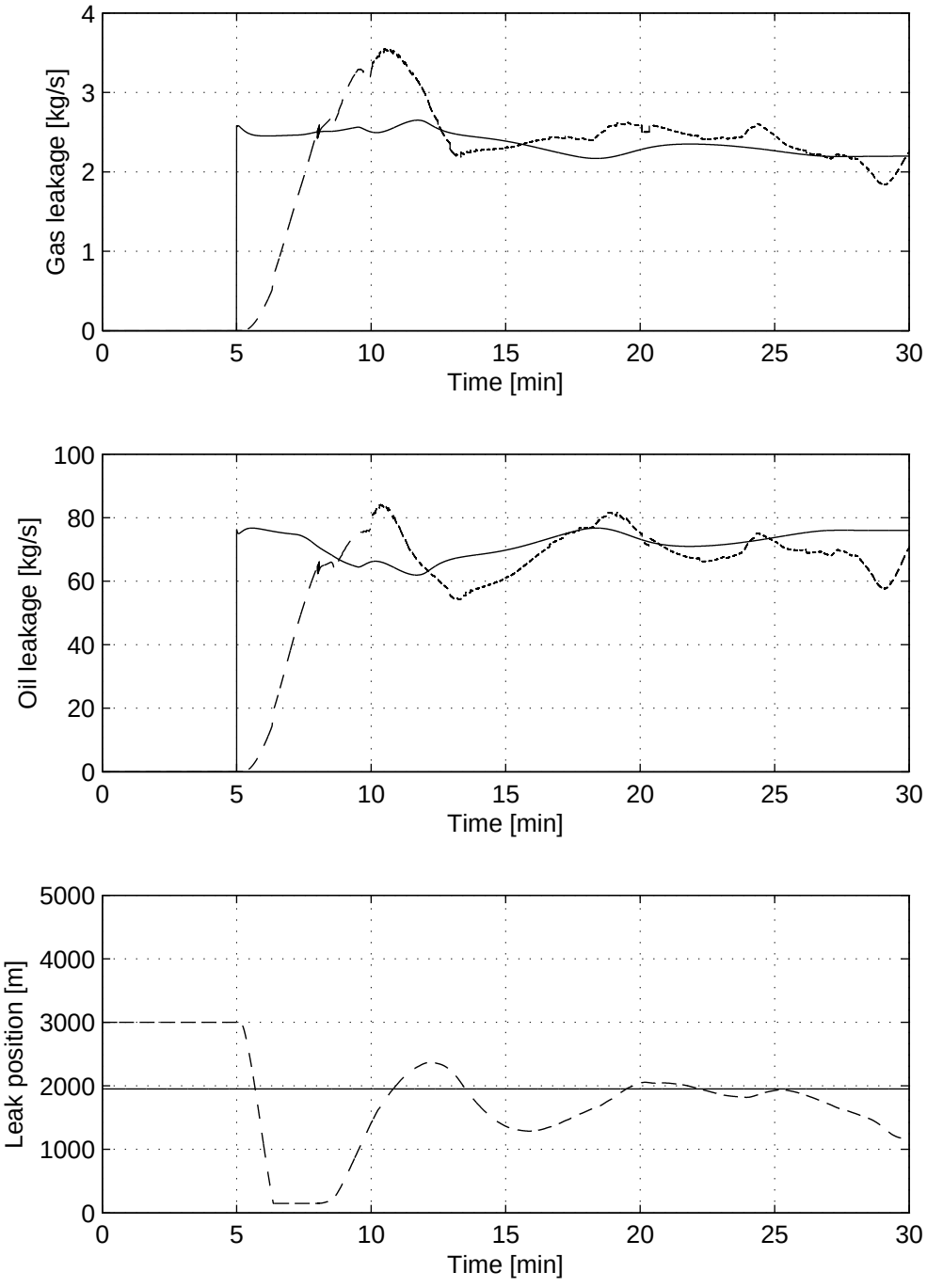

Figure 4.18: Estimates of leak parameters during the shutdown scenario. $\hat{\epsilon}_l$ is 10% off.

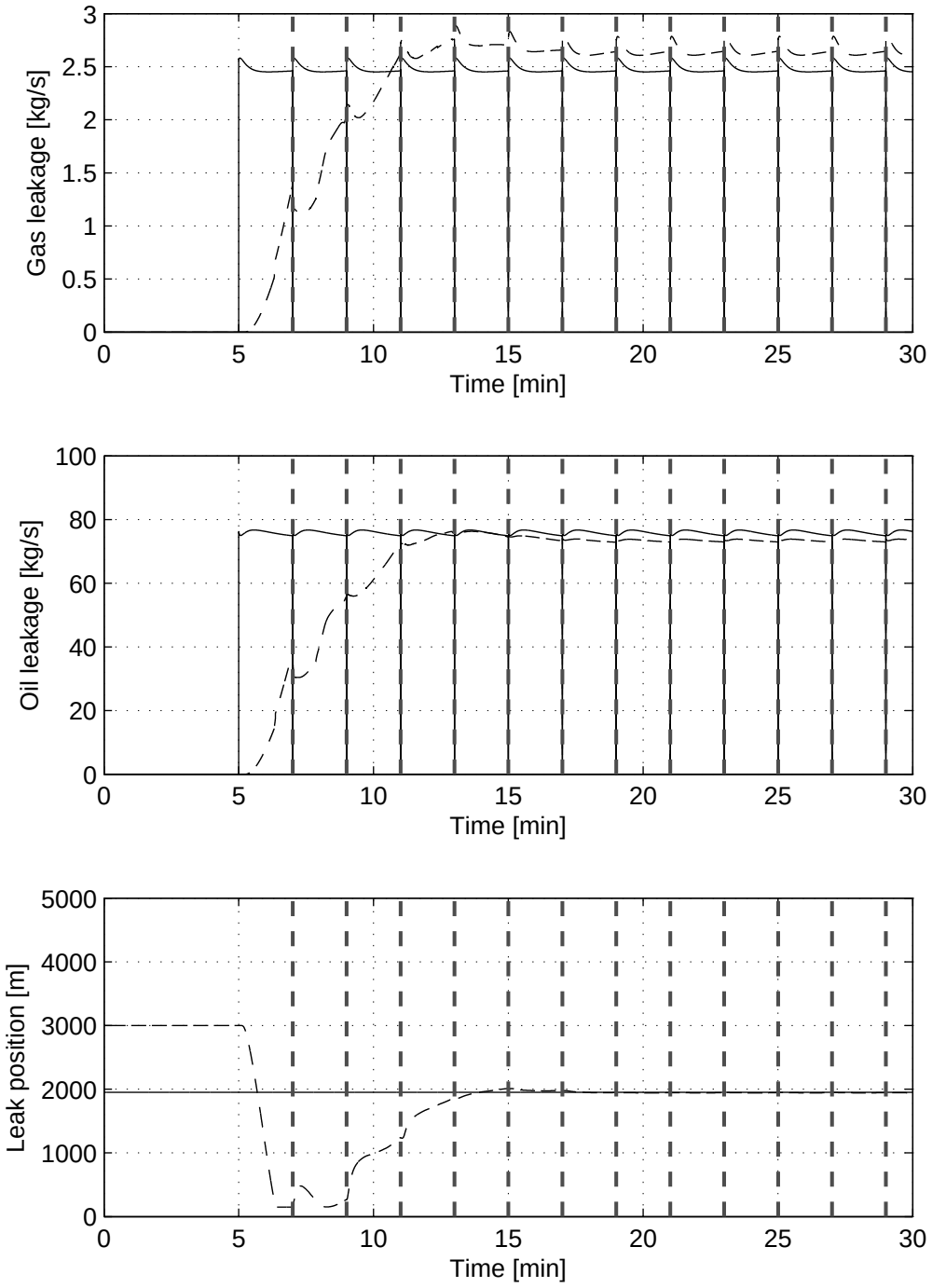

Figure 4.19: Estimates of leak parameters during the shutdown scenario. Only data from two minutes after leak occurense is used. There is a 10% error in ϵ_l. Stippled lines indicate estimates while the solid line is real values. Horizontal lines indicate a reset of model and observer.

Chapter 5

Discussion

In this chapter, the main results presented in the previous chapter will be discussed. The discussion is partitioned into sections corresponding to how they were presented. The chapter is finished by a discussion on future work.

Notice that the boundary conditions will be labeled output injection, but based on a linearized model, they are more an approximation.

5.1 Convergence

When convergence is concerned, for both flow regimes, there are variations in performance when looking at the different variables. In general, when prioritizing pressure, output injection must be said to be favorable. On the other hand, for the mixed flow example, gas velocity and volumetric fraction converge slower when output injection is employed. When looking at the short term graphs, however, the lines alternate on being lower. Oil velocity and pressure seem to converge faster with the new boundary conditions. Initially, they both seem to have a profile similar to that found for pressure in single phase systems (Aamo et al. 2005). This is promising, but it is not surprising that mixed flow behave similar to single-phase flow. If well mixed, it may be considered as a single medium. On the other hand, especially during the first 10 minutes when there is a lot of changes going on, the observer has many sections with varying degree of slugging. This does not seem to ruin the good effect these boundary conditions have on convergence. It is reassuring that the boundary condition also work for slug flow, when slug flow, although often avoided, is one of the two most common flow regimes in two-phase flow(Lu et al. 2006).

Not considering fraction, in stratified flow, all variables seem to converge faster when output injection is employed. Error in fraction is almost identical for all three cases. Although all variables seems to profit, pressure does not seem to converge quite as fast as in mixed flow. Something that looks like steady state error is observed in

stratified flow. This is actually because of the slow oil phase, which have not yet had time to flow through the pipeline after 100 minutes. After 2 hours and 20 minutes, this error would have faded.

The simulations in mixed flow showed that the observer not employing output injection had converged to the model within 15 minutes, while the observers with output injection use close to one hour. Any time-window less than 10 minutes favor output injection. Note that most cases of adaption presented in the previous chapter have more or less converged within 10 minutes. When it comes to the stratified flow example, convergence in general is a lot slower than the mixed flow examples. While the observer not employing output injection used 15 minutes to converge in mixed flow, it uses more than two hours in stratified flow. Remember that the phase velocities in this flow regime is slower than in mixed flow. The faster response seen on the $\mathbb{L}_2$-norm is due to the pressure waves propagating fast through the pipeline, while the slower response is linked to the lower eigenvalues of the model. The slow dynamic is related to the phase velocities, which is faster for mixed flow, and hence the convergence is also faster.

Output injection at inlet compared to output injection at both ends, does not seem to change considerably. Remember that output injection could not be implemented at outlet as it should. Only pressure is set, while the boundary conditions give values for both m_G and m_L. Optimally, fraction should have been specified at outlet. Another limiting factor is that pressure was modified by (3.3) instead of being set directly. The effect of adding this reduced output injection at outlet is not as evident as that of output injection at inlet. Most variables see a slight increase in performance or is unchanged, except for oil velocity in stratified flow for which performance is reduced. A less restricted model would probably benefit more by these boundaries than OLGA does, and hence, all results to follow would perhaps have been affected.

When considering the case with varying boundaries, again, fraction is the only variable that does not benefiting from output injection. Actually, fraction seems to diverge, which is alarming. However, performance is again increased most in terms of pressure, which is promising. The pulse-like inflow is probably not realistic in a real system, where changes would be less often, smaller in magnitude or more ramp-like.

5.2 Leak adaption

The adaption laws seem to work as intended. Independent of flow regime, both leakage and position are estimated within the 30 minute simulation. Restarting the observer work as intended, but limit its features to offline estimation. Leak detection systems are available today, it is the estimation of position which is new, and hence

emphasized. Therefore, using this observer offline together with a leak detection system should be as useful as observing online.

While output injection improved performance both in terms of quantification and location when the flow regime was mixed flow, quantification in stratified flow was slower. Locating the leak, on the other hand, was faster also in this case. In most practical scenarios, location is of greater interest than quantification, and output injection must be said to have a positive effect in both examples. Note that in Figure 4.8, leak position adaption reaches the lower boundary. It is kept constant at 150m for a while. The longer an observer is bounded, the further it would have fluctuated away, and the longer it would take to come back if it was not bounded. As the case without output injection stays bounded longer, output injection would probably give an even better advantage if they were not bounded. Still, output injection end up reducing convergence-time even when both cases reach the lower restriction on $\hat{x}_l$.

Also note that in the examples with stratified flow, both the case with and without output injection end up at a steady state error in leak position. This is related to the apparent steady state error in the convergence, which actually is no steady state error but an error due to slow convergence. Although the pressure waves have long since reached the ends of the pipeline, differences in mass inside the pipeline causes a slight difference in inlet pressure drop, which affect the leak position.

When testing the observer on many different leaks, in most cases, it converge eventually. Performance vary much, however, from one case to another, and if the observer was individually tuned, convergence-time could have been improved drastically. In a realistic system, the leak is not known, and tuning is not an option. Therefore, it is important that one observer is able to handle a wide range of leaks. Running several different observers concurrently could be an option in a real-time system, increasing the range and performance of the system in total.

In both flow regimes, the leak with the least leakage seems harder to estimate. In the stratified flow regime, the lesser leak was not located at three of four positions. Also, leaks toward the end of the pipeline seem harder to locate than leaks in the first half of the pipeline. This is because all leaks start at zero leakage, which will make the adaption of position start drifting toward inlet. Not until the leakage is near quantified does the leak approach its real position, which would at that point be closer if it was in the first half of the pipeline. This is also the reason why the initial observer leak position is in the last half of the pipeline, and not in the middle. A more aggressive tuning would quantify the leakage faster, but would make the observer less stable, decreasing the range of cases it would succeed.

A perhaps surprising fact, is that leaks in stratified flow with a larger leakage will have an overshoot in estimated leakage, while small leakage will be quantified slower, with the estimated value seldom exceeding true value. This can be observed by $\bar{f}_G$ and $\bar{f}_L$, which is negative for severe leakage, indicating the overshoot. This

phenomena is not observed in mixed flow.

Adaption in mixed flow converge every time, but always with $\bar{x}_l$ positive. This is due to the undershoot observed in Figure 4.8, which is present in almost every scenario. Another interesting fact is that all $\bar{f}_G$ and $\bar{f}_L$ are positive also. This information would not have been observed if mean deviation was measured instead. The main reason why it is always positive is, again, because leakage start at zero. When a leak is detected, it is not likely to be zero, and a jump in leakage could have been initiated. A non-zero leakage would in most cases be no worse guess than zero, and $\bar{f}_G$ and $\bar{f}_L$ would improve. Considering what was mentioned above, this could perhaps reduce $\bar{x}_l$ also.

The few cases where the observer did not position the leak, was observed in stratified flow, and would actually converge eventually. As the leakage was slowly quantified in these cases, an error built up inside the observer, which corrupt the adaption. More aggressive tuning would limit this error. Since convergence is slow in stratified flow, it is important that the leak parameters are estimated fast. The faster the observer reaches some steady values, the higher is the chance they are correct. If the observer uses a long time to find steady values, it certainly has been wrong at some point, and an error has been built up depending on how long it has been wrong.

All in all, this one observer seems able to handle most cases, eventually finding the leak position and correct quantification. This is a promising result, as stability is important when considering its robustness. It is also reassuring that very little time was put into tuning. Since the adaption can both be too slow and too fast, it is important that coefficients which are neither too slow nor too fast in one case also work for most others.

5.2.1 Leakage fraction unknown

When estimating a leak with a wrong guess of fraction, not in any case does the adaption seem to settle. Either it oscillates, or it drifts off. The guesses at $\hat{\epsilon}_l = 0.95$ and $\hat{\epsilon}_l = 0.5$ are rather unrealistic, as the total gas flow in the pipe is 5%. Still, adaption with these values does tend to drift in the correct direction. In the mixed examples, they even start oscillating around the correct position, even when $\hat{\epsilon}_l$ is off by 1800%. This is promising, but the examples in stratified flow does not seem to be as robust. In fact, none of these tests settle, but leak position estimate drifts away. There seem to be a connection between $\bar{f}_G$, $\bar{f}_L$ and in which direction the position adaption is drifting. The only case where $\hat{x}_l$ drifts toward outlet is the case when gas fraction in leakage is guessed too low. Also $\bar{f}_G$ and $\bar{f}_L$ have oposite sign when $\hat{x}_l$ is too low, compared to when it is guessed too high. If this is a general trend, it may be used for to obtain a better estimate of ϵ_l. Still, in the two cases where estimated fraction is closest to its real value, position estimates are not far off, and give a clear indication to where the leak could be. Also note that all four

graphs cross at one point which is near the correct position. Perhaps could these trends be used to estimate leakage fraction. As an example, starting with $\hat{\epsilon}$ at a high value, lowering and running simulations for many values until the drifting changes direction, should give a good estimate.

Simulations in a mixed flow regime, instead of drifting when $\hat{\epsilon}_l$ is too low, oscillate at a position slightly closer to inlet than the actual leak. Both when $\hat{\epsilon}_l$ is off by 50% and 200% does the adaption give very good estimates of position. Just as when ϵ_l was known, $\bar{x}_l$ has positive values due to undershoot. The amplitude of oscillation seems to vary, and have a higher amplitude the more fraction is off. This means that the third parameter, leakage fraction, can be identified. A search algorithm trying to minimize position oscillation could be used to find the correct value. Both this method, and the example for stratified flow, require steady flow to work. As leaks often occur with changes in production, it is perhaps unlikely that conditions are steady.

When using mass flow fraction as $\hat{\epsilon}_l$, a good indication of leak position is found in all cases, including both flow regimes. As $\hat{f}_G$ is always negative, and $\hat{f}_L$ is always positive, the OLGA leak model have leakage fraction lower than mass flow fraction. The real ϵ_l is approximately 0.033 and 0.028 for mixed and stratified flow respectively, while the flow mass fraction is 0.05 in both models. This means it is off by 40%, but the adaption still gives a good estimates of leak position. The adaption does not drift away, nor does it oscillate as much as the rather rough estimates tested above. This indicates that if mass flow fraction is not a good enough estimate of leakage fraction, the estimate does not have to be perfect in order to give a good indication on position.

5.2.2 Varying boundaries

A sinusoidal inlet flow was employed on the models. Clearly, when the model flow pattern is stratified flow, the observer is not able to converge fast enough. Adaption diverge to zero in all three cases presented. In mixed flow, however, good estimates of leak position is found even with the most severe sinusoidal inlet flow. This result is directly related to the convergence study of Section 4.1. Convergence was shown to be slower in stratified flow, and clearly not fast enough to handle this kind of inlet flow. The conclusion of these scenarios are easy. Observers with mixed flow handle production changes better than observers with stratified flow.

5.2.3 Biased measurements

The first set of simulations consider a $\pm 1\%$ bias, and in most cases, adaption converges towards a fairly good estimate. Only one case does not, which is the scenario with a positive bias on both flow rates conducted with a stratified flow model. Still,

even in this case, $\bar{x}_l$ is not far off. All other scenarios with stratified flow have t_c only marginally different from the case with no bias at all. $\bar{f}_G$ and $\bar{f}_L$ seem also rather unaffected. There is a trend in $\bar{x}_l$, however, where negative bias cause lower values. This is simply because lower flow rates cause a lower pressure drop, and hence estimated position drifts towards outlet to compensate.

For mixed flow, the bias on oil flow seems to affect the convergence time t_c, while bias on gas flow seems not to. Still, every case converge within ten minutes, and again the biases have little effect on leak magnitude. $\bar{x}_l$ still seem correlated to the bias sign. t_c values in the mixed regime should not be compared to t_c values in the stratified regime. Clearly, this observer adopt to stratified flow faster. This is dependent on the observer coefficients, however. Some tuning could change convergence times the other way around, being faster in mixed flow. Since the observer seemed to handle these lesser errors quite well, the new set of scenarios with larger biases were conducted.

With five percent bias on flow rates, almost every case diverge. Only when bias on oil flow is negative correlated to the bias on gas flow, does the observer converge. Also, this is only the case when the flow pattern is stratified. Clearly, 5% is too far off for to find the correct position. However, note that in most cases, $\bar{f}_G$ and $\bar{f}_L$ are small. This is because the outlet pressure is constant, which means the difference in pressuredrop end up affecting inlet pressure values, which again only affects leak position adaption. Consequently, c_v is more or less unaffected by these biases.

When it comes to pressure, a 0.1 bar bias does not seem to affect the convergence of position, independent of sign. $\bar{f}_G$ and $\bar{f}_L$, on the other hand, is both affected. Bias on fraction, however, does affect convergence of position. The bias used on fraction is ± 0.01. This is a rather large error as volumetric fraction typically ranges from 0.02-0.06 in this thesis. In this case, the error is approximately 25% of real value. The negative bias on fraction changes t_c from 5.7 to 8.4, which is a 50% increase. In terms of absolute value, this must be considered robust, but process equipment may have problems measuring exact fraction, especially when leaks occur. Leakage might even change the flow pattern, which would render the equipment made for the original flow regime useless.

Next, the bias on fraction is increased to ± 0.05, while the bias on pressure is increased to ± 0.2 bar. This may seem unreasonable, as the bias on pressure in percentage is nothing compared to the bias on volumetric fraction. However, measuring pressure is far easier than measuring volumetric fraction. Perhaps not surprisingly, the 0.2 bar bias on pressure does not prevent the observer from obtaining good estimates of leak parameters. On the contrary, the 0.05 bias on fraction causes the observer to diverge with high values of $\hat{x}_l$. This may very well be the weakest link of this observer, as volumetric fraction is not something one usually measure.

5.2.4 Shutdown scenario

With a perfect estimate of $\hat{\epsilon}_l$, the observer seems to handle the drop in flowrate well. As pointed out already, this is not a real shutdown, only a drastic change in production. Looking at the leakage estimate, it follow that of the model, while the position seems to. With the small error in leakage fraction, however, the observer does not settle, although it does give an indication to where the leak might be.

When adapting to the short data set between the time the leak is detected and shutdown, the observer find an almost perfect estimate of leak position, even with the error in $\hat{\epsilon}_l$. For an offline system, this is a very important result. It allows the operator to shut down almost immediately after detection, and there can still be good estimates of position. By extracting a short dataset, one can also avoid sudden production changes or other changes preventing the observer from converging. It also give the observer a chance to try out many values of $\hat{\epsilon}_l$, and if close to the true value, adaption should settle. If $\hat{\epsilon}_l$ is far off, the observer will likely oscillate or drift instead. On the other hand, some oscilliation must be expected due to noice and modelling error.

5.3 Future work

Even though the observer seems to work reasonable in most scenarios, aspects such as temperature and inclination is ignored. Constant inclination would probably not be a problem when modeled correct, but a pipeline with varying inclination would certainly put the observer to the test. Especially slug flow in inclined pipelines would test performance, as slugging is harder to model. Large changes in temperature could also prove critical, but again it would depend on the model. These are fields which clearly should be investigated.

Another significant part of the model which has not been investigated is friction. When this type of observer was studied for single-phase flow, friction adaption was an important field(Hauge 2007). As adaption of friction factor may to some extent neglect modeling error, scenarios such as bias on measurements could most certainly benefit from this feature. Friction adaption in two-phase flow should not prove more difficult than it was for a single phase, but unfortunately the OLGA Matlab toolbox license used in this thesis did not allow tuning of friction.

When using this observer, volumetric fraction must be measured. In order to avoid this, other measurements could be included instead, and used to calculate an estimated fraction. One option could be to measure flow rates and phase velocities instead. Using the formula $w_k/u_k = m_k$ for phase k, one could produce ϵ from these. Most probably this would prove just as hard, as the two sets of measurements are linked. Mass flow with an accuracy of 2-3% would be hard to measure, not to mention the problems that could arise because of correlation between measurements in

phase velocities and mass flow. In a stratified flow regime, a slip relation should be included, and perhaps adapted to fit the model. Such thoughts could perhaps ease the implementation.

OLGA prevent output injection from being used at outlet. A less restrictive model could improve convergence and hence also adaption and its robustness.

The observer does not estimate $\hat{\epsilon}_l$, but there seems to be patterns in behavior related to its error. A search algorithm trying to minimize oscillation or drifting could prove to solve this problem, but would limit the system as an offline observer. For example, in mixed flow, any error in $\hat{\epsilon}_l$ caused the estimate $\hat{x}_l$ to either oscillate or converge. As long as the boundaries are somewhat steady at the time the leak occur, a window in time following the occurrence may be reused giving endless adaption. There are known methods for finding the $\hat{\epsilon}_l$ which minimizes these oscillations. Similar, in stratified flow, adaption of $\hat{x}_l$ does not seem to settle unless $\hat{\epsilon}_l \approx \epsilon_l$. It should be possible to derive similar algorithms for such cases, searching for a good estimate of ϵ_l.

Simulations showed that if the estimated position or leak magnitude did not converge, it did give an indication on the values. As it is only two of the systems four characteristics that reach outlet and inlet, it should only be possible to adopt two leak parameters. However, after estimation, one of the estimated parameters could be set fixed, while leakage fraction was estimated instead. For example, leak magnitude was often found near correct, even in difficult scenarios. With c_v fixed at the final estimate, leak position and leakage fraction could be estimated running through the dataset a second time. This could of course be repeted any number of times.

The tuning parameters are both upper and lower bounded, and optimal tuning vary within the regimes. Perhaps tuning parameters could have been expressed in terms of inlet flow or something similar. This could both improve performance and make the observer more stable.

The velocity of pressure waves should be somewhat equal throughout the pipeline. When a leak occur, there would most probably be a delay between pressure drop at outlet and at inlet. This delay could have been used to estimate position, which could be the initial position of x_l. In addition, there should be a jump at c_v when a leak was detected, as the leak is most certainly not zero. If successful, this could improve adaption considerably.

This thesis to some extent mirror the Luenberger-type observer for single phase(Aamo et al. 2005) and make it work on two phases. Many pipelines include water in addition to oil and gas. It is not unlikely that the observer might also work for three phases, either by treating oil and water as one medium or by expanding the model. This might require more measurements, however.

Chapter 6

Conclusion

The set of general boundary conditions derived is based on a linearized model of the system, and can be implemented on any hyperbolic flow model. The boundary conditions are implemented on an observer in order to obtain output injection, and with it, improved convergence.

The observer is a Luenberger-type observer, and employs OLGA, a computational fluid dynamics simulator, as its model. The boundaries are controlled through Matlab, and model measurements are also generated by an OLGA model. The general boundary conditions improve convergence when the time window is limited. The effect is more evident when the model has a mixed flow pattern, as opposed to a stratified.

A set of adaption laws is presented, adapting to the pressure waves generated by the occurrence of a leak. When implementing them on the observer, it successfully identifies leak position and leakage as long as there is an estimate of leakage mass fraction. Tests using the mass flow fraction as an estimate on leakage fraction prove to be sufficient. The adaption laws are valid only before the slower dynamics generated by the leak reach the outlet. The observer is programmed to reuse measurements if this give a too short timewindow. This is also used to avoid large production changes as in the case of a shutdown, and successfully identify the leak only using a short dataset. This does not prevent the observer from running online, but it must do calculations offline after a leak is detected.

The observer is tested on a wide range of scenarios, both with distributed and separated flow. An observer with a fixed suboptimal set of coefficients seems to handle most cases. The observer seems to be more robust to production changes when the flow regime is distributed. Minor leaks are harder to identify than larger.

The observer depends on four measurements both at inlet and outlet, and if the measured or estimated volumetric fraction deviates too much, the observer does not converge. Tests showed that the observer could handle a small bias on all

measurements, but diverged if the bias was too severe, and it was especially sensitive to error in fraction.

All in all, the observer handle most scenarios, and could probably perform better with different tuning. However, there seem to be two reasons for concern. Fraction in leakage is not adapted, and a good estimate must be found in some other way. Also, the observer is dependent on good measurements of volumetric fraction which might prove hard to obtain.

Bibliography

Aamo, O. M., Salvesen, J. & Foss, B. A. (2005), *Observer design using boundary injections for pipeline monitoring and leak detection*, Norwegian University of Science and Technology.

Besson, T., Tchousso, A. & Xu, C.-Z. (2006), *Exponential Stability of a Class of Hyperbolic PDE Models from Chemical Engineering*, In Proceedings of the 45th IEEE International Conference on Decision & Control.

Chung, M. S., Lee, S. J. & Chang, K. S. (2001), *Effect of interfacial pressure jump and virtual mass terms on sound wave propagation in two-phase flow*, Journal of Sound and Vibration 244(4), 717-728.

Drew, D. A. (1979), *The analysis of virtual mass effects in two-phase flow*, International Journal of Multiphase Flow 5.

Egeland, O. & Gravdahl, J. T. (2002), *Modeling and Simulation for Automatic Control*, Marine Cybernetics AS.

Feng, J., Zhang, H. & Liu, D. (2004), *Applications of fuzzy decision-making in pipeline leak localization*, In Proceedings of IEEE International Conference on Fuzzy Systems.

Hauge, E. (2007), *Advanced leak detection in oil and gas pipelines using a nonlinear observer and OLGA models*, Norwegian University of Science and Technology.

Hodne, K. (2007), *Leak detection in two-phase oil and gas pipelines by parameter- and state estimation*, Norwegian University of Science and Technology.

Hu, R., Ye, H., Wang, G. & Lu, C. (2004), *Leak detection in pipelines based on PCA*, In Proceedings of the 8th IEEE International Conference on Control, Automation, Robotics and Vision.

Liu, Y., Yang, W. & Wang, J. (2008), *Experimental study for the stratified to slug flow regime transition mechanism of gas-oil two-phase flow in horizontal pipe*, Higher Education Press, co-published with Springer-Verlag GmbH.

Lu, G.-Y., Wang, J. & Jia, Z.-H. (2006), *Experimental and numerical investigations on horizontal oil-gas flow*, School of Mechanical Engineering, Shanghai Jiaotong University.

Nilssen, C. R. (2005), *Leak Detection for oil- and gas pipelines by parameter- and state estimation*, Norwegian University of Science and Technology.

Tiselj, I. & Petelin, S. (1997), *Modelling of Two-Phase Flow with Second-Order Accurate Scheme*, Journal of Computational Physics 136.

Toumi, I. & Kumbaro, A. (1996), *An Approximate Linearized Riemann Solver for a Two-Fluid Model*, Journal of Computational Physics 124.

Zhang, J. (1996), *Designing a Cost Effective and Reliable Pipeline Leak Detection System*, Pipeline Reliability Conference, Houston, USA, November 19-22.

Appendix A

Interpolation

A second order interpolation scheme is used to estimate measurements of volume-variables at boundaries between sections. The distance between the three measurements to be used and the position of the estimate is illustrated in Figure 3.1 and 3.2. Consider the general second order equation

$$\alpha(x) = ax^2 + bx + c \tag{A.1}$$

The estimate will be denoted $\alpha_0 = \alpha(0)$, while the three measurements will be denoted α_1, α_2 and α_3 at the position $x = \Delta x/16$, $x = 3\Delta x/16$ and $x = 6\Delta x/16$ respectively. Searching the parameters a, b and c, consider (A.1) evaluated at the different points:

$$\alpha_0 = \alpha(0) = c \tag{A.2}$$

$$\alpha_1 = a(\frac{\Delta x}{16})^2 + \frac{\Delta x}{16}b + c \tag{A.3}$$

$$\alpha_2 = a(\frac{3\Delta x}{16})^2 + \frac{3\Delta x}{16}b + c \tag{A.4}$$

$$\alpha_3 = a(\frac{6\Delta x}{16})^2 + \frac{6\Delta x}{16}b + c \tag{A.5}$$

which yield a system of equations to determine the three unknown constants. In matrix form the equations may be written

$$\begin{bmatrix} (\frac{\Delta x}{16})^2 & \frac{\Delta x}{16} & 1 \\ (\frac{3\Delta x}{16})^2 & \frac{3\Delta x}{16} & 1 \\ (\frac{6\Delta x}{16})^2 & \frac{6\Delta x}{16} & 1 \end{bmatrix} \cdot \begin{bmatrix} a \\ b \\ c \end{bmatrix} = \begin{bmatrix} \alpha_1 \\ \alpha_2 \\ \alpha_3 \end{bmatrix} \tag{A.6}$$

Solved for a, b and c,

$$\begin{bmatrix} a \\ b \\ c \end{bmatrix} = \begin{bmatrix} \frac{1}{10}(\frac{16}{\Delta x})^2 & -\frac{1}{6}(\frac{16}{\Delta x})^2 & \frac{1}{15}(\frac{16}{\Delta x})^2 \\ -\frac{9}{10}(\frac{16}{\Delta x}) & \frac{7}{6}(\frac{16}{\Delta x}) & -\frac{4}{15}(\frac{16}{\Delta x}) \\ 9/5 & -1 & 1/5 \end{bmatrix} \cdot \begin{bmatrix} \alpha_1 \\ \alpha_2 \\ \alpha_3 \end{bmatrix} \tag{A.7}$$

Realizing that only the last row of (A.7) is needed to produce the estimate, the resulting equation becomes

$$\alpha_0 = \frac{9}{5}\alpha_1 - \alpha_2 + \frac{1}{5}\alpha_3 \tag{A.8}$$

Notice that this equation is valid in both ends of the pipeline, as the section-sizes are equal, a redefinition of the x-axis leads to identical results,

$$\alpha_m = \frac{9}{5}\alpha_{m-1} - \alpha_{m-2} + \frac{1}{5}\alpha_{m-3} \tag{A.9}$$

where subscript m denote the outlet value, while α_{m-1}-α_{m-3} are the three known values closest to outlet.

Appendix B

Simulation properties

Table B.1: Pipe and simulation properties

Property	*Value*
Pipe length	5000m
Pipe roughness	$1 \cdot 10^{-5}$
Pipe diameter	20 inches
Segment length	100m
Inflow temperature	$4°C$
Ambient pressure	1 bar

Table B.2: Simulation data - Position adaption stratified flow example

Property	*Value*
Time step	0.02s
Inlet flow rate gas	5 kg/s
Inlet flow rate oil	91 kg/s
Outlet pressure	50 bar
Dominant flow regime	Stratified Flow
Gas leakage	80%
Oil leakage	40%

Table B.3: Simulation data - Position adaption mixed flow example

Property	*Value*
Time step	0.02s%
Inlet flow rate gas	40 kg/s
Inlet flow rate oil	730 kg/s
Outlet pressure	50 bar
Dominant flow regime	Mixed Flow
Gas leakage	38%
Oil leakage	9.5%

Table B.4: Simulation data - Magnitude adaption stratified flow example

Property	*Value*
Time step	0.02s%
Inlet flow rate gas	5 kg/s
Inlet flow rate oil	91 kg/s
Outlet pressure	50 bar
Dominant flow regime	Stratified Flow
Default gas leakage	80%
Default oil leakage	40%

Table B.5: Simulation data - Magnitude adaption mixed flow example

Property	*Value*
Time step	0.02s%
Inlet flow rate gas	40 kg/s
Inlet flow rate oil	730 kg/s
Outlet pressure	50 bar
Dominant flow regime	Mixed Flow
Default gas leakage	25%
Default oil leakage	25%

Table B.6: Observer coefficients

Property	*Value*
Initial leak position	4000m
κ_{x_G}	0.2
κ_{x_L}	0.2
κ_{u_L}	$0.2\dot{1}0^{-4}$
κ_{u_L}	$0.2\dot{1}0^{-4}$
c_G	314.5 m/s
c_L	1161.3 m/s
k_L	$1.2113 \cdot 10^9$

Table B.7: Observer coefficients

Property	*Value*
Initial leak position	3000m
κ_{x_G}	0.2
κ_{x_L}	0.2
κ_{u_L}	$0.4 \cdot 10^{-4}$
κ_{u_L}	$0.4 \cdot 10^{-4}$
c_G	314.5 m/s
c_L	1161.3 m/s
k_L	$1.2113 \cdot 10^9$

Appendix C

Additional plots

This section holds some additional plots not included in the main thesis, but might be of interest to the reader.

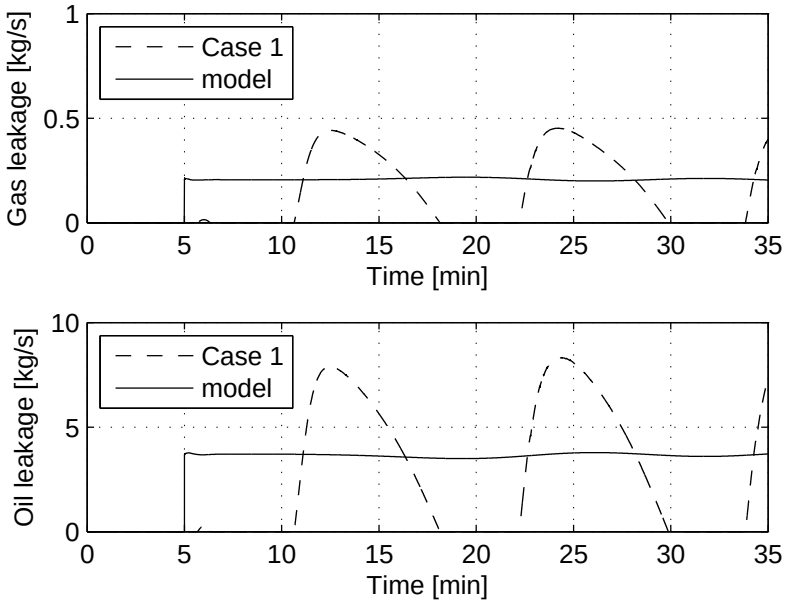

Figure C.1: Leak magnitude adaption for Case 1 with varying boundaries in stratified flow.

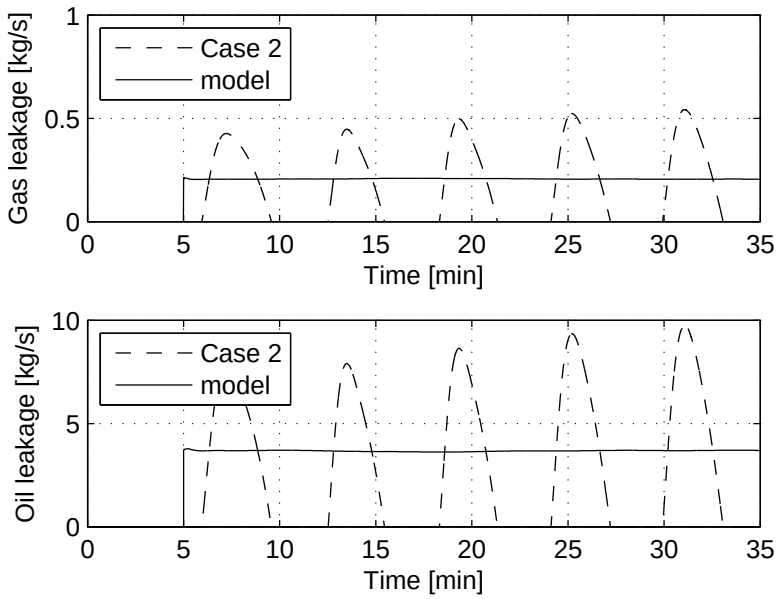

Figure C.2: Leak magnitude adaption for Case 2 with varying boundaries in stratified flow.

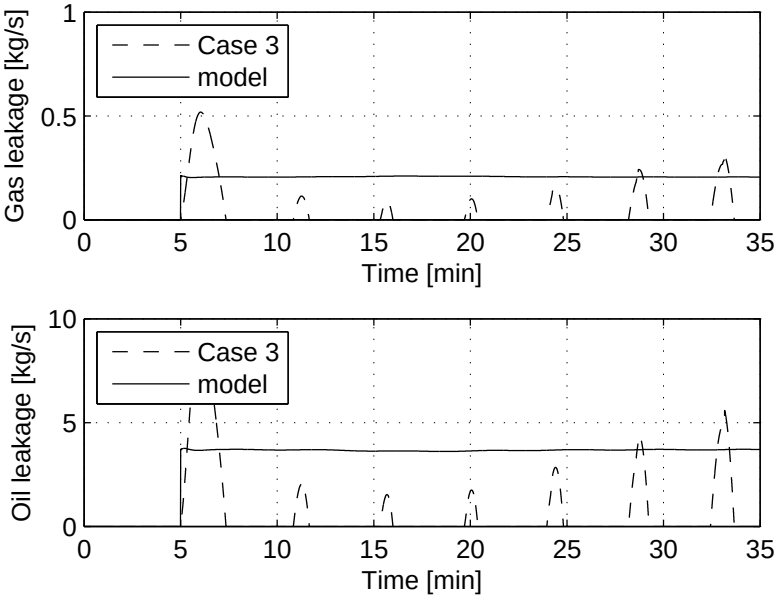

Figure C.3: Leak magnitude adaption for Case 3 with varying boundaries in stratified flow.

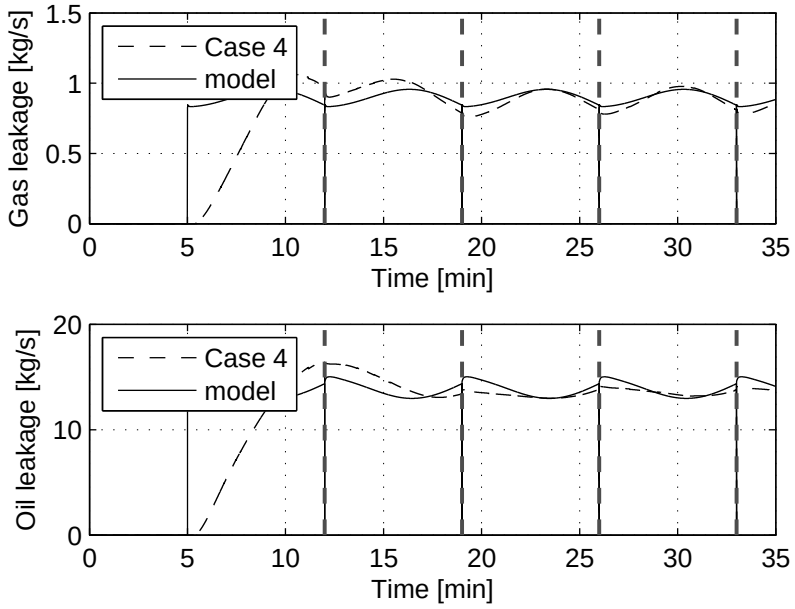

Figure C.4: Leak magnitude adaption for Case 4 with varying boundaries in mixed flow.

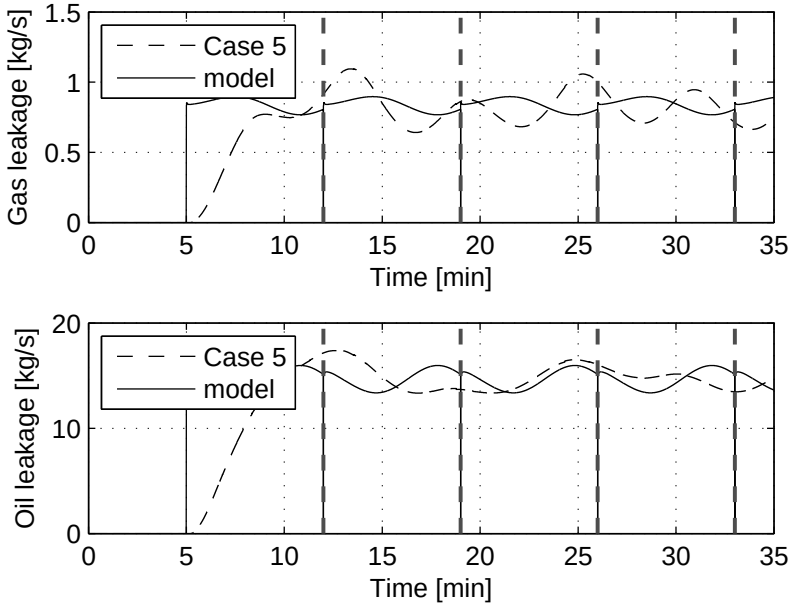

Figure C.5: Leak magnitude adaption for Case 5 with varying boundaries in mixed flow.

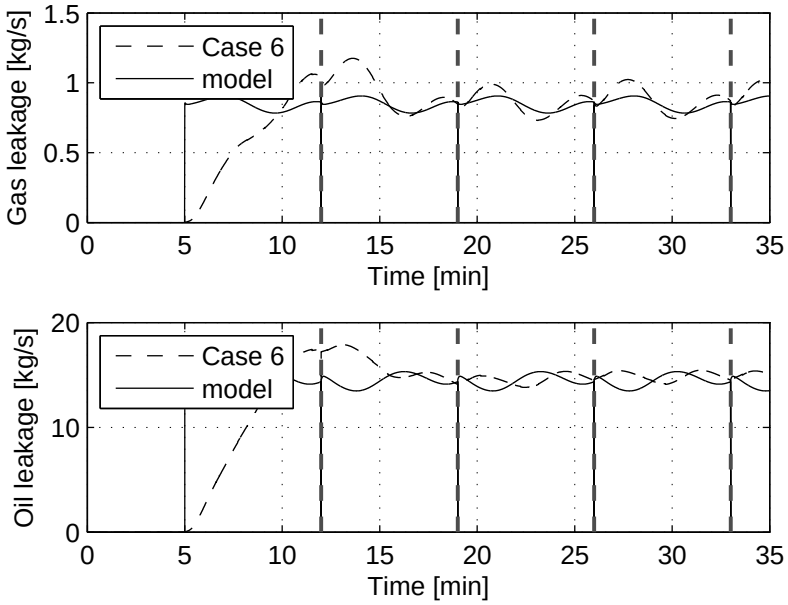

Figure C.6: Leak magnitude adaption for Case 6 with varying boundaries in mixed flow.

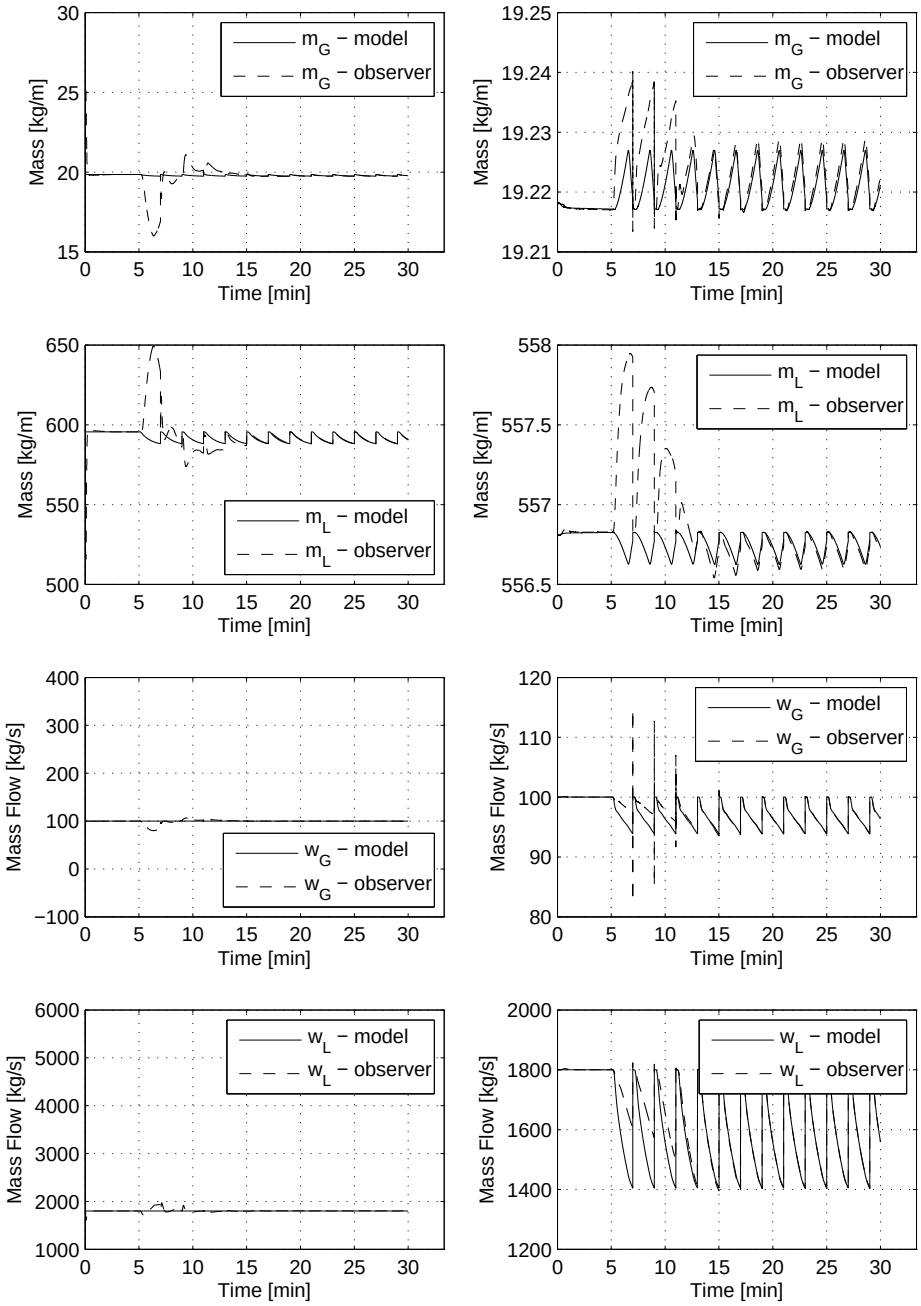

Figure C.7: Boundary values with restart every second minute after the leak is detected.